SGRE Response to VSM Grid Code Spec V6_AJ010420:

- The allowable bandwidth of control

- The practical impact and effect of grid-forming devices: their stiffness contributions, inertia, damping (external and internal) and drooped responses following grid events.

- Testing grid-forming devices against declared parameters (e.g. inertia, damping, drooped response) using the “Network Frequency Perturbation” plot

Project name:	National Grid GC0137		
Dept.:	SGRE OF TE TD EDT FCV CCO		
Resp. dev.:		**Creation date:**	30/04/20
Revision date:	14/07/2020	**Revision:**	1
Approved (date):	14/07/2020	**Initials:**	AJR

Document Details

Document Save Date:

Document History

Rev Number	Revision Date	Author	Changes
1.0	14/07/20	Andrew J Roscoe Thyge Knueppel	R1 released to National Grid and GC0137

Contents

References

[1] National_Grid_ESO, "Draft Grid Code – Grid Forming Converter Specification 27th March 2020 V6_AJ010420," 2020. .

[2] National_Grid_ESO, "Stability Pathfinder Phase Two: Technical Performance Requirements," 2020.

[3] E. Lewis, "Enstore notes for GB Grid Forming Converters – 003.docx," 2020.

[4] Q. C. Zhong and G. Weiss, "Synchronverters: Inverters that mimic synchronous generators," *IEEE Trans. Ind. Electron.*, vol. 58, no. 4, pp. 1259–1267, 2011.

[5] F. Tayyebi, A.; Gross, D.; Anta, A.; Kupzog, F.; Dorfler, "Frequency Stability of Synchronous Machines and Grid-Forming Power Converters," *IEEE J. Emerg. Sel. Top. Power Electron.*, p. 15, 2020.

[6] M. Yu *et al.*, "Use of an Inertia-less Virtual Synchronous Machine within Future Power Networks with High Penetrations of Converters," *19th Power Systems Computation Conference (PSCC)*. Genoa, Italy, 2016, doi: 10.1109/PSCC.2016.7540926.

[7] L. Reguera Castillo and A. J. Roscoe, "Experimental Validation of a Novel Inertia-less VSM Algorithm," *IEEE ISGT (Innovative Smart Grid Technologies North America)*. Washington DC, USA, 2017, doi: 10.1109/isgt.2018.8403384.

[8] L. Zhang, L. Harnefors, and H.-P. Nee, "Power-Synchronization Control of Grid-Connected Voltage-Source Converters," *IEEE Trans. Power Syst.*, vol. 25, no. 2, pp. 809–820, 2010.

[9] A. Roscoe *et al.*, "A VSM (Virtual Synchronous Machine) Convertor Control Model Suitable for RMS Studies for Resolving System Operator / Owner Challenges," *15th Wind Integration Workshop*. Vienna, 2016.

[10] A. J. Roscoe and S. M. Blair, "Choice and Properties of Adaptive and Tunable Digital Boxcar (Moving Average) Filters for Power Systems and other Signal Processing Applications," *IEEE Applied Measurements in Power Systems (AMPS)*. Aachen, Germany, 2016, doi: 10.1109/AMPS.2016.7602853.

[11] M. Yu *et al.*, "Instantaneous Penetration Level Limits of Non-Synchronous Devices in the British Power System," *IET Renew. Power Gener.*, vol. 11, no. 8, pp. 1211–1217, 2016, doi: 10.1049/iet-rpg.2016.0352.

[12] A. J. Roscoe, S. J. Finney, and G. M. Burt, "Tradeoffs between AC power quality and DC bus ripple for 3-phase 3-wire inverter-connected devices within microgrids," *IEEE Trans. Power Electron.*, vol. 26, no. 3, pp. 674–688, 2011.

Glossary and table of nomenclature

AVR	Automatic Voltage Regulator
CC	Current Control
CHIL	Controller Hardware-In-The-Loop
DOL	Direct On Line
D_f	Frequency/power droop slope, pu frequency per pu power
δ_{RG}	Angle (radians) between (virtual) rotor voltage and HV grid for a (V)SM
δ_{RS}	Angle (radians) between (virtual) rotor voltage and (virtual) stator terminals in a (V)SM
Δf	Magnitude of frequency modulation (Hz) when creating an NFP plot.
ΔP	Magnitude of power modulation response (pu) when creating an NFP plot
f_0	Nominal system frequency (Hz)
$f_{NFP_{mod}}$	Frequency (Hz) of frequency and power modulation when creating an NFP plot
$F_\delta(s)$	A small-time-constant filter on the perception of δ_{RS} , added to both the real VSM control system, and the system model for SM
$F_S(s)$	A small-time-constant filter on the evaluation of the damping power P_S, , added to both the real VSM control system, and the system model for SM
FRT	Fault Ride Through
GF	Grid Forming
H	Inertia (pu) of SM or VSM in seconds
k_s	Damping power (pu) per pu slip
K_ϕ	$K_\phi = 1/X$ and represents the pu stiffness contribution of a grid-forming device
$\mathrm{K}_{\phi MVA}$	Grid stiffness or synchronising torque contribution in MVA
MOAS	Mass On A Spring
PHIL	Power Hardware in the Loop
P_m	(Virtual) mechanical power input to a (V)SM rotor, from a (virtual) prime mover/governor
P_δ	The component of the real transient power output (pu) due to δ_{RS} across reactance X in a (V)SM, assuming voltage is 1pu. For a $\mathrm{VSM_{Int}}$ $P_\delta = P_{(V)SM}$, the total transient power output.
P_{Set}	Power setpoint (pu)
P_S	Damping power (real/external or virtual/internal) due to the slip of ϕ_R against ϕ_S
P_{SExt}	Damping power (real/external) which is equal to P_S for a SM or $\mathrm{VSM_{Ext}}$, but zero for a $\mathrm{VSM_{Int}}$.
$P_{(V)SM}$	The total real transient power output (pu) of the device, from (12)or (13) as appropriate.
$\phi_{\Delta P}$	Phase of the power modulation response when creating an NFP plot
ϕ_R	Electrical angle (radians) of the (virtual) rotor in a (V)SM
ϕ_S	Electrical angle (radians) of the (virtual) stator terminals in a (V)SM
R_{NFP}	Complex value of power response when creating an NFP plot
ROCOF	Rate of Change of Frequency
RTDS	Real-Time Digital Simulator
SGRE	Siemens Gamesa Renewable Energy

SM	Synchronous Machine
VSM	Virtual Synchronous Machine
(V)SM	(Virtual) Synchronous Machine
VSM0H	Virtual Synchronous Machine with Zero Inertia (but a fast-responding droop response)
WTG	Wind Turbine Generator
THDv	Total Harmonic Distortion of voltage (assessing the harmonic components only)
TDv	Total Distortion of voltage (assessing all non-fundamental spectral components)
τ_δ	Time constant for $F_\delta(s)$
τ_P	Time constant (in seconds) of the drooped frequency/power response, i.e. governor/prime-mover response.
τ_S	Time constant for $F_S(s)$
ω_0	Nominal system frequency (radians/second)
X	The primary reactance of the SM or VSM device, in pu. For a real SM, this is X'_d, the transient reactance. For a converter, this is normally considered to be the impedance of the primary filter inductor. This can be thought of as the reactance between the (virtual) rotor and (virtual) stator in a (virtual) synchronous machine.
X_G	The additional reactance, in pu, between the (virtual) stator and a convenient grid "point of common coupling" (e.g. a point on the HV grid) that is to be considered
ζ	Damping ratio of the SM or VSM rotor dynamics. $\zeta = 1$ corresponds to critical damping.

1 Introduction

This document follows the release of V6 of the GC0137 "Draft Grid Code – Grid Forming Converter Specification 27th March 2020". [1]. Since then the Stability Pathfinder Phase 2 has also been launched, with its own requirements document [2].

Section 2 contains some specific comments on [1] and [2]. In these comments, specific statements are made concerning the behaviour of Synchronous Machines (SMs), Virtual Synchronous Machines (VSMs), or both (V)SM in general. These comments are the result of many concepts, conclusions and results that are analysed in the subsequent sections of this document. Significant conclusions can be drawn about the appropriate types of quantities of damping to be provided, within a grid powered by a mix of generation types. Also, towards the end of this document, an extremely useful visualisation technique, the "Network Frequency Perturbation" (NFP) plot is introduced, along with a technique of adding masks for acceptable performance ranges. This could be used to provide a key part of a Grid Forming specification for Grid Forming (GF) converters. The NFP plot could also be provided by each GF converter owner/operator/manufacturer for a device, clearly describing and quantifying the device's performance across the range of grid perturbation scenarios.

Section 4 describes the development of models which can be used to analyse the response of (V)SM devices to HV grid phase/frequency events, either in the time or frequency domains.

Section 5 uses the models developed in section 4 to produce time-domain examples of device responses to HV grid phase/frequency events. It is shown that the initial power output from VSM devices can be commensurate with the output from SM devices, even with the VSM devices only have "internal" damping. Potentially, masks could be produced from time-domain responses to phase and ROCOF events that could be used to type-test device compliance in simulation (using a client user model), in a power-hardware-in-the-loop (PHIL) environment, or site testing. It is also shown that providing high levels of "external" damping from a GF converter will likely be unproductive due to the effect of current-clipping during larger phase-step events.

Section 6 develops models and shows time-domain examples of an inertia-less VSM0H grid-forming converter, which provides very fast drooped response that is equivalent to a damping power.

Section 7 examines SM, VSM and VSM0H devices connected in parallel, power-sharing during load steps. This shows that all devices can contribute immediately to power sharing, in << 20 ms, even if the VSM devices have only "internal" damping. It is also shown that drooped response with low time constants can also have a large effect, at least comparable in magnitude to the inertial power output, and also providing damping power proportional to frequency deviation.

Section 8 introduces the Network Frequency Perturbation (NFP) plot. This is a frequency-domain plot of the active-power response of a device to frequency (and phase) perturbations of grid voltages. It allows the response of a device to be summarised across all perturbation frequencies on a single bode plot (actually 2 plots: 1 for amplitude response, 1 for phase response). The NFP plot, when interpreted correctly, allows the droop, inertia and damping response to be determined, without running and plotting multiple time-domain examples. The NFP plot can be determined analytically:

- from the (V)SM or VSM0H control system diagram if it is linearised appropriately
- or it can be obtained from sweeping grid frequency perturbations in a simulation linked to a client user model
- or it can be obtained from sweeping grid frequency perturbations in a PHIL test environment containing the actual (V)SM hardware.

- or it can be obtained through on-site measurements with special injections made by the converter
- or it might be possible to deduce the NFP plot from background variations over time periods.

Finally, section 9 extends the use of the Network Frequency Perturbation (NFP) plot to show how it might be used to create pass/fail masks against declared device parameters. The masks could be applied to the measured NFP plot from a “black box” (V)SM device, to determine its compliance (or not) against a declared parameterisation.

2 Specific comments on "Draft Grid Code – Grid Forming Converter Specification 27th March 2020"

2.1 Definitions of terms

2.1.1 Inertia Power

The "Inertia Power" is very vaguely defined. It also cannot be assessed within a 5 ms window of the start of an event. To understand the contribution of a grid-forming converter to power system stability and robustness following events, or during sustained provision of power to awkward loads, requires knowledge of converter performance across a number of areas:

1) The device's inertia. Eric Lewis calls this "Type 1" power [3].
2) The device's total reactance to the grid (assuming it is grid forming) with a control bandwidth < 50 Hz, which defines its "synchronising torque" and "grid stiffness" contribution. Eric Lewis calls the power which flows transiently due to this mechanism after a phase step as "Type 2" power [3]. It defines part of the transient peak power that a converter makes "instantaneously" due to a phase step (the other part being damping power, if the device has "external" damping). If the device has "internal" damping, then the "Type 2" power defines all the transient peak power that a converter makes "instantaneously" due to a phase step
3) Real "external" damping power. This is the power which a real SM will output due to its damper windings. It contributes to damping rotor oscillations and in a real SM is real and "external". Eric Lewis calls this "Type 3" power [3]. For grid-forming converters, damping is quite likely to be "internal". This does not mean that the device is undamped. For most grid-forming converters the damping will (or can) be higher than for a SM, but the damping will be "internal" or "virtual" and does not actually appear at the terminals directly as a real power. This is explained in detail in sections 3 & 5.
4) Drooped response from a governor/primer-mover or governor/storage system as frequency falls (or rises), with some time constant on the response time. Eric Lewis calls this "Type 4" power [3].

To understand the interaction of these powers and prioritise or define requirements for each, it requires much more than the basic swing equation.

A thorough analysis is presented in sections 3-9. These can be read in conjunction with the reports from Eric Lewis/Enstore [3] and also the report/examples from Alastair Frew/Drax . Broadly, there is commonality between all three document sets, although there are some differences in terminology, and some differing opinions on damping and inertia requirements.

2.2 ECC.6.3.19.3 iii) Bandwidth

What response and stimulus variables are considered in the transfer function used to assess bandwidth?

The proposed bandwidth is "below 5Hz". This is normal for the active governor and AVR control systems of a SM coupled to a prime mover/governor and AVR, where prime-mover power or field voltage are the responses to

frequency or voltage changes. However, when the inherent damping of a SM is also considered, and active-power output is considered the response variable, the SM system can respond with a bandwidth that can be considered to extend above 5 Hz. Within the broader context of converter-interfaced renewables, such an absolute limit would be over-constraining and there are some times when a bandwidth > 5 Hz will be required. This includes active damping scenarios. For example in ECC 6.3.19.4 iii) "*The Grid Forming Plant shall be capable of contributing to Active Power and/or Reactive Power oscillation damping*". To be compliant with this damping requirement may require control bandwidth or power, to a frequency/phase event, to extend above 5 Hz. This does not detract from the general concept that to provide grid-forming behaviour requires a rotor-angle response to grid-side voltages which is significantly less than 50 Hz. Specific examples of times when bandwidth may need to be > 5 Hz would be:

1) During close-in faults and during the largest grid phase steps, current-limiting will be required within the grid-forming converter to avoid self-destruction. These "clipping" actions can have control bandwidths > 50 Hz but only persist for the duration of the event (and a small post-event time), and only for converters sufficiently electrically close to the event.

2) It is shown in section 8 that the power response bandwidth of conventional and suitable devices extends beyond 5 Hz, to fulfil the classical "damper winding" response of a SM. Typically while the bandwidth of the rotor angle responses might be considered to be around 5 Hz for conventional SM devices and many VSM devices (Figure 8-4, Figure 8-6, Figure 8-8, Figure 8-10), the actual significant power output response extends over a wider frequency range up to 10-15 Hz (Figure 8-3, Figure 8-5, Figure 8-7, Figure 8-9) for viable (V)SM and VSM0H devices This is a wider bandwidth than the 5 Hz value specified in ECC.6.3.19.3 iii). The exact meaning of "bandwidth" would need to be specific defined to fully understand this, i.e. what response and stimulus variables are in the transfer function used to assess bandwidth? Probably, the intention of the phrase is along the lines of *the response of (V)SM rotor angle to grid phase angle should have a bandwidth below 5 Hz*, but this needs to be clarified.

3) Large mechanical generators such as wind turbines have certain drivetrain damping requirements. Within a device such as a wind turbine, there are two important loops by which active power response is determined if a grid-forming converter is used. First there is the loop within the grid forming converter, whereby the active power output responds to grid frequency/phase. This most closely corresponds to the proposed bandwidth of "below 5 Hz", in that the response of (V)SM rotor angle to grid phase angle might have a bandwidth "below 5 Hz". However, as described in 2) above, this allows power modulations of >5 Hz to appear at high amplitudes if grid phase changes quickly. Second, there is a power "setpoint" that varies in real time. This is required to maintain maximum power point tracking, and to achieve drivetrain damping. The drivetrain damping functions can become active following large electrical or aerodynamic disturbances that significantly excite one of the tower/blade/drivetrain modes. The bandwidth of this path to fulfil all the drivetrain damping requirements can extend to ~15 Hz. The magnitude of power modulations required is dependent on many factors such as prevailing power output, turbine style (geared/direct) etc.

4) In section 4.4 it is shown that fast-acting droop response is essentially the same as a direct "external" damping power, both being powers that are proportional (with a negative gain) to frequency deviations. A drooped response is normally accompanied by a low-pass filter effect, and for a traditional prime mover this can be quite a slow filter with a time constant of seconds or tens of seconds. However, for a GF converter the time constant of response can be much less, indeed for the VSM0H converter assessed in section 6 the control bandwidth is of the order of 10-15 Hz. This can be seen on the rotor-angle response plots in Figure 8-4, Figure 8-6, Figure 8-8, Figure 8-10. This converter provides a large quantity of damping power and illustrates the point that having a bandwidth > 5 Hz (but << 50 Hz) is not necessarily a bad thing.

2.3 ECC.6.3.19.4 ii)

In this section the proposal to use a 5 ms window to assess performance makes sense, compared to the 5 ms window proposed for inertia which is inappropriate (see Definition of "Inertia Power" above).

A thorough analysis of likely device responses to grid phase steps is presented in sections 3-7. Essentially, assuming the device is a SM or a GF converter the response magnitude will be determined largely by the total device-to-grid impedance, which for a SM includes the transient reactance X'_d. While a real SM also provides some additional power due to real "external" damping, in practice many GF converters can provide the same (or more) power, immediately following grid phase steps (or load steps), even if they only provide "internal" damping, if their total connection impedance is lower than that for a SM. This can occur since GF converters can have local device impedances lower than commensurate SM X'_d, but similar upstream connection impedances.

In ECC.6.3.19.4 ii), should there be a link with the requirement to ride through ±50 degree phase steps, as required by DC0079 ?

2.4 ECC.6.3.19.4 iii) Active Power and/or Reactive Power oscillation damping, also called Synchronising Torque.

This section needs to be significantly clarified and expanded. Significant analysis in this document (Sections 3-9) examines the effects of real "external" and virtual "internal" damping that, for a GF converter, provide an equivalent function to the damper windings in a real SM. Active-power damping, and its relationship with phase/frequency modulations, needs to be much better quantified in the GF specification. The NFP plot offers one way of doing this. (See sections 8 & 9). Typically while the bandwidth of the rotor angle responses might be considered to be around 5 Hz for conventional SM devices and many VSM devices (Figure 8-4, Figure 8-6, Figure 8-8, Figure 8-10), the actual significant power output response extends over a wider frequency range up to 10-15 Hz (Figure 8-3, Figure 8-5, Figure 8-7, Figure 8-9) for viable (V)SM and VSM0H devices This is a wider bandwidth than the 5 Hz value specified in ECC.6.3.19.3 iii).

Significant findings of sections 5 include that:

- There might be some value to the network of providing "external" damping via a GF VSM_{Ext} solution, with conventional levels of damping, and similar post-event decaying rotor oscillations to a conventional SM.
    - However, creation of the VSM_{Ext} algorithm is not trivial, and GF manufacturers will likely express a strong preference to provide an "internally" damped GF VSM_{Int}.
    - Provision of a VSM_{Ext} GF converter which provides high levels of "external" damping is probably not viable. Any benefit during dynamic situations may be severely reduced due to current clipping due to the large damping powers surpassing 1 pu. Also it can raise the bandwidth to ~40 Hz and move the rotor resonant frequency to unexpected values such as ~8 Hz, with high amplitudes. The analogy would be with a vehicle that is so highly damped that instead of providing a smooth ride, the dampers are so stiff that road surface vibrations are transmitted direct to the vehicle body, providing a noisy and rattly ride.
- Most GF converter VSM offerings are likely to offer virtual "internal" damping, VSM_{Int}
    - The algorithm is much more obvious/simple compared to VSM_{Ext}.

- VSM_{Int} can be provided with conventional levels of damping (with typical post-event decaying rotor oscillations to a conventional SM)
- VSM_{Int} can also viably be provided with much higher levels of damping, up to critical or even above.
- Offering high damping in a virtual "internal" way, does not increase the risk of overcurrent during dynamic events. In fact, the opposite is probably true.
- Increased "internal" damping does not significantly affect the immediate response to phase steps between 0-50 ms, but it does tend to decrease the power feed-in over a period between 50 ms – 500 ms following a large load step or loss of generation infeed, compared to VSM_{Int} with lower damping, or conventional SM with external damping, or VSM_{Ex}.

There are also other types of damping that are referred to, both in the draft GF spec and also in the Stability Pathfinder Phase 2 Requirements [2]. These seem to refer to active damping schemes that

- *detect sub-synchronous frequency oscillations*
- *inject active or reactive current adequately in antiphase to achieve a reduction in oscillations at the Grid Entry Point*

These appear to refer to a different active set of schemes with some thresholds/triggers. Traditionally this function would have been provided by a Power System Stabiliser (PSS).

- In the modern context, with GF VSM converters that could provide higher levels of "internal" damping than a traditional SM, would such an active function actually be required, or does it just risk introducing new oscillations? Having discussed this point internally within SGRE, our feelings are that, as shown in section 7 of this report, a highly-damped VSM, even with "internal" damping, can be effective at damping lower-damped (V)SM generators and reducing or eliminating their tendencies to swing. Using a "passive" damping scheme, at many distributed GF converters, ought to be intrinsically "safe". On the other hand, attempting to design, parameterise and tune an *active* damping system involving many interacting units, with an algorithm that required *detection* and *injection*, might be extremely complex/risky. Furthermore, wind turbines have mechanical modes in the 0.5-2 Hz region, so any active-power injection done in this frequency region might cause a conflict with the turbines' own drivetrain damping mechanisms.

- In the context of GF VSM, is a reactive/voltage response to a sub-synchronous frequency oscillation appropriate? Clearly in the context of large SM with large prime movers, modulating reactive power with a PSS made sense, compared to slower-acting governor responses available at large thermal stations. However, in a VSM context, adjustment of active power directly (with a faster response available) might be a much more appropriate method. Does introducing reactive power modulations as a response to frequency deviations simply risk confusing the situation with cross-couplings? Another consideration is that GF converters are often connected at the ends of long lines/cables, making meaningful reactive-power contribution harder to quantify. If such a reactive-power modulation scheme is required, this might be better achieved at more central locations by STATCOM devices.

2.5 ECC.6.3.19.5 ?) Harmonic and Unbalance requirements

Harmonic requirement specifications seem to have been removed entirely from V6? Surely the converters must be able to withstand some certain minimum level of voltage harmonics, balanced and/or unbalanced, and also certain levels of unbalanced voltage? What is the EN50160 equivalent for THDv and unbalanced voltage at HV and EHV?

This is important. Many converter transformers, as installed today, have been specified for very low harmonic currents. This is understandable, since the current-control converters were specifically designed to operate at very low THDi levels, in order to meet the connection agreements. If those converters (or future installations) are operated as GF converters, then the THDi that occurs is a function of the network loads connected, and THDv at the point of common coupling (PCC). This is largely out of the control of the GF converter unless it is supplying a dominant part of the local grid stiffness. The upshot is that there needs to be a usable specification on tolerance to harmonic (and unbalanced) voltages at the PCC, against which GF converter hardware needs to be (re)assessed and/or designed.

3 Summary of conclusions from sections 4-7

This section highlights the conclusions sections from several individual sections that follow, containing links to the relevant sections and plots/tables that lead to the conclusions. This section is mostly of use if the report has been read before in its entirety, to quickly relocate areas where conclusions have been drawn. If reading the report for the first time, the reader may want to skip ahead to section 4 to follow the narrative.

(Section 4.3) Grid Stiffness and Synchronising Torque are essentially the same property describing small-signal response, but in a converter-dominated context need to be considered separately from the property Fault Level, aka Short Circuit Level, which describes a large-signal response. For a grid-forming device, the small-signal property Grid Stiffness is determined by the device-to-grid impedance (and $X_d{}'$ for a SM), but Fault Level needs to be assessed separately, accounting for SM electromagnetics ($X_d{}''$), or converter current limits/clipping.

(Section 4.4) A fast-acting drooped frequency response can be considered as damping.

(Section 4.11) In a VSM converter there is a range of damping available, since this is configured by software. Damping up to critical ($\zeta = 1$) or above is possible, without power efficiency considerations. Implementing real "external" damping power as it exists in a real SM is not trivial, and would probably require > 5 Hz control bandwidths to implement such that it matched the real damping power profile of a real SM. However, evidence in following sections and plots suggests that virtual "internal" damping may be quite adequate in a system scenario to provide the required damping.

(Section 5.1) Response to phase steps

- The power response ramps rapidly to a peak within 20ms of the step/jump
- The dominant peak power output magnitude is inversely proportional to the total device-to-grid impedance, and is independent of $\mathrm{inertia}\ H$
- The power response of real SM and VSMExt is further augmented with external damping power. For conventional levels of damping the external damping power accounts for approximately one third of the initial peak power output
- If VSMExt was implemented, damping would have to be restricted to conventional levels, otherwise the damping power required would often cause overcurrent clipping within the VSMExt device, counteracting any potential beneficial effect.
- In VSMInt is used, it allows damping to be increased to critical with ζ=1, without any increased risk of over-current clipping in the converter. This provides a much more damped response, without subsequent rotor/power swings.
- Use of conventional damping levels with ζ<1 allows the initial peak power transient on the "1st swing" to be sustained for slightly longer. However, this is at the expense of adding decaying rotor/power oscillations.
- Increasing the inertia also increases the duration of the initial "1st swing" power output proportionately, and the energy in the "1st swing".
- For all devices in phase step/jump scenarios, with the exception VSM devices that can make an extremely fast droop response, the drooped prime mover response is too slow to have any significant impact on power response to a phase step/jump. Therefore, for most devices, the transient responses to phase steps/jumps can be effectively considered as if the devices were operating as synchronous condensers. By the time the event response finally finishes, the total energy infeed from every device is therefore approximately zero.
- For all VSM devices, large close-in phase steps can push a converter towards/into current clipping, depending on the magnitude of the phase step, device-event impedance, and the pre-event operating powers (active and reactive) of the converter.

(Section 5.2) Response to constant-ROCOF frequency ramp

- Similarly to a phase step/jump scenario, the largest actual power flows are due to the P_δ component, via the "Type 1" inertia power [3]
- The real external damping power P_{SExt} (which is only non-zero for SM and VSM$_{Ext}$ devices) has a smaller magnitude then P_δ. However, it does play a role in accelerating the real power infeed on SM and VSM$_{Ext}$ devices, giving them a slightly faster power infeed than equivalently-damped VSM$_{Int}$ devices.
- For SM and VSM$_{Ext}$, increasing the damping ratio ζ increases the initial rate of power increase, and also decreases the level of decaying rotor oscillations after the start of the event.
- For VSM$_{Int}$, increasing the damping ratio ζ **decreases** the initial rate of power increase, but still decreases the level of decaying rotor oscillations after the start of the event.
- The effect of droop-related frequency response through governor and prime-mover action ("Type 4" power [3]) plays a much larger part in ROCOF events than it does in phase step/jump events.
    - In Group A, the SM prime movers have a response time constant of τ_P=4 s, emulating gas turbines. This allows them to increase their infeed noticeably beyond the 0.08 pu and 0.16 pu inertial contribution for the H = 4 and H= 8 devices respectively. In this case (Figure 5-3) the prime mover can add a further ~0.08 pu power contribution by the time 2 seconds have elapsed after the event start, an equivalent power to the H = 4 contribution. In Group A, the VSM devices have no primary frequency response configured, so their response is purely due to inertia.
    - In Group B, the SM prime movers have a response time constant of τ_P=10 s, emulating steam turbines. By contrast the VSM devices have a much faster droop response time constant of τ_P=1 s. This means they can deliver a a further ~0.2 pu power contribution by the time 2 seconds have elapsed after the event start, an equivalent power to an H = 10 contribution.
- Essentially, the VSM$_{Int}$ devices with $\zeta = 1$ will feed in slightly less power than a traditional SM (with equivalent H) within the first 500 ms of such a "potted" constant-ROCOF event, unless $\tau_P < 0.5$ s. The power feed-in rate can be increased by lowering ζ (at the expense of rotor oscillations) or by moving to a VSM$_{Ext}$ control strategy, or by decreasing D_f for a more aggressive droop response, or by reducing τ_P. The possibility for offering drooped responses from VSM$_{Int}$ or VSM$_{Ext}$ converters (potentially with $\tau_P < 0.5$ s), in conjunction with increased damping, means that the VSM converters could actually play a bigger role in managing frequency nadir than a traditional SM. Indeed, if the local energy available supported $\tau_P < 0.5$ s, then the power ramp rate of VSM$_{Int}$ might match that of an SM with external damping, by substituting very-fast droop response power in place of external damping power – the two types both offering damping (see section 4.4).

(Section 5.3) Response to phase step/jump coincident with constant-ROCOF frequency ramp

- According to the "potted" theoretical situation where a negative-going phase step/jump coincides with the beginning of a linear frequency ramp (falling), the models for all (V)SM devices predict an initial thump of power output, followed by a "lull" about 250 ms after the phase step, before the inertial and droop-response power subsequently increases. This power profile, using the model of Figure 4-1, assumes that there is some infinite bus within the system against which the (V)SM devices can "swing". While the model used is reasonably accurate for this "potted" scenario, it needs to be appreciated that when there is no infinite bus, and all the power is provided by a collection of interlinked (V)SM units and other devices, the power transients may not contain this "lull". Section 7 investigates this further and shows that in real power-sharing scenarios lacking any "infinite bus", the "lull" does not exist coincidentally at all devices.

(Section 6) Summary conclusions for VSM0H responses to phase steps and ROCOF

- Figure 6-3 (left column) shows that the VSM0H response to a phase step is of a similar order to a SM or VSM (compare the left column $P_{(V)SM}$ plot of Figure 6-3 with Figure 5-2).
- Figure 6-3 (right column) shows that the VSM0H response to a frequency ramp starts slower than that of a SM or VSM, but that it can then exceed that of a SM or VSM that has a slower droop response time constant τ_P, because the time constant on the VSM0H droop response is so small. (compare the right column plots of Figure 6-3 with Figure 5-3).
- Figure 6-4 shows the VSM0H response to the combined phase step and frequency ramp. Compared to Figure 5-5, which shows the responses of SM and VSM devices (with inertia) to the same event, the VSM0H device provides a similar response to the initial phase step, followed by a slightly smaller response than (V)SM between 40 ms and 500 ms (no inertia), but then rapidly followed by a steadily increasing power output which can increase faster than (V)SM, with a parabolically increasing cumulative energy output.
- VSM devices could also be equipped with very fast-acting droop response with very small τ_P, if the energy source attached to the DC bus supported it. This would create a VSM device possessing inertia, plus also a fast-acting droop response. This would provide a large response throughout the entire post-event period.

(Section 7) Summary of conclusions from islanded load-step scenarios
Simulations of islanded load-steps with 2 and 3-generator systems comprising SM, VSM and VSM0H power sources shows that all grid-forming devices contribute to the initial load step, whether damping is external or internal. The initial power share infeed is dominated by the stiffness contribution K_{ϕ} that is determined by impedance, although the presence of real external damping does additionally increase a device's contribution. Inertia does not affect the magnitude of the initial power infeed.

There are 3 distinct phases to the post-event period:

1) 0-50 ms (Figure 7-3). The initial responses are due to the phase step effect. The power transient dominantly comes from $\mathrm{VSM_{Int}}$, primarily because in this example it has a lower total impedance to the grid. There is an external damping power contribution from the SM, but it has little affect during the first 50 ms, and/or is not large enough to outweigh the lower impedance effect of the $\mathrm{VSM_{Int}}$.

2) 50 ms – 350 ms (H =4) and 50 ms – 500 ms (H =8) (Figure 7-3) During this period the differences in damping ratio and internal/external damping of the 2 devices have an impact. Firstly, the higher damping ratio of the $\mathrm{VSM_{Int}}$ means that its rotor slows faster, reducing its δ angle faster than the more lightly-damped SM. Secondly, while the external damping power appears directly at the device terminals, the internal damping effect is indirect, so for the $\mathrm{VSM_{Int}}$ the damping power is purely "virtual". These two effects combined mean that the SM provides nearly double the transient (new load) power compared to the $\mathrm{VSM_{Int}}$ during this period, even though both devices have the same H value.

3) 0.5 s onwards (Figure 7-2). As frequency falls at a more stable rate, with ROCOF gradually arrested and reversed, both devices provide the same inertia, and damping power reduces. However the $\mathrm{VSM_{Int}}$ with τ_P=1 s can respond faster on the droop response, compared to the steam turbine. Therefore, it outputs more power as frequency falls, and from 0.5 s onwards, this power is much larger than the inertial contribution, as ROCOF is stabilised and frequency reaches the nadir at ~3.5 s and then begins to rise again. Only much later, >20s after the event, is the steam turbine prime mover able to "catch up" to its fair share of power output. Note, that if the converter was not able to provide a drooped response, then the plot would look quite different from 0.5 s onwards.

An interesting feature of this power-sharing scenario (Figure 7-2) is that the SM power output does not have the classic decaying oscillations of the grid-connected scenarios (compare with SM devices B1 & B2 in Figure 5-5), even though the damping ratio of the SM is $\zeta \ll 1$. This is because it has no infinite bus to swing against. It can only swing against the VSM_{Int}, which is configured for $\zeta=1$. This is a good example of where a critically-damped VSM, even in the VSM_{Int} form with internal damping, can provide a more stable power-sharing partner than another traditional SM [5].

When VSM0H devices with zero inertia are added to the generation mix:

Referring again to the 3 distinct phases to the post-event period:

1) 0-50 ms (Figure 7-6). The VSM0H provides the same phase-step response as the VSM_{Int}, both of which, in this example, provide more response than the SM because they have a lower total impedance to the grid.
2) 50 ms – 350 ms (H =4) and 50 ms – 500 ms (H=8) (Figure 7-6) During this period the VSM0H provides less contribution than SM or VSM, because it provides neither inertia nor bandwidth-unlimited external damping power.
3) 0.5 s onwards Figure 7-5). The VSM0H provides more power than SM, and faster than VSM, simply because its response on the droop slope is faster than either, with τ_P<<1 s ($\tau_P \approx 0.010$, see section 6)

The overall result is that the VSM0H

- Contributes a proportionate share of immediate response to the load step (phase step),
- then does little to limit the initial ROCOF,
- but thereafter quickly contributes power as frequency drops, and has a significant effect on minimising the peak frequency deviation (compare Figure 7-5 with Figure 7-2), and general post-event oscillations.

4 Simplified linearised models for SM and VSM devices connected to an HV grid

4.1 Context for a (V)SM embedded within the power network

Figure 4-1 shows the context of a SM or VSM embedded within the power system. In this analysis, the SM rotor or VSM bridge is separated from the stator (or virtual stator) by a pu reactance X. This is the pu transient reactance X'_d in a SM, or the primary filter reactance in a VSM. However, the total impedance to the grid also includes other upstream elements including transformers and transmission lines. In this analysis, only the dominant inductive series elements are considered, and both (V)SM induced rotor and grid voltage magnitudes are considered to be nominal at 1pu. Angle δ_{RS} describes the angle between the (virtual) rotor and the (virtual) stator, while δ_{RG} describes the angle between the (virtual) rotor and the distant upstream grid. Figure 4-1 also shows a parallel current and power path via a squirrel-cage icon. This represents, in a real SM, the damper windings which introduce an additional real power flow that is proportional to the slip frequency between ϕ_R and ϕ_S.

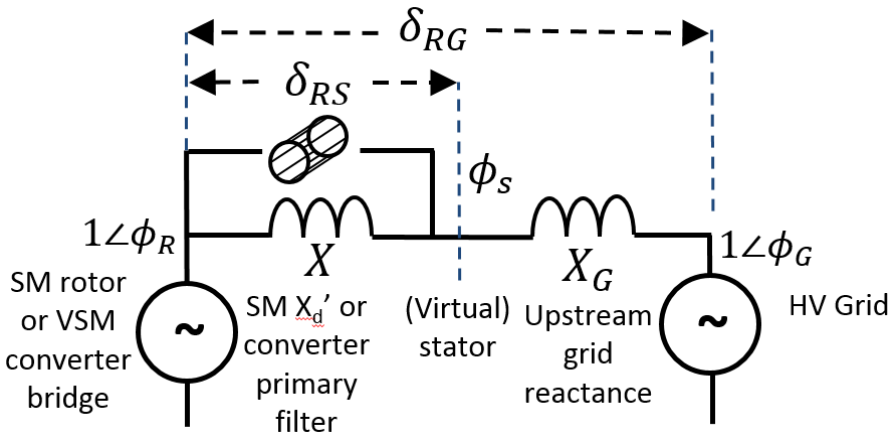

Figure 4-1 : Context for SM or VSM embedded within power system

4.2 Rotor frequency and electrical frequency are not the same

Before, moving on with further analysis, it is useful here to stress that within a (V)SM, the (virtual) rotor speed is not necessarily the same as the frequency perceived in the power system or at the machine stator terminals.

For a SM, the fundamental equation of motion of the rotor is given by:

$$\left(P_{M\ in\ pu} - P_{E\ out\ pu}\right) = \Delta \mathrm{P} = -\left(\frac{2H}{\omega_0}\right)\frac{d\omega_{rotor}}{dt} \quad (1)$$

This is a fundamental energy balance, between pu power imbalance ΔP and the rotor speed.

However, (1) is often rewritten as:

$$\Delta \mathrm{P} = -\left(\frac{2H}{f_0}\right)\frac{df}{dt} \quad (2)$$

It is crucial to remember that this is only an approximation. Equation (2) makes an assumption that the electrical frequency of voltages is exactly equal to rotor speed. The issue is that during dynamic situations, (2) is not correct. It is not correct because:

1) The rotor angle and rotor per-unit speed is not the same as the stator voltage angle and per-unit frequency. They are linked by the 2nd-order relationships derived later in section 4.6. This is a much more dynamic relationship than "being the same"!

2) When any device makes a perception of frequency at the electrical stator terminals or another network point, this is invariably done using a measurement window/filter and some form of processing algorithm. These massage the output values, in a way that can only be understood properly with intimate knowledge of the inner workings of the measurement device and its algorithms.

Only in the case where $(d\omega/dt)/\omega_0$ and $(df/dt)/f_0$ are equal and constant, and at steady state, can (2) be considered correct. This will only be true when system ROCOF is not changing, and there are no phase steps, etc. Essentially any time there is a dynamic event where grid-forming power response is important, (2) will not provide an accurate assessment. This is important to remember, because (2) appears many times in the post-analyses of dynamic network events!

4.3 Types and mechanisms of power response

As described in [3] there are 4 different types of power response that can be drawn from a (V)SM:

1) Power due to inertia, as the machine rotor slows down or speeds up. Eric Lewis calls this "Type 1" power [3].

2) Power due to a sudden phase step/jump of the electrical network, causing power to be transiently drawn-from, or pushed-into, a (V)SM. Eric Lewis calls the power which flows transiently due to this mechanism after a phase step as "Type 2" power [3]. A (V)SM, like a battery, does not "inject" power. Power is drawn-from, or pushed-into it by loads and other devices.

3) Real "external" damping power. This is the power which a real SM will output due to its damper windings, represented as the squirrel-cage icon in Figure 4-1. It contributes to damping rotor oscillations and in a real SM is real and "external". Eric Lewis calls this "Type 3" power [3]. For grid-forming converters, damping is quite likely to be "internal". This does not mean that the device is undamped. For most grid-forming converters the damping can be configured to be higher than for a typical SM, but the damping is "internal" or "virtual" and does not actually directly appear at the terminals as a real power that mimics a squirrel-cage winding. The internal damping does, however, damp the virtual rotor motion and thus indirectly affects the real power exchange, and causes the VSM to interact with other devices in a damped manner.

4) Drooped response from a governor/primer-mover or governor/storage system as frequency falls (or rises), with some time constant on the response time. Eric Lewis calls this "Type 4" power [3].

It should be noted that types 1) and 2), i.e. the responses due to phase jumps/steps and inertia are (dominantly) both subtypes of the same fundamental principle whereby power is drawn-from, or pushed-into, a (V)SM device due to the "delta" angle δ_{RS} at the (virtual) machine, across it's reactance X (Figure 4-1). Assuming that voltages are 1 pu:

$$P_\delta = \frac{sin(\delta_{RS})}{X} \approx \frac{\delta_{RS}}{X} \text{ if } \delta_{RS} \text{ small so that } sin(\delta_{RS}) \approx \delta_{RS} \quad (3)$$

i.e. the power flow is roughly proportional to the angle δ_{RS}, and inversely proportional to X (Figure 4-1).

This relationship is fundamental for a (V)SM. Essentially the rotor is considered to be an "infinite bus" "voltage source" at angle ϕ_R, separated from the electrical stator terminals by reactance X (pu). Assuming that the device is a SM or (V)SM, i.e. it is grid forming with a primary control-loop bandwidth << 50 Hz acting on ϕ_R, then the "synchronising torque" and "grid stiffness" contribution of a (V)SM device in MVA can be calculated by following the "voltage source behind an impedance" rationale:

$$Grid\ Stiffness\ Contribution = Synchronising\ Torque\ Contribution = \mathrm{K}_{\phi MVA} \quad \text{MVA} \tag{4}$$

where $\mathrm{K}_{\phi MVA} = S_{RatingMVA}\mathrm{K}_{\phi}$ MVA (5)

and $\mathrm{K}_{\phi} = \frac{1}{X}$ pu (6)

The Grid Stiffness Contribution K_{ϕ} defines the dominant part of the transient peak power that a converter makes "instantaneously" due to a phase steps/jumps. It also quantifies the synchronising torque contribution. These are "small signal" properties.

> [Note. evaluation of (4)-(6) for an SM with $X = X''$ – the subtransient reactance, will reveal it's classical "Fault Level" and "Short Circuit" contribution, at it's stator terminals, typically ~8 pu since X'' is typically ~0.125 pu, whereas X' may be in the region of 0.3. This describes a "large signal" property. Determination of "Fault Level" and "Short Circuit" contribution require a different analysis for a VSM since during a local/deep fault, while device impedance may be in the same ~01.25 region, the currents will be clipped with a control bandwidth above 50 Hz. For a VSM, while K_{ϕ} and $\mathrm{K}_{\phi MVA}$ give an indication of the small-signal stiffness and synchronising torque contribution of a (V)SM device, they do not give an indication of the large-signal fault response which requires current-clipping and a temporary control bandwidth above 50 Hz].

Compared to type 1 and type 2 power, governed by (3), type 3 power, i.e., real external damping power, represented as the squirrel-cage icon in Figure 4-1, is a slip-related power flow P_S . This is proportional to the slip frequency $d\delta_{RS}/dt$ between ϕ_R and ϕ_S, where $\delta_{RS} = (\phi_R - \phi_S)$. This is a quite different mechanism to the type 1 and type 2 power. It is not a natural property of the reactance X. In a SM it is due to the damper windings which are represented as the parallel branch in Figure 4-1.

$$P_S = \frac{k_S(d\delta_{RS}/dt)}{\omega_0} \tag{7}$$

where k_S is the power (pu) per pu slip.

If real external damping power P_S had to be produced from a VSM, it would need to be "forced" through the reactance X by making "synthetic" adjustements to ϕ_R and therefore δ_{RS}, so that the required external damping power, equivalent to (7), actually emerged via (3). This would probably require a control bandwidth > 5 Hz.

When any network disturbance occurs, perturbations to δ_{RS} occur in all connected (V)SM devices, but at different rates and trajectories for every device. For example, when a large generation unit is suddenly tripped, it's power infeed is lost and the immediate result is a negative-going phase step on the HV network that is largest at points electrically close to the event. (V)SM devices that experience the largest phase step will respond most with "instantaneous" type 2 (phase step/jump) power transients to match the power deficit, and this sudden despatch of energy from their rotors will slow their rotor frequencies. While devices further from the event may experience a much smaller (or no) phase step/jump, each will see a gradually increasing δ_{RS} as they become advanced, relative to the devices closer to the event which are already slowing down. This will, in turn, lead to all (V)SM devices slowing down as they all provide inertial (type 1) response – which is a much more gradually increasing power than the phase step/jump (type 2) power. In turn, the detected change in speed/frequency will cause governors and prime mover responses in all devices configured to provide a drooped (type 4) response. Changing prime-mover power at all relevant (V)SM devices initially acts to accelerate or decelerate their rotors, which feeds through, in time, to modified δ_{RS} trajectories and subsequent power output, dominantly via (3).

Therefore it can be seen that following any event, for each and every (V)SM device, the 4 different types of power response, rotor response, and prime mover response are all related in a complex manner. Furthermore, all the responses at every (V)SM device are inter-related through their electrical connections which affects the electrical angles at the stators (ϕ_S) of each and every (V)SM device.

4.4 Fast-acting drooped frequency response can be considered as damping

In section 4.2, it is noticeable that a real (external) power output which is proportional to the slip between a SM rotor and stator is a damping power. Essentially, if an SM rotor was to remain at a constant speed, the damping power due to slip would make a positive power output proportional to the frequency drop on the grid by (7).

It is interesting, and extremely useful, to note that an immediately-acting drooped frequency response, whereby power output was:

$$P_{droopResponse} = \frac{(f_0 - f)}{D_f \cdot f_0} \tag{8}$$

would also provide a power output directly proportional to a grid frequency drop. This means that a fast-acting governor and prime-mover response coupled to a droop slope effectively provides a similar damping function as SM (external) damping to the grid. However, this is only true when the response is reasonably fast. Within a tradition SM system such as a gas/steam turbine or hydro unit, time constants on prime mover responses are measured in seconds and this adds significant phase lag. If the phase lag becomes too great, governor and prime-mover response can no longer be considered as damping, and indeed, can contribute to resonance at frequencies where the phase lag approaches 90° [See later diagram Figure 4-2 and imagine performing an OLTF gain/phase margin assessment of the droop response in conjunction with $(1/2Hs)$]

In a real gas turbine or steam turbine:

$$P_{droopResponse} = P(s)\frac{(f_0 - f)}{D_f \cdot f_0} \tag{9}$$

where $P(s)$ is the response of the governor and prime mover. This could be a simple or a complex transfer function, but for a real gas/steam turbine has a time constant of the order of seconds. This means that the drooped response contribution to damping is reduced. However, some VSM systems coupled to DC busses may be able to offer $P(s)$ with extremely small time constants, if copious energy is available at the DC bus. Examples would include systems including battery, supercapacitor or flywheel energy storage. Therefore, some VSM systems will be able to offer significant real damping output power even though it is technically delivered via "type 4" droop response, rather than type 3 "external damping".

It should also be noted that:

- There is another subtle difference between droop response and pure damping power. Natural damping power in a SM is proportional to the deviation of the rotor speed to the stator electrical frequency, both of which vary in real time, and the response is due to the difference between the two. A drooped frequency response is proportion to the frequency deviation from some (generally) static frequency setpoint, although the setpoint can be adjusted in real time.
- Within the "Synchronverter" architecture [4] [5], the rotor damping is explicitly provided by a virtual/internal damping power that is described as a droop response proportional to frequency deviation from nominal.
- A branch of grid-forming converters called VSM0H [6] [7], Power Synchronisation [8] or Droop control [5] exists in which there is no attempt to introduce an inertia term. However the converters offer a fast-acting droop (and hence damping) response which can offer large amounts of damping and robustness during frequency events, and a significant effect on frequency nadir. Such a converter is described and analysed in section 6.

4.5 Dominant Parameters defining (V)SM power response

The performance of a (V)SM during normal operation (anything but the closest faults) is defined largely by the following parameters (Figure 4-1):

- X, the primary reactance of the SM or VSM device, in pu. For a real SM, this is X'_d, the transient reactance. For a converter, this is normally considered to be the impedance of the primary filter inductor. This can be thought of as the reactance between the (virtual) rotor and (virtual) stator in a (virtual) synchronous machine.
- X_G, the additional reactance, in pu, between the (virtual) stator and a convenient grid "point of common coupling" that is to be considered.
    - Essentially the "grid stiffness" and "synchronising torque" provided by a (V)SM at a point on the HV network are defined (and can be quantified) by its rating in VA divided by $(X + X_G)$
- H, the inertia of the (V)SM, in seconds
- ζ, the damping ratio of the (virtual) rotor oscillations following a disturbance. ζ is commonly in the region of 0.25 for a SM, but can optionally be much larger for a VSM.
- Whether the damping power is "external" or "internal"/"virtual" [5]. For a SM, the damping power is inherently "external" and appears directly as a real power at the terminals. For most practical VSM schemes presented to date in literature, the damping is "internal".

- D_f, the frequency/power droop slope. Typically 4 % for a unit responding aggressively or managing frequency within an islanded network. $D_f \to \infty$ for a device which provides zero droop response, such as a renewable device operating under a maximum-power-extraction regime and zero curtailment.
- τ_P, the time constant of the drooped response (if any is available) from the prime mover / governor. For a VSM, the prime mover might be a battery or energy store attached to a DC bus and τ_P could be a matter of ms, or even considered to be ”instant”. For a pumped-hydro scheme, τ_P will be larger but still ”useful” for “fast response”. For a turbo-diesel or CCGT, τ_P could run to several seconds. For a large steam turbine, τ_P could exceed 10 seconds.

Therefore, even in a simple model of a grid-forming (V)SM there are 7 degrees of freedom – parameters that can vary between SM and VSM devices. The number of degrees of freedom can be reduced by considering that:

- X, X_G, (and therefore $(X + X_G)$) are essentially fixed by device and network hardware. In some circumstances, X for a VSM can be manipulated upwards or downwards within reason, but there are cost and filtering implications.
- In a VSM, there are constraints on available energy for inertia and droop responses, dependent on the energy storage on the DC bus. This may constrain $D_f \to \infty$ or define viable values of H. However, often $\tau_P \to 0$ in such devices, if $D_f < \infty$ is viable, and if energy can be rapidly extracted from the DC bus without collapsing it.

However, in general, if the potential for energy storage, however small, is allowed-for within a VSM, a range of different options for combinations of H, D_f, τ_P are still available. This means that, even considering that $(X + X_G)$ is not freely tunable, there are still 5 degrees of freedom to examine in any comparison of SM and VSM performance. All these 5 parameters, of which 2 describe damping within a (V)SM, have a significant impact on the stability of the (V)SM device and its interaction with the power system.

4.6 Small-signal linearised model of (V)SM

In the context of Figure 4-1, Figure 4-2 shows a simplified small-signal control diagram representing the relationship between angles and power flow for a SM or a typical VSM [9]. Several different VSM implementations have been proposed in the literature which will not have identical properties, but for the purpose of the analysis and discussion presented within this report, the generic implementation shown in Figure 4-2 is considered appropriate. In Figure 4-2, $\omega_0 = 2\pi f_0$ with f_0 set to 50 or 60 Hz. The rotor-stator angle δ_{RS} is determined through a reactive divider from δ_{RG}. It is important to split the total rotor-grid reactance into the two parts X and X_G, so that the local (V)SM rotor-stator angle δ_{RS} can be considered. This is because the damping power in a real SM is a function of the damper windings providing a squirrel-cage induction-machine torque (power) which is dependent on the slip between rotor and stator angles. Considering the slip between rotor and distant grid would be a slightly incorrect analysis. It is also useful to always be reminded that the device’s performance is not only governed by its own local impedance, but also by the grid impedances between it and other devices/loads.

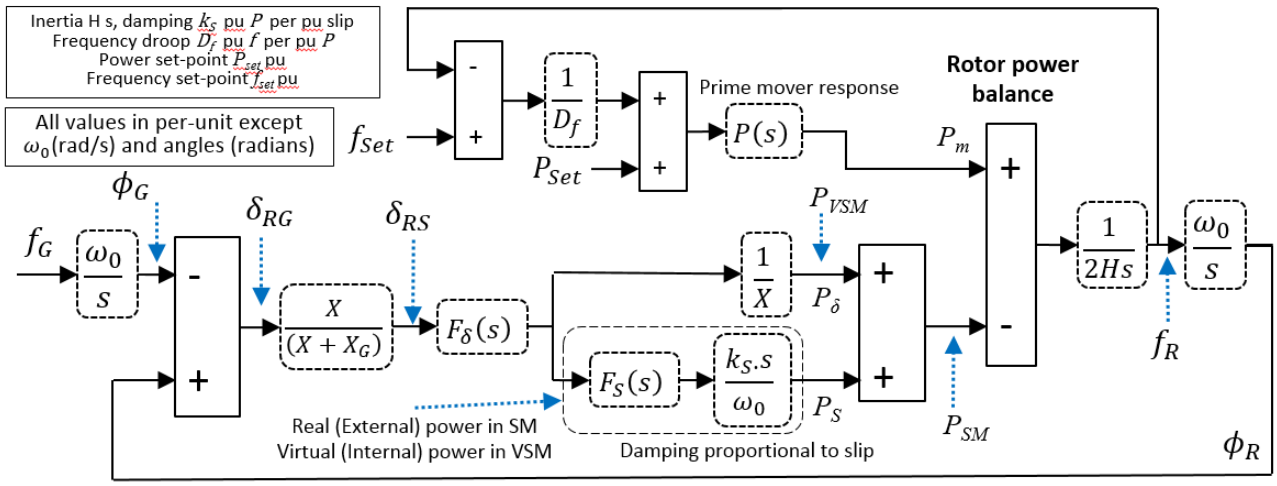

Figure 4-2 : Simplified linearised model of SM or VSM embedded within power system, assuming voltage ~1pu, frequency ~1pu, and $sin(\delta_{RS}) \approx \delta_{RS}$ [9]

4.7 External and Internal damping

The power output from a real SM consists of two parts: The power P_δ due to δ_{RS} across X

$$P_\delta = \frac{\delta_{RS}}{X} \tag{10}$$

plus the damping power P_S due to the slip of ϕ_R against ϕ_S, i.e.

$$P_S = \frac{k_S(d\delta_{RS}/dt)}{\omega_0} F_\delta(s)\, F_S(s) \tag{11}$$

The total power output at the stator for a real SM is given by the sum of these two powers:

$$P_{SM} = P_\delta + P_S \tag{12}$$

A positive P_{SM} acts to decelerate the SM rotor. Meanwhile a governor loop including a droop slope D_f (pu frequency per pu power) and prime mover response $P(s)$ acts to adjust the power output in a power-sharing scenario. The inertia H (in s) determines the rotor acceleration from the power balance, and this in turn determines the rotor angle trajectory, which closes the loop.

Within a typical VSM, using a control methodology similar to Figure 4-2 there is a difference in the actual electrical power output, compared to a real SM. While the controller can calculate the damping power term due to slip, the actual power flow across the reactor X is only due to δ_{RS}, so the actual electrical power output at the virtual stator is given only by:

$$P_{VSM} = P_\delta \tag{13}$$

Thus when a controller equivalent to Figure 4-2 is used to create a VSM, its damping can be said to be “internal” or “virtual” [5] [3], i.e. the damping power is internal only, and does not directly appear at the (virtual) stator terminals. Such a device could be called “VSM_{Int}”.

By contrast, a real SM can be said to possess "external" damping, since the damping power appears directly as a real power at the stator terminals. It might be possible to modify a VSM algorithm so that it behaved as "VSM_{Ext}", i.e. with external damping, so that the damping power genuinely appeared at the (virtual) stator terminals by (12). A controller to achieve this using converter hardware is not presented here, and it would require significant non-trivial adjustment and augmentation compared to Figure 4-2, due to the need to force a slip-related power flow contribution across a filter inductor which does not naturally provide such behaviour, while still maintaining a stable closed loop with << 50 Hz bandwith [9]. However, its possibility is considered as VSM_{Ext} within this report, and its behaviour predicted.

In some later plots the power P_{SExt} is plotted, to represent the real slip-related external damping power. This is:

$$\begin{aligned} &P_{SExt} = P_S \text{ for a real SM or } VSM_{Ext} \\ &P_{SExt} = 0 \text{ for a } VSM_{Int} \end{aligned} \tag{14}$$

4.8 Practical rationalisation of simplified model with reality

A model such as Figure 4-2 can provide reasonable phasor-based emulations of (V)SM responses to events. However it cannot represent the most dynamic effects such as decaying DC currents and intra-machine magnetic effects. Rationalising the predictions of the simplified model of Figure 4-2 against a MATLAB® Simulink model of a wound-rotor machine with default parameters, and also considering the practicalities of implementing a VSM algorithm, lead to the following assumptions in the approach which follows:

A boxcar filter $F_\delta(s)$ with a time length $\tau_\delta = 1/f_0$ is applied to the signal δ_{RS}, i.e. [10]

$$F_\delta(s) = \frac{1}{s\tau_\delta}(1 - e^{-s\tau_\delta}) \tag{15}$$

In reality this relates to the fact that stator currents do not change instantly, even following a discrete phase step at ϕ_G or ϕ_S, due to the system and device inductances. In a VSM such a filter is also a useful practical addition, placing filter zeros at all $\mathbb{N}f_0$, reducing noise and removing harmonic power-ripple feedback components.

Similarly, it is found that insertion of an additional boxcar filter $F_S(s)$ with a time length $\tau_S = 4/f_0$ is necessary to provide a reasonable approximation of external slip-related damping power output from a real SM when subjected to a grid phase step. A physical interpretation of this could be that it takes time to establish the low-frequency currents within the damper windings, although this has not been fully investigated. Within a VSM algorithm, some equivalent filtering here is also desirable to keep the damping path transfer function "proper", i.e. with at least as many poles as zeros. However, within a VSM, applying a lower value such as $\tau_S = 1/f_0$ can be beneficial to increase the accuracy of the subsequent predictions in (20)-(22), especially as ζ is increased towards 1, since (20)-(22) assume $F_\delta(s) \approx 1$ and $F_S(s) \approx 1$.

In reality the prime mover response $P(s)$ may be a complicated transfer function, due to both governor controls and prime mover hardware. In the following analysis, a simple filter is assumed:

$$P(s) = \frac{1}{(1 + \tau_P s)} \tag{16}$$

Typical values for a steam turbine could be 10 s or more. For a VSM, τ_P can be in the low ms range depending on the energy source coupled to the DC bus.

The model of Figure 4-2 can easily be implemented in (for example) Simulink, to produce time-domain traces for various grid phase angle trajectories representing phase steps and/or ROCOF events.

4.9 Closed-loop response of isolated (V)SM without prime mover, i.e. synchronous condensor or (V)SM with constant Pm

In parallel with simple time-domain simulations of Figure 4-2, a more analytical approach pays dividends. The response of local rotor angle ϕ_R to HV grid angle ϕ_G in the context of Figure 4-1 and Figure 4-2 can be written as shown in (17).

$$\frac{\phi_R}{\phi_G} = \frac{\left(\frac{\omega_0}{s}\right)\left(\frac{X}{(X+X_G)}\right)F_\delta(s)\left\{\frac{1}{X}+F_S(s)\frac{k_S\cdot s}{\omega_0}\right\}}{\left(2Hs+\left[\left(\frac{\omega_0}{s}\right)\left(\frac{X}{(X+X_G)}\right)F_\delta(s)\left\{\frac{1}{X}+F_S(s)\frac{k_S\cdot s}{\omega_0}\right\}\right]+\frac{P(s)}{D_f}\right)} \tag{17}$$

In its full form this is difficult to analyse or understand. However, if the simplifications are made that $F_\delta(s) \approx 1$ and $F_S(s) \approx 1$ (both reasonably approximate for analysis << 50 Hz), and in the absence of a prime mover response ($D_f \to \infty$), then (17) reduces to:

$$\frac{\phi_R}{\phi_G} \approx \frac{\left(\frac{k_sX}{2H(X+X_G)}s\right)+\left(\frac{\omega_0}{2H(X+X_G)}\right)}{\left(s^2+\frac{k_sX}{2H(X+X_G)}s+\frac{\omega_0}{2H(X+X_G)}\right)} \tag{18}$$

This represents a 2nd-order bandpass filter plus a 2nd-order lowpass filter.

The denominator of these terms reveals a lot about the 2nd order transfer function behaviour [The full time-domain response, equivalent to (18) is derived in section 10 (Appendix A) for reference].

$$s^2+\frac{k_sX}{2H(X+X_G)}s+\frac{\omega_0}{2H(X+X_G)} \Leftrightarrow s^2+2\zeta\omega_n s+\omega_n^2 \tag{19}$$

Where ζ is the damping ratio ($\zeta = 1$ corresponds to critical damping), and ω_n is the undamped resonant frequency in rads/s. Therefore the device will respond to phase steps on ϕ_G with decaying sinusoidal ϕ_R with:

$$\text{undamped resonance at } \omega_n = \sqrt{\frac{\omega_0}{2H(X+X_G)}} \tag{20}$$

$$\text{damping ratio } \zeta = \frac{k_sX}{4H\omega_n(X+X_G)} \tag{21}$$

$$\text{damped natural resonance at } \omega_d = \omega_n\sqrt{(1-\zeta^2)} \tag{22}$$

(20) and (21) can also be re-manipulated to reveal the following relationships, any of which can be used when they are convenient or useful:

$$k_s = \frac{4\zeta H\omega_n(X+X_G)}{X} \quad \text{(inverse of (21))} \tag{23}$$

$$\zeta = \frac{k_sX}{2\sqrt{2H\omega_0(X+X_G)}} \quad \text{(20) \& (21)} \tag{24}$$

$$k_s = \frac{2\zeta\sqrt{2H\omega_0(X+X_G)}}{X} \quad \text{(inverse of (24))} \tag{25}$$

Equation (17) for a (V)SM also allows the output power response to be determined, for a grid frequency disturbance f_g (Figure 4-2).

For a real SM or VSM_{Ext}:

$$\left(\frac{P_{SM}\,or\,P_{VSM_{Ext}}}{f_g}\right) = \frac{\left(\frac{X}{(X+X_G)}\right)F_\delta(s)\left\{\frac{1}{X}+F_S(s)\frac{k_S\cdot s}{\omega_0}\right\}(\phi_R-\phi_G)}{\left(\frac{\phi_G}{\left(\frac{\omega_0}{s}\right)}\right)} \tag{26}$$

which manipulates to:

$$\left(\frac{P_{SM}\,or\,P_{VSM_{Ext}}}{f_g}\right) = \left(\frac{\omega_0}{s}\right)\left(\frac{X}{(X+X_G)}\right)F_\delta(s)\left\{\frac{1}{X}+F_S(s)\frac{k_S\cdot s}{\omega_0}\right\}\left(\frac{\phi_R}{\phi_G}-1\right) \tag{27}$$

and similarly for a VSM_{Int}:

$$\left(\frac{P_{VSM_{Int}}}{f_g}\right) = \left(\frac{\omega_0}{s}\right)\left(\frac{X}{(X+X_G)}\right)F_\delta(s)\left\{\frac{1}{X}\right\}\left(\frac{\phi_R}{\phi_G}-1\right) \tag{28}$$

In both (27) & (28), the value ϕ_R/ϕ_G is obtained via (17).

Equations (27) & (28) are extremely useful for evaluating the Network Frequency Perturbation (NFP) plot, analysed in section 8. These equations define the active-power responses of (V)SM devices to changes in grid frequency and phase.

4.10 (V)SM analogy with “mass on a spring”

The practical significance of (18)-(25) is that, ignoring the effects of prime mover torque adjustments i.e. “Type 4” power, the (V)SM rotor behaves like a mass on a spring (in zero gravity) with a damper. The analogy is presented briefly in Figure 4-3 and Table 4-1. The inertial rotor mass is connected via a spring (the reciprocal of transient impedance X'_d) and damper to the stator electrical angle (the left hand of Figure 4-3 and Table 4-1). This is analogous to a mass on a spring in zero gravity (the right hand of Figure 4-3 and Table 4-1). Neglecting the extra complications of grid impedance X_G, the equations of motion for these two analogous systems are derived and summarised in Appendix B, section 11, showing the similarity in the forms, and expressions for resonant frequency and damping.

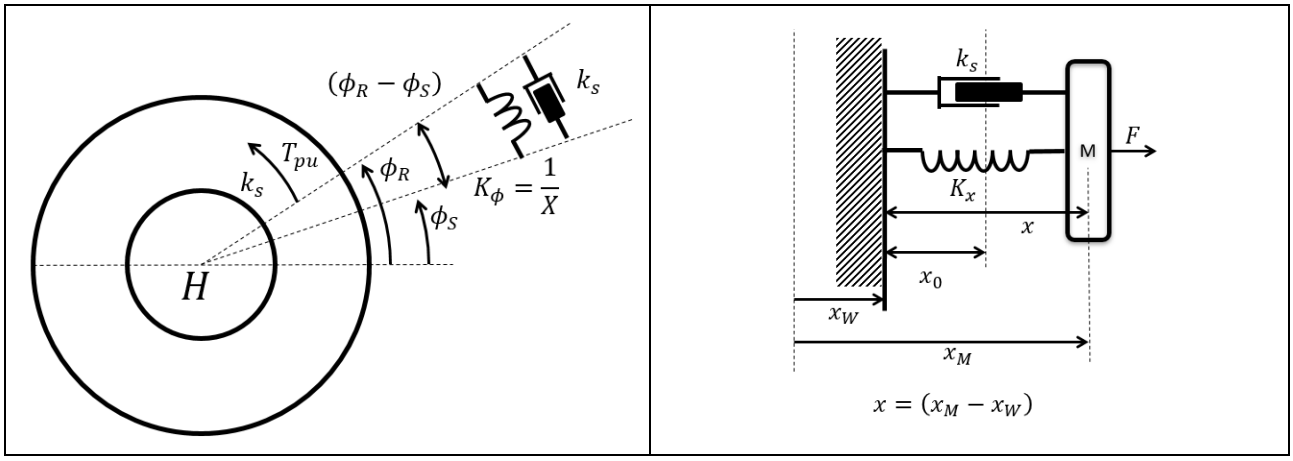

Figure 4-3 : Analogy between (V)SM rotor (left) and "mass on a spring in zero gravity" (right)

(V)SM rotor			Mass on a spring		
$\boldsymbol{T_{pu}}$	Torque	pu	F	Force	N
ϕ_R	Rotor angle	rad	x_M	Mass position	m
ϕ_S	Stator electrical angle	rad	x_W	Wall position	m
H	pu inertia	s	M	Mass	kg
$K_\phi = \frac{1}{X}$	"Spring stiffness" Reciprocal of transient impedance	1/pu	K_x	Spring stiffness	N/m
k_s	damping	pu per pu slip	k_s	damping	Ns/m
ω_0	Nominal speed	rad/s			

Table 4-1 : Analogy between (V)SM rotor (left) and "mass on a spring in zero gravity" (right)

When considering the relative motion of the rotor and stator angles, the analogy with the mass-on-a-spring (MOAS) is extremely helpful. When the (V)SM is connected to a stiff grid, it is equivalent to the wall and its position x_W (Figure 4-3) being rigid and fixed. The mass (or rotor) can oscillate against it. In the "potted" scenarios of grid phase angle to be presented in section 5, the analogy is that the wall is solid and stiff, but is itself being moved by a fixed mechanism following an absolutely predetermined ("potted") trajectory, which can excite motion and resonances in the mass/rotor.

In the other extreme, if the (V)SM is completely islanded from other power sources, then the equivalent analogy is that the wall is paper-thin, with zero mass, and is free to move. In this scenario the wall will move to suit the mass, and it is impossible for the mass (or rotor) to resonate with it.

In the middle of these extremes lie the more complex scenarios of multi-generator systems. These correspond to multiple MOAS connected together via point(s) of common coupling. The motion can be very complex, involving multiple damped resonances. One example which is easier to understand is that if one lightly-damped system is coupled to a more heavily-damped system, the better-damped system can help to dampen the resonance on the more lightly-damped system. A good example of this is shown later in section 7.1, in which a critically-damped VSM is shown to eliminate rotor swings in a SM when they are power-sharing.

4.11 Choice of damping ratio and damping strategy

Given a choice of inertia H, damping ratio ζ, and knowing the reactances X and X_G, the above equations allow k_s to be configured within the shown VSM algorithm. While ζ in a real SM installation is typically in the region of 0.25, being limited by practical and efficiency constraints in the machine design, ζ could (for example) be chosen to be 1.0 in a VSM, leading to response which is roughly "critically" damped, and reducing the chances of sub-synchronous oscillation with other network equipment.

All the above analysis raises the following questions:

1) If it could be implemented, is there a case for adding the extra difficulty and complexity of providing external damping with VSM_{Ext}, compared to the base case of implementing VSM_{Int}?
2) Are there any positive or negative consequences of implementing values of damping ratio ζ towards (or above) 1?

4.12 Choice of inertia and droop response

Similarly, within a VSM device, the inertia H, droop slope D_f and prime mover response time τ_P may all be selectable via software, and indeed may quite viably be tuned online via real-time adjustments. While there will be constraints on the viable ranges of these three parameter settings due to the connected hardware systems, there may still be many permutations of the available settings of the 4 values, even for systems with relatively little stored energy. This especially applies if the prime mover (e.g. wind turbine) is being operated curtailed, i.e. backed off from maximum-power-tracking, so that inertia and drooped frequency-response services can be offered without significant energy storage.

5 Time-domain examples of (V)SM device responses to HV grid phase/frequency events

In this section, time-domain traces of power response are shown, using the simplified linearised model of Figure 4-2, to various "potted" grid scenarios at HV, consisting of idealised and predefined phase steps/jumps, linear frequency ramps (constant ROCOF), and combinations of the phase steps with frequency ramps.

In the pages and plots which follow, there are 8 traces on each plot, representing 8 different (V)SM configurations of device.

There are 2 groups of 8 devices, making a total of 16 devices analysed.

- Group A equips the SM units with D_f=4 % droop slope, and τ_P=4 s to represent a gas turbine or hydro plant. The droop slope on the VSM devices $D_f \longrightarrow \infty$ making the VSM (virtual) governor/prime-movers and P_m unresponsive to steady-state frequency changes. In this case, the SMs are (alone) responsible for maintaining frequency towards nominal at steady-state, while the VSM units provide support only during the dynamic phase steps and ROCOF ramps.
- Group B equips every device with a D_f=4 % droop slope. The SM devices represent steam turbines with τ_P=10 s, while the VSM devices have τ_P=1 s. In this case, both SM and VSM devices are responsible for maintaining frequency during steady-state operation. However, the VSM devices can respond much faster via their (virtual) governors and thereby despatch power from their DC busses much faster than the steam turbines can provide additional power to the SM devices .

In detail, Table 5-1 lists the configurations for each group of 8 test devices:

			Common to both groups		**Group A**	**Group B**
	Device 1 (Plot trace 1)	SM (steam turbine)	X=X$_d$'=0.3 pu X_G=0.15 pu ζ = 0.25 τ_S = 0.08	H = 4 s	D_f=4 % τ_P=4 s	D_f=4 % τ_P=10 s
	Device 2 (Plot trace 2)			H = 8 s		
	Device 3 (Plot trace 3)	VSM$_{Int}$	X=X$_d$'=0.07 pu X_G=0.22 pu	H = 4 s, ζ = 0.25 τ_S = 0.02	$D_f \longrightarrow \infty$	D_f=4 % τ_P=1 s
	Device 4 (Plot trace 4)			H = 8 s, ζ = 0.25 τ_S = 0.02		
	Device 5 (Plot trace 5)			H = 4 s, ζ = 1 τ_S = 0.02		
	Device 6 (Plot trace 6)			H = 8 s, ζ = 1 τ_S = 0.02		
	Device 7 (Plot trace 7)	VSM$_{Ext}$		H = 4 s, ζ = 1 (External) τ_S = 0.02		
	Device 8 (Plot trace 8)			H = 4 s' ζ = 0.25 (External) τ_S = 0.08		

Table 5-1 : Group A and Group B device configurations

Clearly, there are many other permutations of device design which could be analysed. The 16 devices in Table 5-1 attempt to give an overview, while limiting the number of plots and traces to a reasonable quantity.

On each page are shown 10 plots. Group A devices (5 plots) are shown on the left, and Group B devices (5 plots) on the right. The five plots shown in each column (for each Group) on each page are:

$P_{(V)SM}$	The total real transient power output (pu) of the device, from (12) or (13) as appropriate.
P_δ	The component of the real transient power output (pu) due to δ_{RS} across reactance X in a (V)SM, assuming voltage is 1pu. For a VSM$_{Int}$ $P_\delta = P_{(V)SM}$, the total transient power output.
P_{SExt}	Damping power (real/external) which is equal to P_S for a SM or VSM$_{Ext}$, but zero for a VSM$_{Int}$
$\int P_{(V)SM}dt$	The cumulative energy transient following the event, i.e. the integral of $P_{(V)SM}$ against time, in pu.seconds
$\Delta f = f_R f_0$	The frequency deviation or each (V)SM device's (virtual) rotor, in Hz. f_R (Figure 4-2) is in pu so to obtain the Hz value the plot shows $f_R f_0$

Table 5-2 : 5 Plots shown for each Group on each page

5.1 Response to phase steps

The first scenario to be examined is a mid-range negative phase step/jump of -5° at HV (see Figure 4-1). This is not as large as phase steps regularly seen on the HV grid due to (for example) lightning strikes causing transmission line breakers to open and reclose, but nevertheless the -5° step/jump is enough to draw a significant power transient from all (V)SM devices connected through reasonable pu reactances/impedances.

In this scenario the phase step is isolated, and there is no accompanying underlying frequency slide. Therefore, unless a drooped governor and prime mover response is extremely fast-acting, such "type 4" [3] droop responses play little part in the scenario. The devices are all effectively operating as prime-mover-less synchronous condensers in this scenario, in their response to the transient.

By contrast, the component P_δ plays a large role, since the phase step immediately draws a significant -5° angle across $(X + X_G)$ (Figure 4-1) and a proportion of this across the local (V)SM reactance X, causing a relatively large, and "instantaneous" (within <<20 ms) power transient by (9). Therefore the "type 2" [3] phase step/jump power (dominant) and "type 1" inertia power (to a lesser extent) power play a large part.

Figure 5-1 shows the results on a relatively wide scale, which masks much of the detail. Detail is examined subsequently in Figure 5-2.

The main point of note from Figure 5-1 is that the output power transient of the VSM$_{Ext}$ devices with ζ=1 (Devices A7 & B7) surpasses 1 pu, and in fact extends to 2.75 pu. This shows that if a damping ratio toward 1.0 is desirable, then it could be counter-productive to also implement external damping in the converter as VSM$_{Ext}$, since it can easily push the converter into overcurrent, leading to current-clipping and negation of any apparent benefit, for only mid-range phase-step scenarios. VSM$_{Ext}$ is more viable during phase steps if the damping is lowered to ζ=0.25, commensurate with the SM (i.e. Devices A8 & B8), and τ_S is increased to $4/f_0$ (80ms), which brings the peak power transient into line with a real SM. This, however, re-introduces the decaying rotor oscillations that a real SM has.

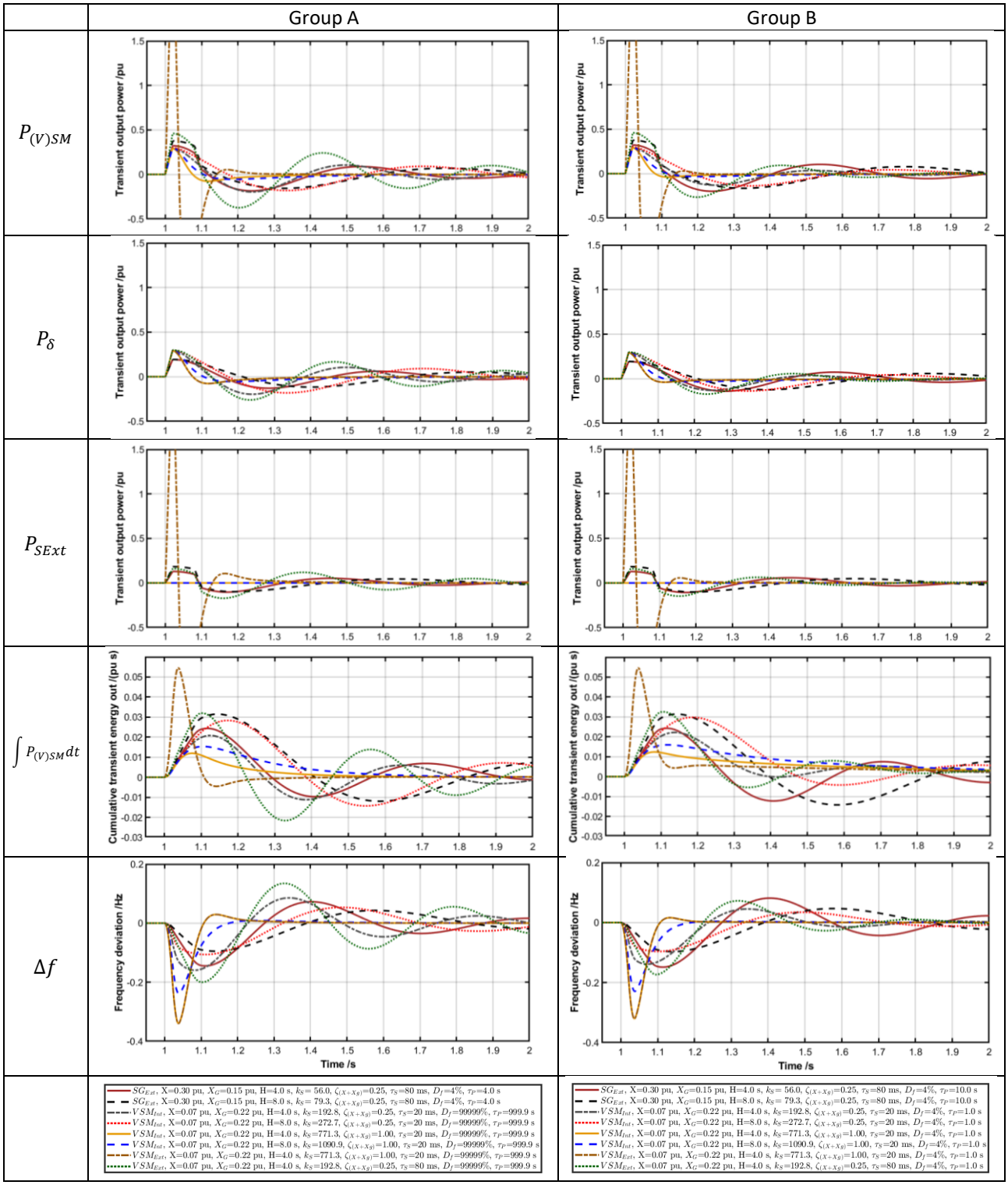

Figure 5-1 : Responses of Group A & B devices to a -5° phase step/jump at HV (Figure 4-1). Wide view. See Figure 5-2 for zoom

The other point of note from Figure 5-1 is that traditional SM, and the VSM devices with ζ=0.25 (Devices A/B 1-4 & 8), all show the familiar post-event decaying rotor and power oscillation swings against the "infinite bus" at HV. Meanwhile, the critically-damped VSM devices A/B 5-7 do not result in rotor or power swings.

Figure 5-2 shows a zoomed-in version of Figure 5-1 showing just the first 200ms of the transient, on the same y scales. This allows the transient performances of the 8 devices in each of the 2 Groups to be better compared.

Apart from the VSM_{Ext} device with critical damping (Device A/B 7), that attempts to make an unviably large response due to external damping, the total real power immediately drawn from the other devices (A/B 1-6 & 8) by the phase step is not dissimilar across the devices, at 0.3-0.4 pu. P_δ is larger for the VSM devices, due to their slightly lower $(X + X_G)$ in the scenario presented (and hence their higher grid stiffness K_ϕ from (6)). However the SM and VSM_{Ext} devices have the external damping power P_S added to the actual power output, causing them to have a higher total transient peak power contribution $P_{(V)SM}$ than the VSM_{Int} devices.

The peak power is independent of the inertia H, but the time for the power to settle back to zero is doubled, if H is doubled. The transient energy pulses are thus doubled if H is doubled, although the cumulative energy settles back towards zero as post-event time passes, unless the droop slope and (virtual) prime mover response are aggressive enough to respond significantly to the brief event. This is unlikely following an isolated phase step unless τ_P is extremely small.

In this phase-step scenario, arguably the VSM_{Int} devices with ζ=1 provide a useful and practical response, having a fast rise-time to an appropriate peak value, and thereafter being highly damped. However, if the devices were already operating towards 1 pu output power, they could be pushed towards current limit.

On the other hand, the initial power transient infeed is more sustained for VSM_{Int} if damping ζ is lowered to 0.25, i.e. for devices A/B 3 & 4. The lower damping means that the rotor on those VSM_{Int} devices A/B 3 & 4 slow down less than the ζ=1 VSM_{Int} devices A/B 5 & 6, leading to a more sustained power output and higher energy output during the "first swing". The penalty, however, is that that extra energy is ultimately drawn back again from the grid during the decaying rotor oscillations that are introduced with ζ<1. Since governors and prime movers are generally (and in these scenarios, but not necessarily in a VSM) too slow to act on a phase step, the devices are all effectively operating as prime-mover-less synchronous condensers in this scenario, and the cumulative transient energy outputs (the 4th plot of the 5, showing $\int P_{(V)SM}dt$), eventually return to almost zero after the transient responses finally finish, for all devices.

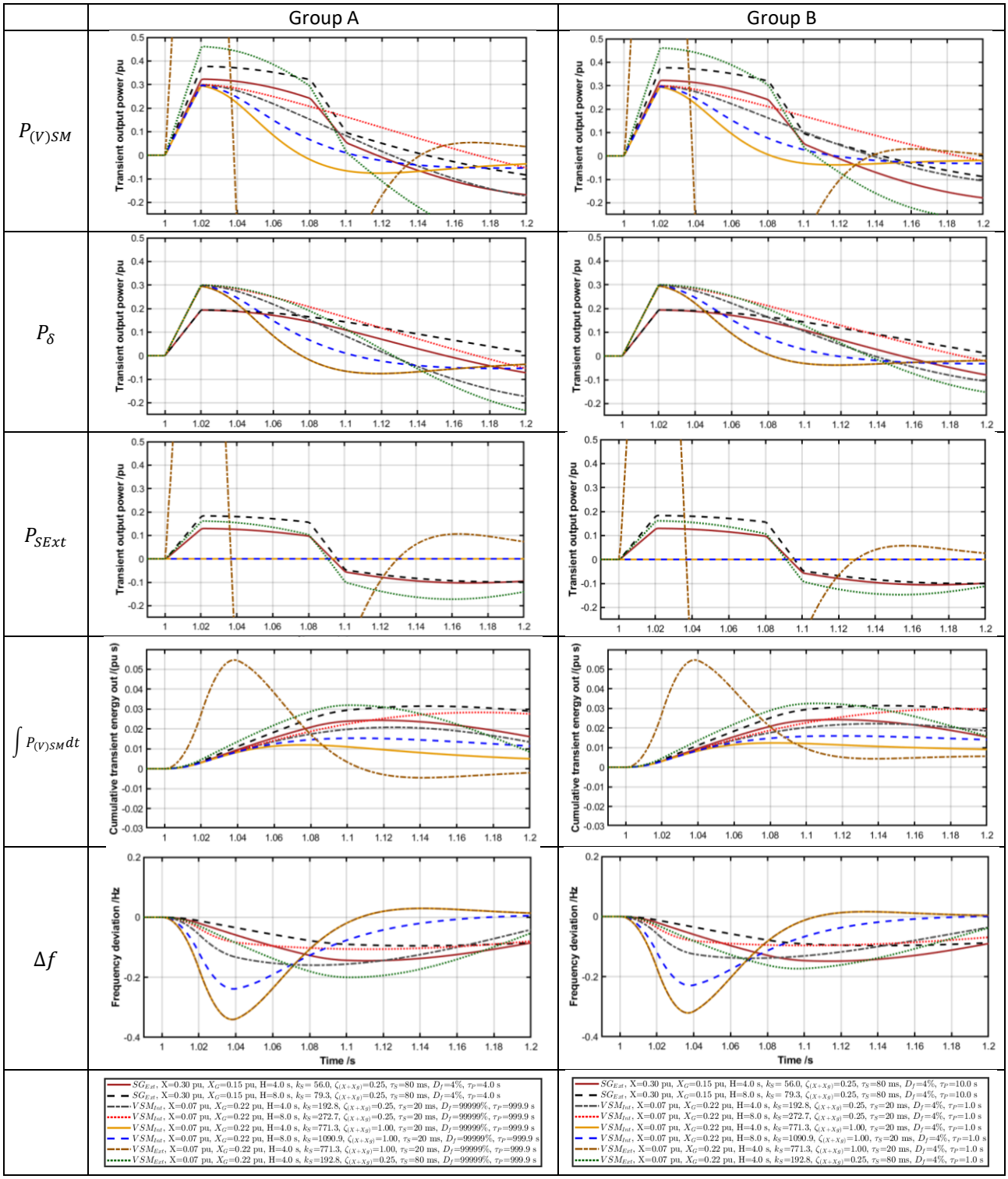

Figure 5-2 : Responses of Group A & B devices to a -5° phase step/jump at HV (Figure 4-1). Zoomed from Figure 5-1

5.1.1 Summary conclusions for phase steps/jumps

- The power response ramps rapidly to a peak within 20ms of the step/jump
- The dominant peak power output magnitude is inversely proportional to the total device-to-grid impedance, and is independent of inertia H
- The power response of real SM and VSM_{Ext} is further augmented with external damping power. For conventional levels of damping the external damping power accounts for approximately one third of the initial peak power output
- If VSM_{Ext} was implemented, damping would have to be restricted to conventional levels, otherwise the damping power required would often cause overcurrent clipping within the VSM_{Ext} device, counteracting any potential beneficial effect.
- In VSM_{Int} is used, it allows damping to be increased to critical with ζ=1, without any increased risk of over-current clipping in the converter. This provides a much more damped response, without subsequent rotor/power swings.
- Use of conventional damping levels with ζ<1 allows the initial peak power transient on the "1st swing" to be sustained for slightly longer. However, this is at the expense of adding decaying rotor/power oscillations.
- Increasing the inertia also increases the duration of the initial "1st swing" power output proportionately, and the energy in the "1st swing".
- For all devices in phase step/jump scenarios, with the exception VSM devices that can make an extremely fast droop response, the drooped prime mover response is too slow to have any significant impact on power response to a phase step/jump. Therefore, for most devices, the transient responses to phase steps/jumps can be effectively considered as if the devices were operating as synchronous condensers. By the time the event response finally finishes, the total energy infeed from every device is therefore approximately zero.
- For all VSM devices, large close-in phase steps can push a converter towards/into current clipping, depending on the magnitude of the phase step, device-event impedance, and the pre-event operating powers (active and reactive) of the converter.

5.2 Response to constant-ROCOF frequency ramp

While grid phase steps cause a very rapid power flow from/to a SM or VSM, a frequency ramp at the HV grid causes a much more gradual power flow change, since the angles δ_{RG} and δ_{RS} initially deviate gradually on a parabolic trajectory against time, i.e.

$$\Delta\delta_{RG} = -\int 360 \cdot ROCOF \cdot t \cdot dt \quad = -180 \cdot ROCOF \cdot t^2 \tag{29}$$

Such a scenario is typical for a device that is electrically distant from the source of the event (e.g. sudden loss of infeed). Taking the same designs of SM, VSM_{Int}, and VSM_{Ext} devices (Table 5-1), and exposing them to a -0.5 Hz/s HV grid ROCOF for 2 seconds leads to the response transients shown in Figure 5-3 (whole 2-second ramp) and Figure 5-4 (zoom on the first ½ second of the ramp). The rows of plots on each page/figure show the measurands listed in Table 5-2.

The "expected" steady-state power outputs during this scenario (once the ramp is established) would be 0.08 pu and 0.16 pu for the H = 4 and H= 8 devices respectively, by the over-simplistic but commonly-applied (2):

$$P_{(V)SM} = -2H \cdot \frac{ROCOF}{f_0} \tag{30}$$

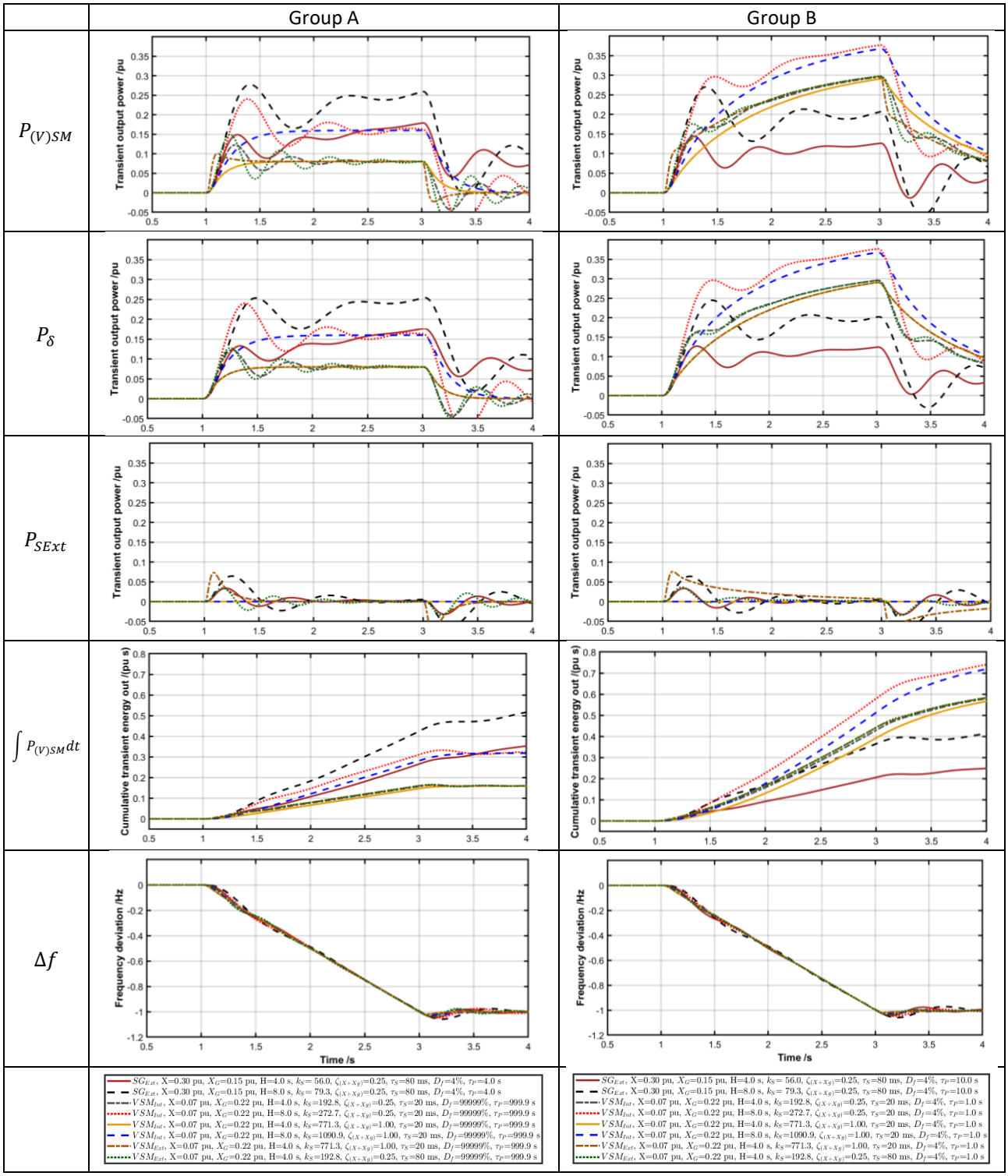

Figure 5-3 : Responses of Group A & B devices to a -0.5 Hz/s ROCOF at HV (Figure 4-1), Wide view. See Figure 5-4 for zoom

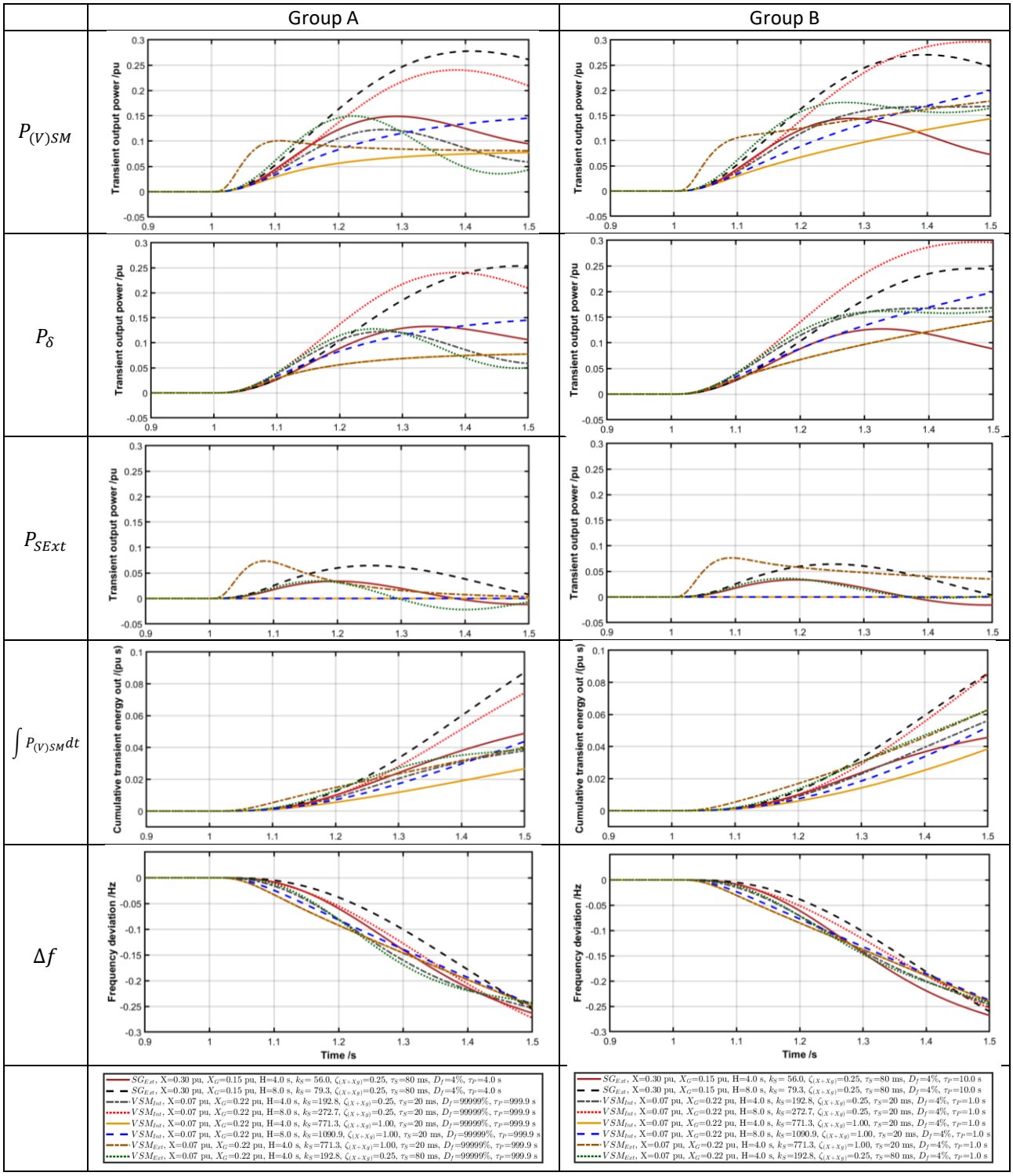

Figure 5-4 : Responses of Group A & B devices to a -0.5 Hz/s ROCOF at HV (Figure 4-1), Zoomed from Figure 5-3

5.2.1 Summary conclusions for constant-ROCOF frequency ramp

- Similarly to a phase step/jump scenario, the largest actual power flows are due to the P_δ component, via the "Type 1" inertia power [3]
- The real external damping power P_{SExt} (which is only non-zero for SM and VSM_{Ext} devices) has a smaller magnitude then P_δ. However, it does play a role in accelerating the real power infeed on SM and VSM_{Ext} devices, giving them a slightly faster power infeed than equivalently-damped VSM_{Int} devices.
- For SM and VSM_{Ext}, increasing the damping ratio ζ increases the initial rate of power increase, and also decreases the level of decaying rotor oscillations after the start of the event.
- For VSM_{Int}, increasing the damping ratio ζ **decreases** the initial rate of power increase, but still decreases the level of decaying rotor oscillations after the start of the event.
- The effect of droop-related frequency response through governor and prime-mover action ("Type 4" power [3]) plays a much larger part in ROCOF events than it does in phase step/jump events.
    - In Group A, the SM prime movers have a response time constant of τ_P=4 s, emulating gas turbines. This allows them to increase their infeed noticeably beyond the 0.08 pu and 0.16 pu inertial contribution for the H = 4 and H= 8 devices respectively. In this case (Figure 5-3) the prime mover can add a further ~0.08 pu power contribution by the time 2 seconds have elapsed after the event start, an equivalent power to the H = 4 contribution. In Group A, the VSM devices have no primary frequency response configured, so their response is purely due to inertia.
    - In Group B, the SM prime movers have a response time constant of τ_P=10 s, emulating steam turbines. By contrast the VSM devices have a much faster droop response time constant of τ_P=1 s. This means they can deliver a a further ~0.2 pu power contribution by the time 2 seconds have elapsed after the event start, an equivalent power to an H = 10 contribution.
- Essentially, the VSM_{Int} devices with $\zeta = 1$ will feed in slightly less power than a traditional SM (with equivalent H) within the first 500 ms of such a "potted" constant-ROCOF event, unless $\tau_P < 0.5$ s. The power feed-in rate can be increased by lowering ζ (at the expense of rotor oscillations) or by moving to a VSM_{Ext} control strategy, or by decreasing D_f for a more aggressive droop response, or by reducing τ_P. The possibility for offering drooped responses from VSM_{Int} or VSM_{Ext} converters (potentially with $\tau_P < 0.5$ s), in conjunction with increased damping, means that the VSM converters could actually play a bigger role in managing frequency nadir than a traditional SM. Indeed, if the local energy available supported $\tau_P < 0.5$ s, then the power ramp rate of VSM_{Int} might match that of an SM with external damping, by substituting very-fast droop response power in place of external damping power – the two types both offering damping (see section 4.4).

5.3 Response to phase step/jump coincident with constant-ROCOF frequency ramp

When a (V)SM device is close to a large disconnection of infeed, the event appears to the device as the combination of a negative-going phase step/jump, combined with a negative ROCOF event, assuming that the loss-of-infeed is large enough to cause a system-wide frequency drop, considering all generation units.

Essentially the responses of the devices (Table 5-1), is the combination of that already shown in sections 5.1 and 5.2. The responses are summarised in Figure 5-5 but few new conclusions need to be drawn, since most already appear in the commentary with sections 5.1 and 5.2.

However, one point of note in Figure 5-5 is that:

- According to the “potted” theoretical situation where a negative-going phase step/jump coincides with the beginning of a linear frequency ramp (falling), the models for all (V)SM devices predict an initial thump of power output, followed by a “lull” about 250 ms after the phase step, before the inertial and droop-response power subsequently increases. This power profile, using the model of Figure 4-1, assumes that there is some infinite bus within the system against which the (V)SM devices can “swing”. While the model used is reasonably accurate for this “potted” scenario, it needs to be appreciated that when there is no infinite bus, and all the power is provided by a collection of interlinked (V)SM units and other devices, the power transients may not contain this “lull”. Section 7 investigates this further and shows that in real power-sharing scenarios lacking any “infinite bus”, the “lull” does not exist coincidentally at all devices.

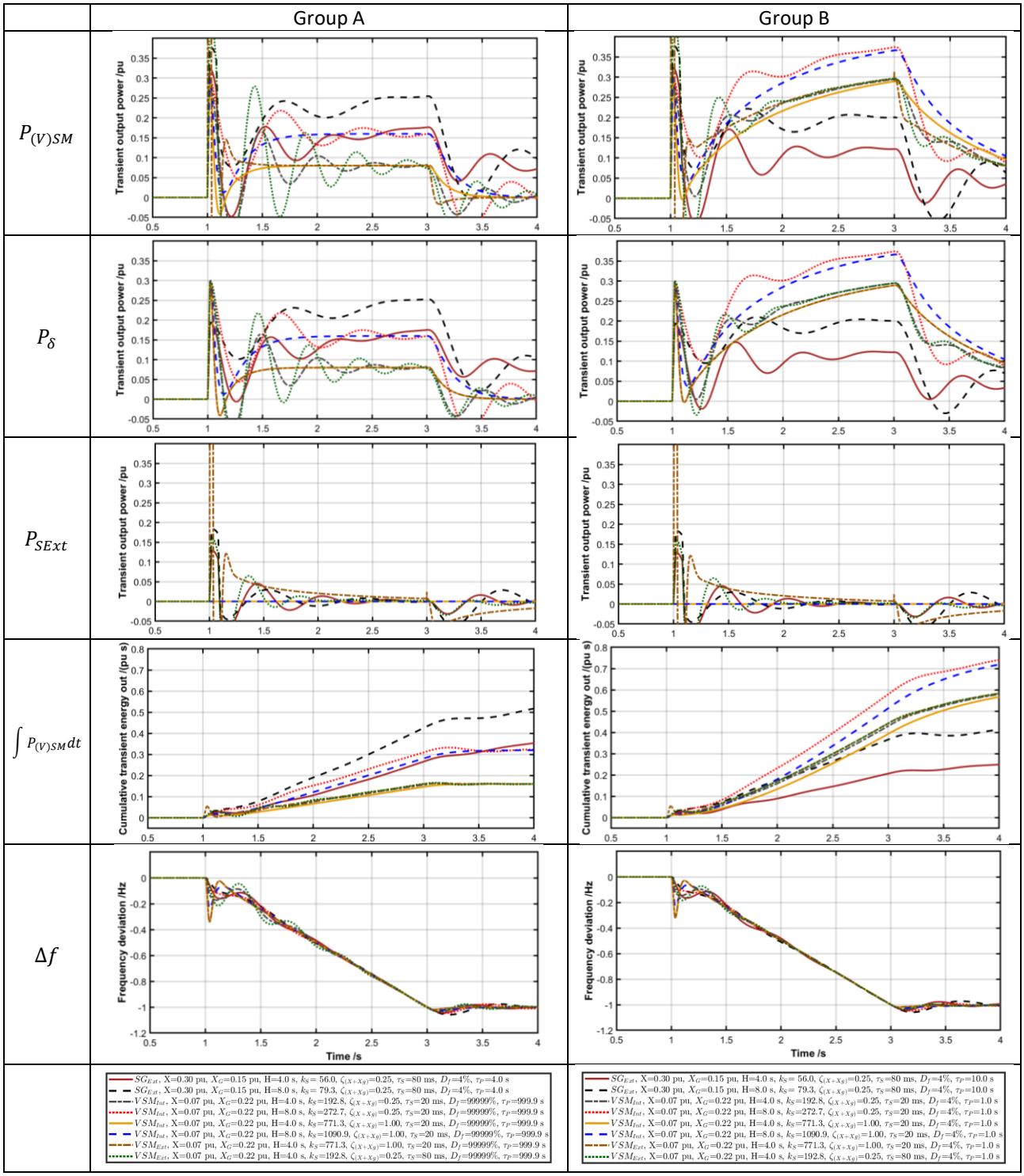

Figure 5-5 : Responses of Group A & B devices to a -5° phase step/jump and -0.5 Hz/s ROCOF at HV (Figure 4-1)

6 An inertia-less grid forming option VSM0H, and time-domain examples of VSM0H responses to HV grid phase/frequency events

The responses to the "potted" ROCOF ramp scenario in section 5.2 suggest that drooped response proportional to $(f_0 - f)$ can provide a significant response during ROCOF ramps, especially if the droop response time constant is small enough (approximately $\tau_P < 0.5$ s). It can never be exactly equivalent to an inertial response, being proportionate to Δf rather than df/dt, but its contribution can be extremely useful in terms of containing frequency nadir. Section 4.4 also discussed and showed how such a drooped response power can be equivalent to a damping power if τ_P is small.

There is a branch of grid-forming converters which makes no deliberate attempt to emulate inertia, but instead operates on a strict droop slope of power response to rotor frequency, with $\tau_P \ll 0.5$ s. Such converter(s) have several names in literature, being called VSM0H [6] [7], Power Synchronisation [8] or Droop control [5]. Their overall control bandwidths are typically < 50 Hz (and hence bandwidth-limited) but not necessarily < 5 Hz as suggested in [1]. Such converters are able to function extremely capably as grid-forming devices and provide large amounts of damping. Essentially their whole dynamic response is damping power. Although there is no deliberate attempt in such converters to achieve VSM_{Ext} behaviour, the bandwidth-limited damping power is effectively external (and real), since the drooped response is via real power. Therefore there is external damping, bandwidth-limited to ~15 Hz.

Because, in a VSM0H converter, $H \to 0$, the controller cannot be modelled by Figure 4-2 nor the equations that follow from it. There is no rotor resonance nor damping ratio to be calculated.

A typical simplified linearised control diagram for such a VSM0H converter is shown below in Figure 6-1 [6]. Essentially this controller simply measures it's active power output, filters the measurement using (in this example) a single-cycle boxcar (moving average) filter with a time length of ~20 ms and latency of ~10 ms, and then applies the resulting frequency, obtained from the droop slope, to the virtual rotor at the converter bridge. Technically the converter does have some finite value of inertia contribution due to the filtering in the power measurement, but this is very small.

Such a converter is capable of power-sharing with other (V)SM devices, or operating a power island independently. If VSM0H devices (alone) are used to operate a power island, then a discrete load step leads to a "step" change in rotor frequency at each VSM0H device, although the "step" is actually a ramp over a time defined by the filter applied to the measured power output.

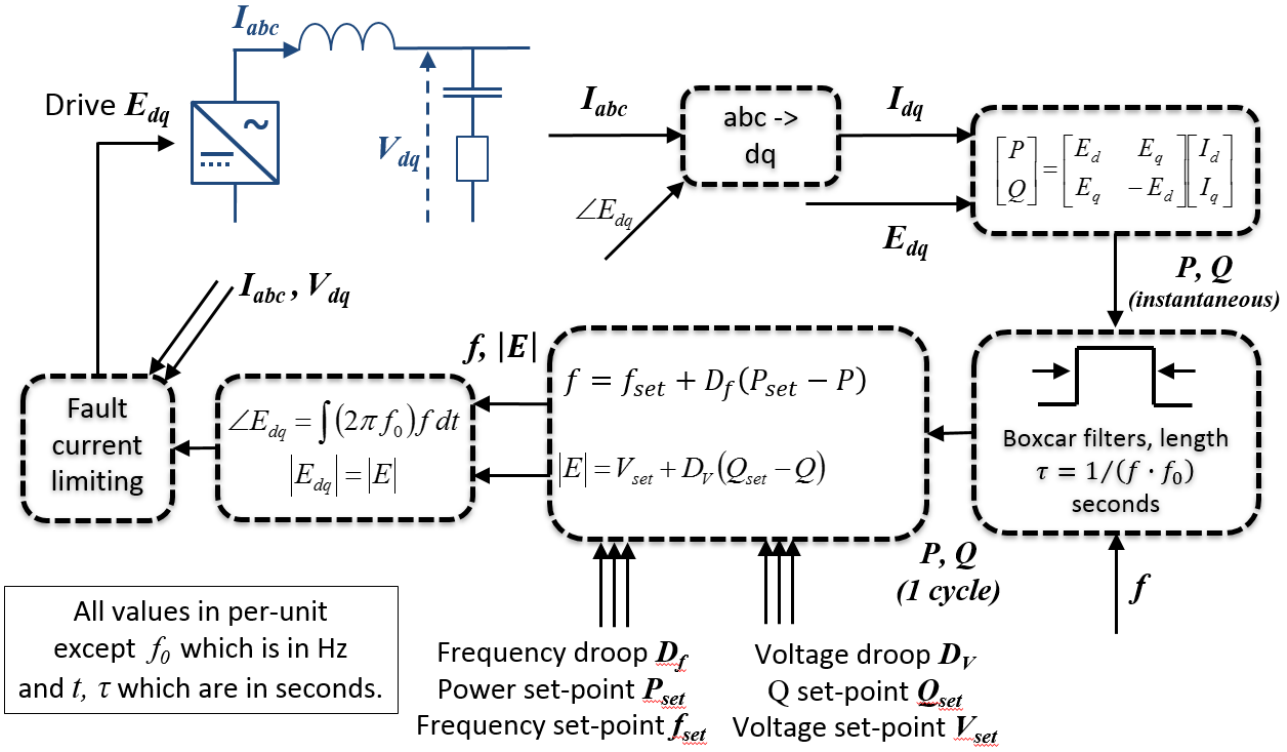

Figure 6-1 : Example controller architecture for a VSM0H / Power-Synchronisation / Droop Control grid-forming converter [6]

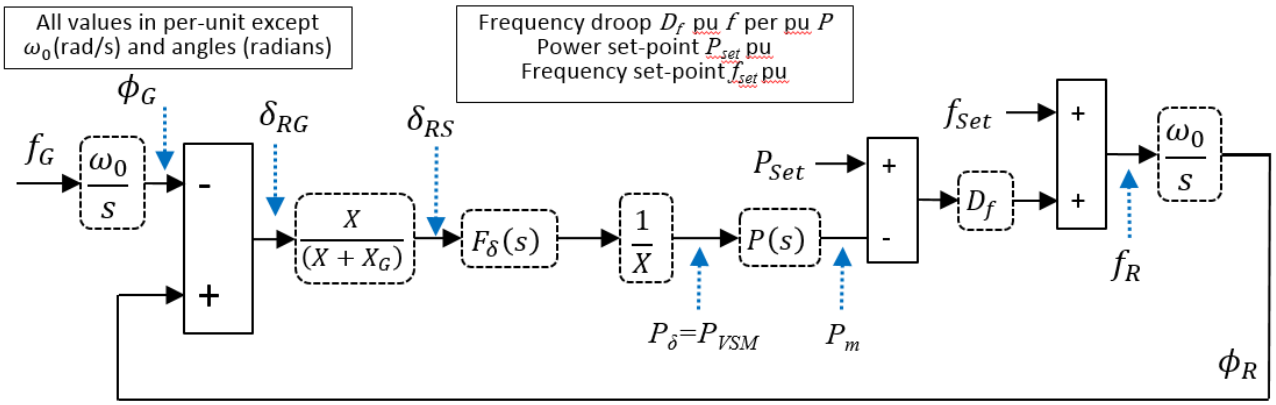

Figure 6-2 : Simplified linearised model of VSM0H embedded within power system, assuming voltage ~1pu, frequency ~1pu, and $sin(\delta_{RS}) \approx \delta_{RS}$

An analysis of the linearised response to system events, mirroring that for VSM in section 4.6, in the context of Figure 4-1, leads to the linearised model (Figure 6-2) and the following response equation for VSM0H that can be compared to (17) & (18).

$$\frac{\phi_R}{\phi_G} = \frac{\left(\frac{\omega_0}{s}\right)\left(\frac{1}{(X+X_G)}\right)F_\delta(s)P(s)D_f}{\left(1+\left(\frac{\omega_0}{s}\right)\left(\frac{1}{(X+X_G)}\right)F_\delta(s)P(s)D_f\right)} \tag{31}$$

To aid the understanding of this, the assumption/simplification can be made that $F_\delta(s) \approx 1$, and that $P(s)$ is implemented as a simple 1st-order lowpass filter (rather than as a boxcar filter):

$$P(s) = \frac{1}{(1+\tau_P s)} \tag{32}$$

in which case:

$$\frac{\phi_R}{\phi_G} \approx \frac{\left(\frac{\omega_0}{\tau_P}\right)\left(\frac{1}{(X+X_G)}\right)D_f}{\left(s^2 + s\left(\frac{1}{\tau_P}\right) + \left(\frac{\omega_0}{\tau_P}\right)\left(\frac{1}{(X+X_G)}\right)D_f\right)} \tag{33}$$

which represents a 2nd-order lowpass filter. This can be compared to the 2nd-order bandpass+lowpass filter which was the approximation of the (V)SM response in the absence of prime-mover response (18). The absence of the bandpass filter component in the VSM0H converter relates to the fact that it attempts to make no inertial response.

$$s^2 + s\left(\frac{1}{\tau_P}\right) + \left(\frac{\omega_0}{\tau_P}\right)\left(\frac{1}{(X+X_G)}\right)D_f \Leftrightarrow s^2 + 2\zeta\omega_n s + \omega_n^2 \tag{34}$$

For typical values $\omega_0 = 2\pi 50$, $(X+X_G) = 0.3$, $D_f = 0.04$ and $\tau_P = 0.010$ (for the single-pole LPF (32)), this leads to

$$\omega_n = \sqrt{\left(\frac{\omega_0}{\tau_P}\right)\left(\frac{1}{(X+X_G)}\right)D_f} \approx 65 \text{ equivalent to ~10 Hz} \tag{35}$$

$$\zeta = \frac{\left(\frac{1}{\tau_P}\right)}{2\omega_n} \approx 0.8 \tag{36}$$

Therefore the VSM0H rotor response with those example parameters, using a single-pole lowpass filter in place of the boxcar filter, and ignoring the effect of $F_\delta(s)$, is approximately a 2nd-order lowpass filter with cutoff frequency ~10 Hz and high, but not critical damping. [Reducing τ_P could, in theory, increase the damping and OLTF stability in the grid-connected context of Figure 4-1 and Figure 6-2 but could make the controller unstable in an islanded scenario and is therefore not recommended.]

The actual response of a VSM0H device, including the effect of $F_\delta(s)$, and accounting for a more complex boxcar filter $P(s)$ (37) being used in the algorithm, instead of a simple low-pass filter, is similar but slightly different to the simplified prediction in (33).

$$P(s) = \frac{1}{s\tau_\delta}(1 - e^{-s\tau_P}) \tag{37}$$

Equation (31) for a VSM0H allows the output power response to be determined, in the context of a grid frequency disturbance described by f_g (Figure 6-2) which mirrors the VSM model context (Figure 4-2):

$$\left(\frac{P_{VSM_{Int}}}{f_g}\right) = \frac{\left(\frac{1}{(X+X_G)}\right)F_\delta(s)(\phi_R - \phi_G)}{\left(\frac{\phi_G}{\left(\frac{\omega_0}{s}\right)}\right)} \tag{38}$$

which manipulates to:

$$\left(\frac{P_{VSM_{Int}}}{f_g}\right) = \left(\frac{\omega_0}{s}\right)\left(\frac{1}{(X+X_G)}\right)F_\delta(s)\left(\frac{\phi_R}{\phi_G} - 1\right) \tag{39}$$

using (31) to evaluate ϕ_R/ϕ_G

Equations (39) is extremely useful for evaluating the Network Frequency Perturbation (NFP) plot, analysed in section 8.

Applying the same -5 °phase step/jump and -0.5 Hz/s ROCOF events used in section 5, to a VSM0H converter (Figure 6-2) leads to the results presented in Figure 6-3. In Figure 6-3, the VSM0H droop slope is set to 4 %, the same as the Group A and B devices in Table 5-1 that had droop response active. The zoomed results to the phase step/jump are shown on the left hand column, and can be compared to Figure 5-2 which shows the (V)SM responses on the same scales, while the responses to the ROCOF event are shown in the right-hand column and can be directly compared to Figure 5-3.

6.1 Summary conclusions for VSM0H responses to phase steps and ROCOF

- Figure 6-3 (left column) shows that the VSM0H response to a phase step is of a similar order to a SM or VSM (compare the left column $P_{(V)SM}$ plot of Figure 6-3 with Figure 5-2).
- Figure 6-3 (right column) shows that the VSM0H response to a frequency ramp starts slower than that of a SM or VSM, but that it can then exceed that of a SM or VSM that has a slower droop response time constant τ_P, because the time constant on the VSM0H droop response is so small. (compare the right column plots of Figure 6-3 with Figure 5-3).
- Figure 6-4 shows the VSM0H response to the combined phase step and frequency ramp. Compared to Figure 5-5, which shows the responses of SM and VSM devices (with inertia) to the same event, the VSM0H device provides a similar response to the initial phase step, followed by a slightly smaller response than (V)SM between 40 ms and 500 ms (no inertia), but then rapidly followed by a steadily increasing power output which can increase faster than (V)SM, with a parabolically increasing cumulative energy output.
- VSM devices could also be equipped with very fast-acting droop response with very small τ_P, if the energy source attached to the DC bus supported it. This would create a VSM device possessing inertia, plus also a fast-acting droop response. This would provide a large response throughout the entire post-event period.

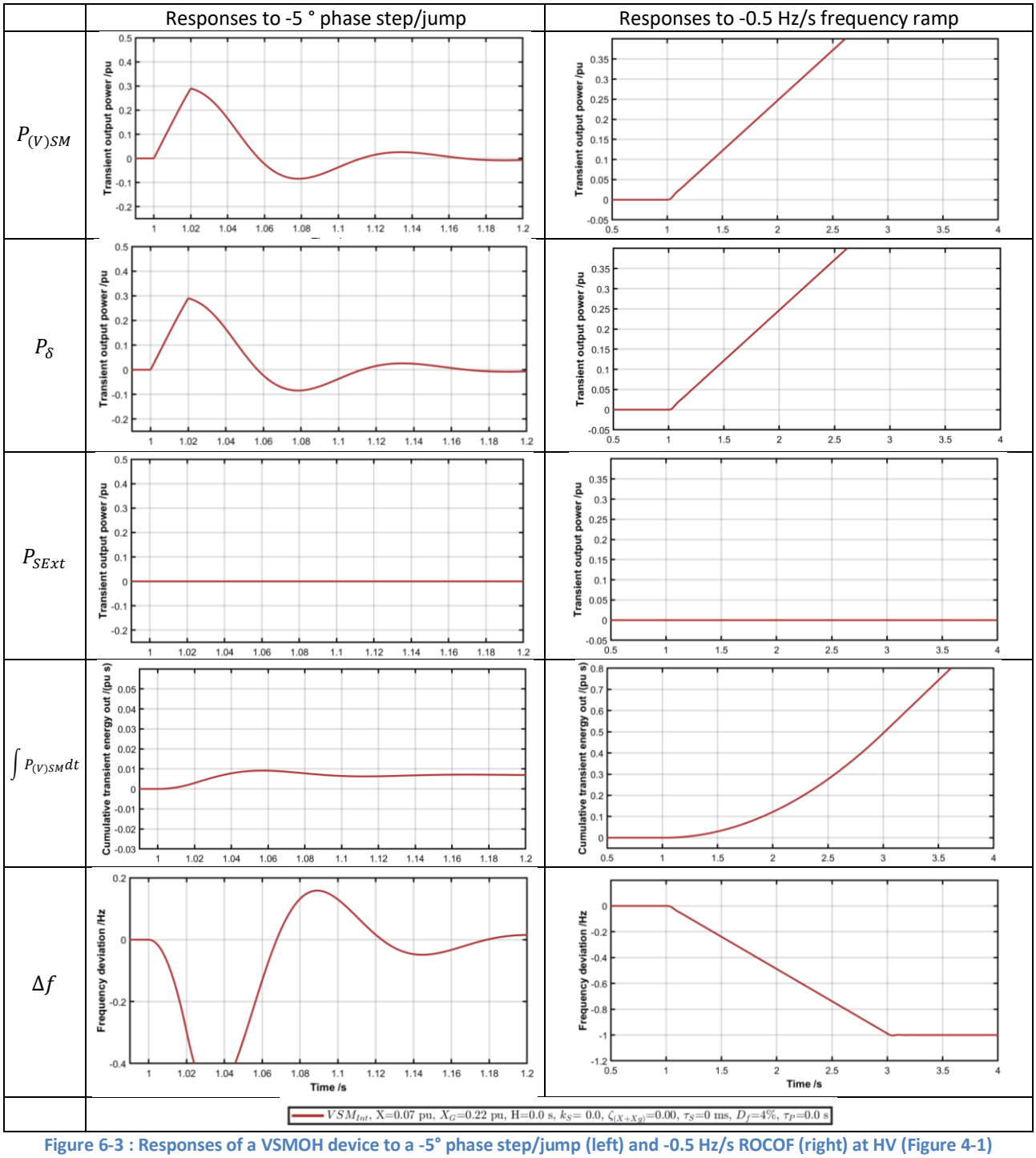

Figure 6-3 : Responses of a VSMOH device to a -5° phase step/jump (left) and -0.5 Hz/s ROCOF (right) at HV (Figure 4-1)

	Responses to -5 ° phase step/jump combined with a -0.5 Hz/s frequency ramp
$P_{(V)SM}$	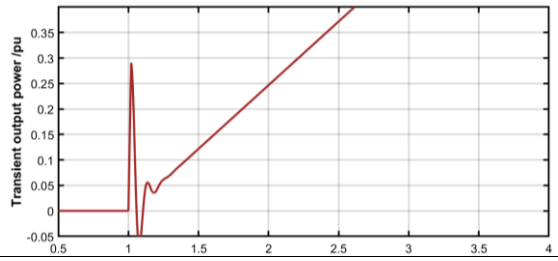
P_{δ}	
P_{SExt}	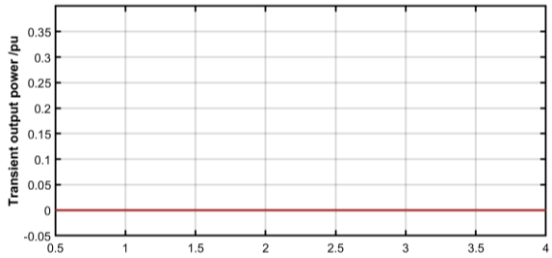
$\int P_{(V)SM} dt$	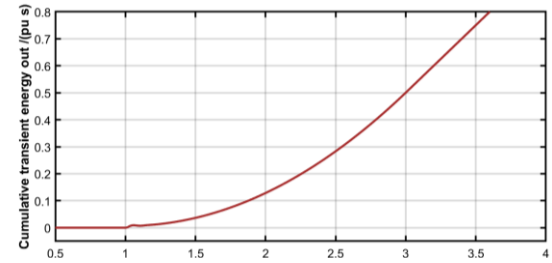
Δf	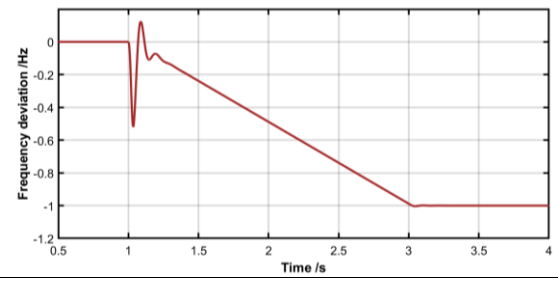
	VSM_{Int}, X=0.07 pu, X_G=0.22 pu, H=0.0 s, k_S= 0.0, $\zeta_{(X+X_g)}$=0.00, τ_S=0 ms, D_f=4%, τ_P=0.0 s

Figure 6-4 : Responses of a VSMOH device to a -5° phase step/jump combined with a -0.5 Hz/s ROCOF at HV (Figure 4-1)

7 Time-domain examples of devices power-sharing in an islanded load-step scenario

Sections 5 and 6 showed theoretical responses of different devices to defined "potted" HV grid voltage phase angle trajectories, from the simplified system model defined in Figure 4-1 and Figure 4-2. Those results suggest that neither SM, VSM_{Int}, VSM_{Ext} or VSM0H can provide an instant power transient, but this is not actually the case. Similarly, discussions in section 5.3 concerning the responses to phase steps and frequency ramps concluded "*According to the "potted" theoretical situation where a negative-going phase step/jump coincides with the beginning of a linear frequency ramp (falling), the models for all (V)SM devices predict an initial thump of power output, followed by a "lull" about 250 ms after the phase step, before the inertial and droop-response power subsequently* increases.*"*. Within an islanded or closed system, on aggregate, the "lull" cannot exist, since the generators, in aggregate, must supply the load power, unless the network voltage and/or frequency collapse.

This demonstrates that while the "potted" grid voltage trajectories and simplified system models (sections 3-7) are useful to categorise device behaviour, they do not reveal the whole story regarding the exact behaviour in an islanded or power-sharing scenario. This particularly applies to the first few cycles when decaying DC currents etc. are present, and the inductances and interactions of all network components are considered. The "potted" scenarios of grid-driven predefined phase and frequency trajectories also don't provide an exact vision of what a power system containing a mix of power sources would do following a given event. The generators will respond as multiple MOAS systems as described in section 4.10.

To investigate further and illustrate these points, this section describes time-domain simulations of 2 and 3-generator power systems (Figure 7-1 and Figure 7-2), in response to a large step load change. This could also be equated to a large loss-of-generation or loss-of-infeed event. The simulations are carried out in MATLAB SimPowerSystem, using:

- Generator 1. A 10 MW / 12.5 MVA Simulink synchronous machine (SM) model, coupled to the steam turbine and governor model, with a total prime mover response time in the order of 10 seconds, consisting of single-pole lowpass filters, ramp-rate limited valve positions, etc. Devices with H=4 and H =8 are approximately equivalent to SM devices B1 and B2 in Table 5-1, used for analysis in section 5.
- Generator 2. A 10 MW / 12.5 MVA simulated VSM_{Int} device with an effective prime-mover response time τ_P=1 s and the droop slope D_f=4 %. The converter hardware is simulated using an average-value model of the converter bridge, which is appropriate for such a study, where PWM switching harmonics have no relevance to the required results. Devices with H =4 and H =8 are equivalent to VSM_{Int} devices B5 and B6 in Table 5-1, used for analysis in section 5.
- Generator 3. A 10 MW / 12.5 MVA simulated VSM0H device with droop slope D_f=4 %. The converter hardware is simulated using an average-value model of the converter bridge. The device is equivalent to that presented in section 6.
- A resistive load which remains constant throughout the scenario, equal to 0.25 pu of the total connected generator active-power capacity.
- A second resistive load which is added as a discrete load step, again equal to 0.25 pu of the total connected generator active-power capacity.

7.1 Two-generator system (SM+VSM) load step scenario

The first two simulations contain just the first two generators, the SM and VSM (Figure 7-1). In the first simulation, the inertia of both units is H =4. In the second simulation, H =8 (both units). The total active power capacity is 20 MW, so the 2 loads are each 5 MW, 0.25 pu of the total generator active-power capacity.

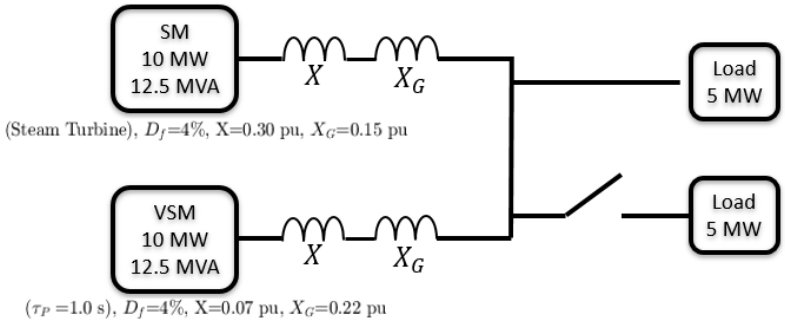

Figure 7-1 : Context for 2-Generator (SM+VSM) load-step scenarios

Figure 7-2 shows power outputs and rotor frequencies, when, at *t*=0 s, the HV load is increased from 5 MW to 10 MW in a discrete step. Figure 7-3 shows the same results, zoomed in to show the first 600 ms in greater detail. The 5 MW new load power is drawn "instantly" (in <<20ms) at the HV bus, and the additional power is provided "instantly" by both devices. This is despite the VSM_{Int} having internal damping. Clearly, having internal damping does not preclude a device providing instant response when it is required for power-sharing.

There are 3 distinct phases to the post-event period:

4) 0-50 ms (Figure 7-3). The initial responses are due to the phase step effect. The power transient dominantly comes from VSM_{Int}, primarily because in this example it has a lower total impedance to the grid. There is an external damping power contribution from the SM, but it has little affect during the first 50 ms, and/or is not large enough to outweigh the lower impedance effect of the VSM_{Int}.

5) 50 ms – 350 ms (H =4) and 50 ms – 500 ms (H =8) (Figure 7-3) During this period the differences in damping ratio and internal/external damping of the 2 devices have an impact. Firstly, the higher damping ratio of the VSM_{Int} means that its rotor slows faster, reducing its δ angle faster than the more lightly-damped SM. Secondly, while the external damping power appears directly at the device terminals, the internal damping effect is indirect, so for the VSM_{Int} the damping power is purely "virtual". These two effects combined mean that the SM provides nearly double the transient (new load) power compared to the VSM_{Int} during this period, even though both devices have the same H value.

6) 0.5 s onwards (Figure 7-2). As frequency falls at a more stable rate, with ROCOF gradually arrested and reversed, both devices provide the same inertia, and damping power reduces. However the VSM_{Int} with τ_P=1 s can respond faster on the droop response, compared to the steam turbine. Therefore, it outputs more power as frequency falls, and from 0.5 s onwards, this power is much larger than the inertial contribution, as ROCOF is stabilised and frequency reaches the nadir at ~3.5 s and then begins to rise again. Only much later, >20s after the event, is the steam turbine prime mover able to "catch up" to its fair share of power output. Note, that if the converter was not able to provide a drooped response, then the plot would look quite different from 0.5 s onwards.

An interesting feature of this power-sharing scenario (Figure 7-2) is that the SM power output does not have the classic decaying oscillations of the grid-connected scenarios (compare with SM devices B1 & B2 in Figure 5-5), even though the damping ratio of the SM is $\zeta \ll 1$. This is because it has no infinite bus to swing against. It can only swing against the VSM_{Int}, which is configured for $\zeta=1$. This is a good example of where a critically-damped VSM, even in the VSM_{Int} form with internal damping, can provide a more stable power-sharing partner than another traditional SM [5].

As would be expected, the higher inertia system shows a smaller total frequency deviation than the lower inertia system. The peak frequency deviation could also be reduced by reducing the response time of the droop response of either the SM or VSM devices. Using a CCGT instead of a steam turbine might offer τ_P<10 s, or the VSM device might be equipped with a "virtual" prime mover with a response time τ_P<1 s. Either or both would provide a quicker arrest of negative ROCOF.

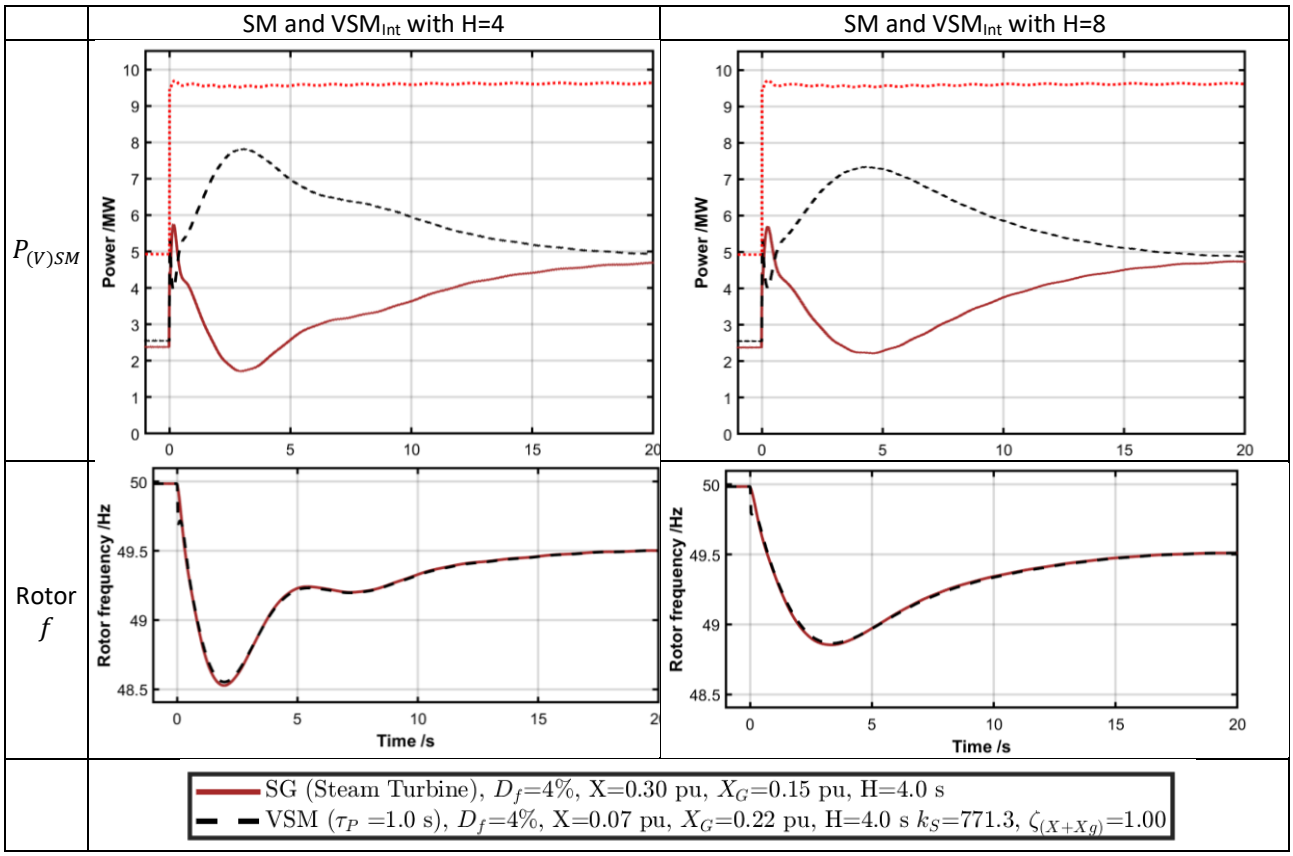

Figure 7-2 : SM and VSM generators subjected to 0.25 pu load step at t=0 s. Whole scenarios.

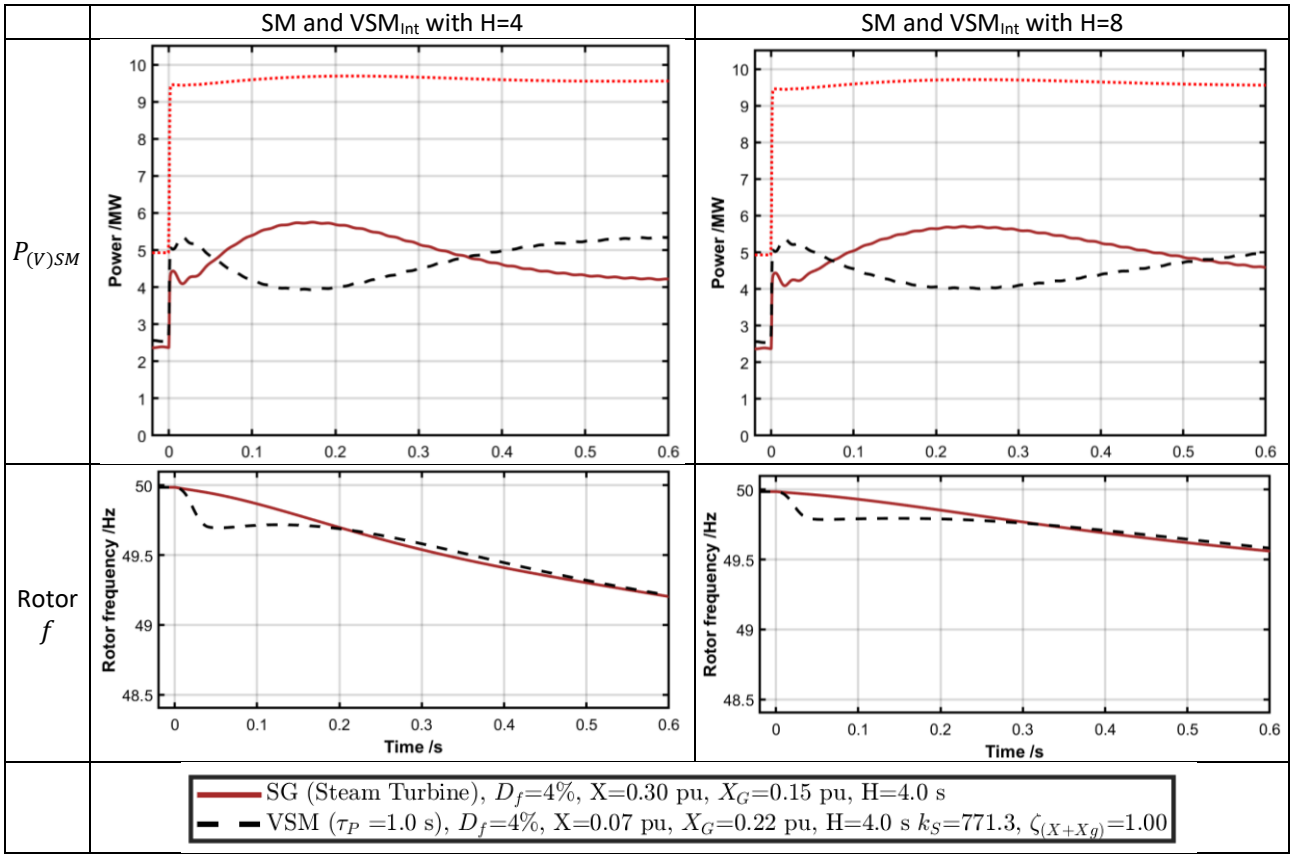

Figure 7-3 : SM and VSM generators subjected to 0.25 pu load step at t=0 s. First 600 ms.

7.2 Three-generator system (SM+VSM+VSM0H) load step scenario

The second two simulations contain three generators: the SM, VSM (and VSM0H Figure 7-4). The total active power capacity is 30 MW, so the 2 loads are each 7.5 MW, 0.25 pu of the total generator active-power capacity. The point of these simulations is to show the effect that a grid-forming VSM0H device can have, even though it provides “zero” (or very low) inertia.

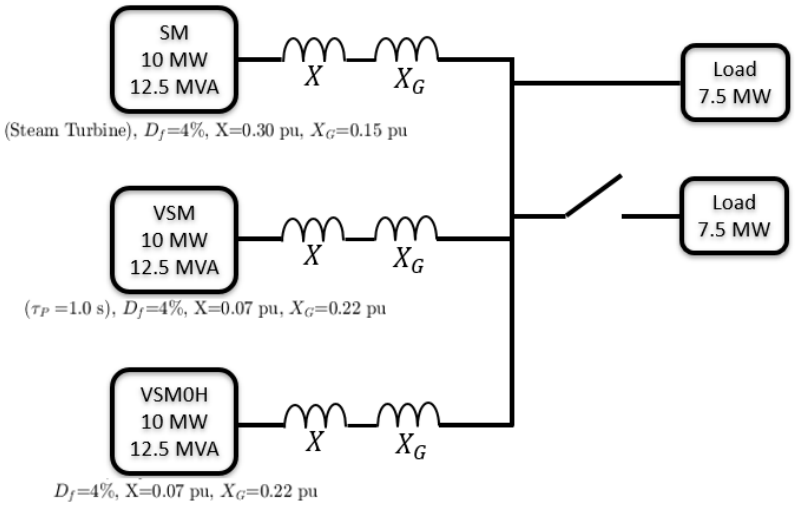

Figure 7-4 : Context for 3-Generator (SM+VSM+VSM0H) load-step scenarios

Figure 7-5 shows power outputs and rotor frequencies, when, at *t*=0 s, the HV load is increased from 7.5 MW to 15 MW in a discrete step. Figure 7-6 shows the same results, zoomed in to show the first 600 ms in greater detail.

Referring again to the 3 distinct phases to the post-event period:

4) 0-50 ms (Figure 7-6). The VSM0H provides the same phase-step response as the VSM_{Int}, both of which, in this example, provide more response than the SM because they have a lower total impedance to the grid.

5) 50 ms – 350 ms (H =4) and 50 ms – 500 ms (H=8) (Figure 7-6) During this period the VSM0H provides less contribution than SM or VSM, because it provides neither inertia nor bandwidth-unlimited external damping power.

6) 0.5 s onwards Figure 7-5). The VSM0H provides more power than SM, and faster than VSM, simply because its response on the droop slope is faster than either, with τ_P<<1 s ($\tau_P \approx 0.010$, see section 6)

The overall result is that the VSM0H

- Contributes a proportionate share of immediate response to the load step (phase step),
- then does little to limit the initial ROCOF,
- but thereafter quickly contributes power as frequency drops, and has a significant effect on minimising the peak frequency deviation (compare Figure 7-5 with Figure 7-2), and general post-event oscillations.

While the results presented here are simulated, there is high confidence in the results since the author obtained a similar power-sharing profile between an SG (turbo-diesel) and VSM0H converter in a laboratory-scale hardware experiment in 2012, evaluating hybrid marine power systems.

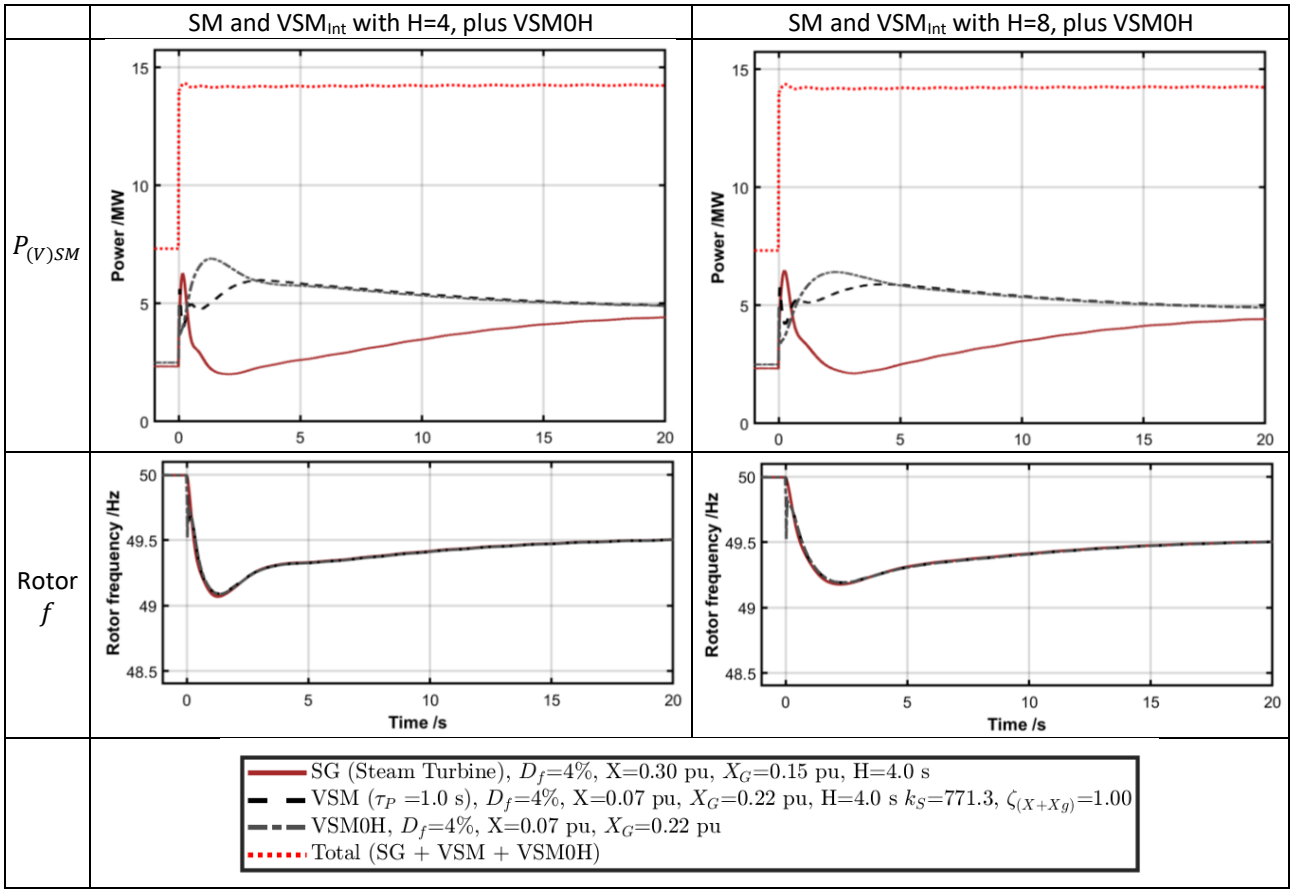

Figure 7-5 : SM, VSM and VSM0H generators subjected to 0.25 pu load step at t=0 s. Whole scenarios.

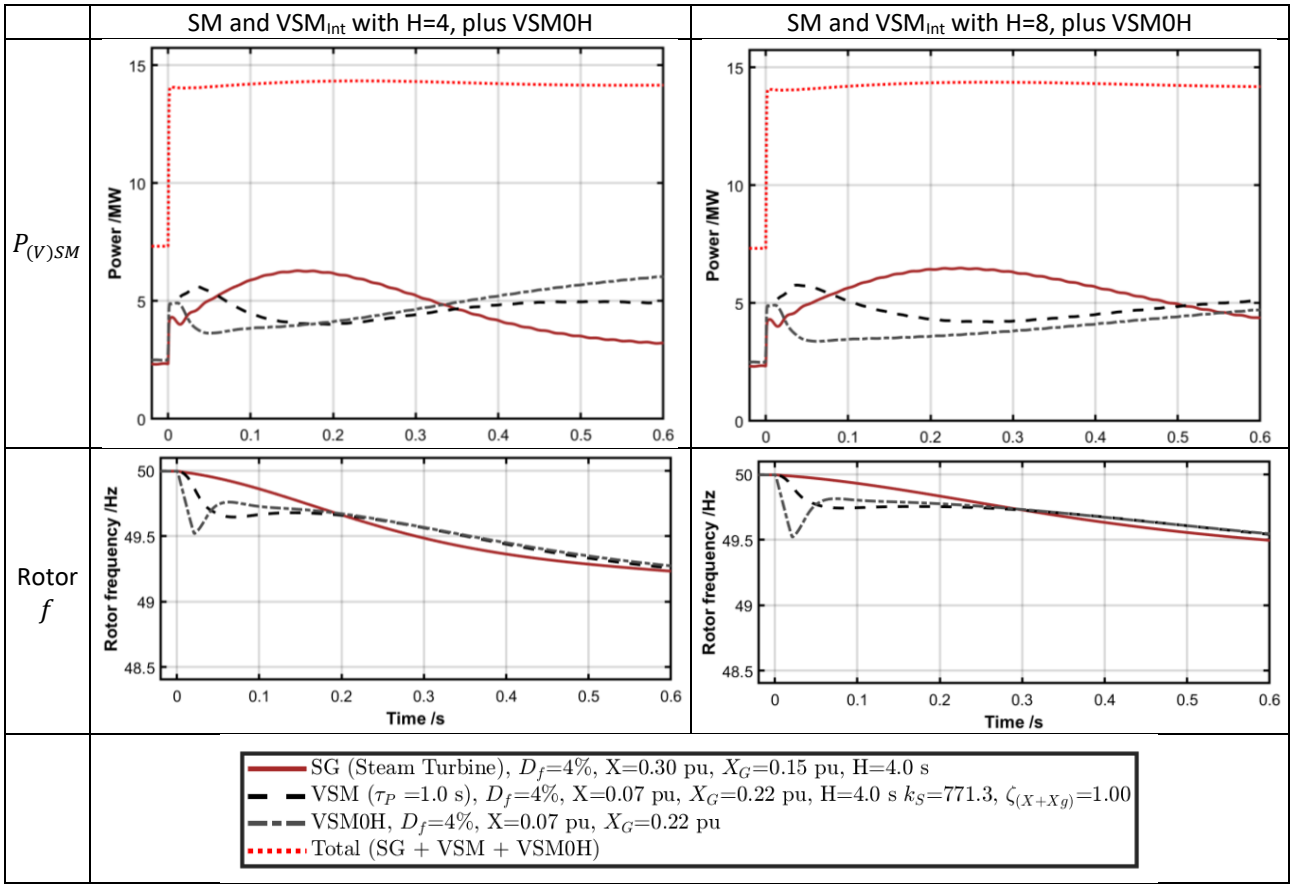

Figure 7-6 : SM, VSM and VSM0H generators subjected to 0.25 pu load step at t=0 s. First 600 ms.

8 The Network Frequency Perturbation (NFP) plot

In a meshed AC electrical network with many generators and loads, frequency and relative phase angles change continuously. In order to gain an understanding of how individual devices contribute to frequency stability and active power balance management, it is useful to examine how that individual device responds to a change in network frequency. The NFP plot [11] allows a clear distinction to be made between devices that provide frequency support through droop-slope type response, and inertial-type response. The method is not a stability assessment technique. However, the results (Bode type plots) give a useful graphical insight into the device behaviour during network disturbances. The NFP plot allows device characteristics to be summarised on a single plot pair (amplitude and phase), that would otherwise require a succession of time-domain cases to explore.

The NFP plot linking frequency and power has been used by the author since 2012 to evaluate the behaviour of grid-forming and non-grid-forming machines and converters. It was first deployed to analyse the "Voltage Drive" grid-forming converter described in [12], and was used as a graphical means to tune that converter to match a conventional SM in both inertia and damping performance. To date, NFP plots have been used to examine the direct link between network frequency (and phase) and active power. This is the most important NPF plot in terms of understanding active power interactions. However this is just the 1st of 4 possible variants. The other three might be valuable to examine in future:

1) NPF plot showing active power responses to frequency modulations, as described in this report
2) NPF plot showing reactive power responses to voltage modulations
3) NPF plot showing cross-linkage of active power responses to voltage modulations
4) NPF plot showing cross-linkage of reactive power responses to frequency modulations

All the analysis and results of the following section refer to the most important 1) power/frequency NFP plot.

An example of an NFP plot is shown in Figure 8-1, and an annotated version in Figure 8-2.

To generate the NFP plot the real or simulated device is placed within a hypothetical or 'test' (e.g. "Power Hardware In the Loop") power system, such as Figure 4-1, in which the grid frequency is forced and modulated in a sinusoidal fashion at frequency f_{NFPmod}, with a small amplitude Δf about the nominal frequency f_0. This can be expressed as:

$$f = f_0 + \Delta f \cos(2\pi f_{NFP_{mod}} t) \tag{40}$$

The value of f_{NFPmod} is swept across a broad range, from ~10^{-3} Hz to ~20 Hz or optionally up to ~50 Hz. The device responds to this changing frequency with a modulated active power output:

$$P_{out} = P_{set} + \Delta P \cos(2\pi f_{NFP_{mod}} t + \phi_{\Delta P}) \tag{41}$$

The amplitude of the frequency modulation Δf is kept small enough that no unnatural saturation of device control loops occur. For example, if the suspected device inertia is H s and droop response is D_f (pu frequency for 1 pu power), then to keep peak output power modulation amplitude below ΔP_{max} pu (i.e. 0.25 pu), accounting for the

approximate expected power output $\Delta P = -2H\,(df/dt)/f_0$ (2) and the differentiation of frequency to df/dt, and also for the droop response:

$$\Delta f < \frac{\Delta P_{max}}{2H}\frac{f_0}{2\pi f_{NFP_{mod}}} \text{ Hz (Inertial limit)}$$
$$\Delta f < \Delta P_{max} D_f f_0 \text{ Hz (Droop limit)} \quad \text{(whichever is smaller)} \tag{42}$$

This would, for example, limit Δf to ~0.5 Hz at low values of modulation frequency, dropping to ~0.01 Hz at a 10 Hz modulation frequency for an $H = 8$ device.

ΔP and $\phi_{\Delta P}$ can be found either by:

- Placement of the actual or simulated device and its transformer impedance(s), including its control system, within a real or simulated test environment (Figure 4-1), and carrying out the modulated sweep described above. In this case, it is important to perform Fourier analysis of both the generated frequency deviation and measured power outputs using coherent sample sets of the frequency (40) used to generate the waveform, and the measured power. The same window lengths and parameters must be used for the Fourier analysis so that not only the magnitude of ΔP is correctly determined, but also its phase $\phi_{\Delta P}$ which must be determined accurately, relative to the phase of the frequency modulation cosine waveform defined by (40).
- It is possible to obtain the NFP plot on-site, for a large-scale multi-MW device and without a test environment. The modulating phase/frequency sweep can be injected as small open-loop adjustments to real-time PWM patterns (voltage angles). Extremely careful Fourier analysis of the local phase changes and the power flows can reveal the NFP plot, on the assumption that the distant upstream grid phase/frequency is relatively steady throughout the test. Essentially the perturbations are applied at the rotor, while the grid phase/frequency stays fixed, compared to the opposite scenario of Figure 4-1. There is a risk of locally elevated levels of flicker and voltage (inter)harmonics during the test period.
- It might also be possible to reverse engineer the NFP plot from natural variations of grid phase/frequency over a test period, if the test period contains suitable grid phase/frequency events to allow the responses to be determined above noise. The phase changes perceived might need to be referenced to represent a point more upstream from the converter (Figure 4-1). No method to practically achieve this is claimed nor presented in this report.
- Classical analysis of the device transfer functions. For instance, for the (V)SM equations (27) & (28) describe the NFP plot shape for SM or VSM_{Ext} (27) and VSM_{Int} (28), while (39) describes the NFP plot shape for VSM0H. The classical analyses presented in section 3 only consider the simplest power-to-angle control loop, and do not account for additional control loops and interactions with voltage magnitude controls. Therefore, for a real device with a complex control system, more advanced state-space models may be required to reveal a truly accurate NFP plot, that accounts for all interacting control loops.

In all cases, the amplitudes of the voltages are kept (or assumed to remain) constant at 1 pu, so that the analysis is purely an examination of the interaction between active power and frequency/phase at the grid.

The response parameters Δ*P*, where ΔP is in per-unit (pu), and $\phi_{\Delta P}$ together form a response R_{NFP}, when normalised to Δf.

$$R_{NFP} = \frac{\Delta P \angle \phi_{\Delta P}}{\left(\frac{\Delta f}{f_0}\right)} \quad (43)$$

Essentially, the NFP plot of R_{NFP} (43) shows the amplitude of the power response of the device, in pu, to a cosinusoidally modulated grid frequency, with the frequency of the modulation swept and plotted as the x axis. The grid frequency modulation amplitudes Δf must in practice be small compared with f_0, and the results are normalised by (43) to a pu modulation amplitude $\Delta f / f_0$ to ensure consistency of plotting.

The NFP amplitude plot shows $|R_{NFP}|$ on the y axis against modulation frequency $f_{NFP_{mod}}$ (Hz) on the x axis. The plot is made by plotting both axes using logarithmic scales. The y axis can either be interpreted as:

- the amplitude of the cosinusoidally varying power response of the device, in pu, to a 1 pu amplitude cosinusoidal grid frequency variation at $f_{NFP_{mod}}$
- or, (with the same values on the x and y axes, and conceptually slightly more meaningful), **the amplitude of the cosinusoidally varying power response of the device, in % pu, to a 1 % pu amplitude cosinusoidal grid frequency variation at $\boldsymbol{f_{NFP_{mod}}}$**. This second format essentially applies a x100 scaling to both numerator and denominator of (43), which cancel out.

The NFP phase plot shows $\angle R_{NFP}$, in degrees on the y axis, against modulation frequency $f_{NFP_{mod}}$ (Hz) on the x axis. The plot is made by plotting the x axis using the same logarithmic scale as the amplitude plot.

8.1 Asymptotes on the NFP plot

There are 2 important asymptotes on the NFP plot, plus a general rule concerning the right-hand side of the plot.

8.1.1 The droop response asymptote

In the most basic case, with a steady-state frequency deviation of Δf Hz, at a very low value of modulated frequency $f_{NFP_{mod}}$, the expected power output will be $\Delta P = (\Delta f / f_0)/D_f$ and $\phi_{\Delta P} = \pi$ (i.e. 180°) as the device responds on a droop slope of D_f pu frequency to 1 pu power. The 180° is important here since as frequency goes down, power output should increase. In this basic case, via (43) essentially:

$$R_{NFP} = -1/D_f \quad (44)$$

because only the drooped response is acting, and all other mechanisms are inactive since the modulation frequency is so low and there are no transient events occurring, just a steady-state offset.

This defines an asymptote on the left-hand side NFP plot. For every device providing a drooped power response to frequency, the NPF plot should merge with an asymptote which is a horizontal line intercepting:

- $|R_{NFP}| = 1/D_f$ on the y axis ($f_{NFP_{mod}} \longrightarrow 0$) of the amplitude plot
- $\angle R_{NFP} = 180°$ on the y axis ($f_{NFP_{mod}} \longrightarrow 0$) of the phase plot

For a traditional SM coupled to a mechanical prime mover and governor system, the droop response has a finite response time and phase lag. Therefore, for all these traditional generators, the amplitude of the droop response $|R_{NFP}|$ is expected to fall below $1/D_f$ as $f_{NFP_{mod}}$ rises above 0 Hz. Likewise it is expected that the phase of the response $\angle R_{NFP}$ will increasingly lag behind 180 ° as $f_{NFP_{mod}}$ rises above 0 Hz.

8.1.2 The inertia asymptote

The second key asymptote is the inertia line. This is defined using the simplistic approximation equation (2) linking electrical frequency and the expected power output during a constant-ROCOF event. It should be remembered that (2), repeated below as (45), ignores all the effects of rotor resonance and damping, and could only be truly accurate during steady-state frequency ramps with constant ROCOF.

$$\Delta \mathrm{P} = -\left(\frac{2H}{f_0}\right)\frac{df}{dt} \tag{45}$$

Accounting for the frequency modulation $f_{NFP_{mod}}$ applied during the NFP process (40) and the differentiation of frequency in (45), the predicted asymptote will be:

$$\Delta \mathrm{P} = -\left(\frac{2H}{f_0}\right)\Delta f 2\pi f_{NFP_{mod}} \cdot -sin\left(2\pi f_{NFP_{mod}} t\right) = \left(\frac{2H}{f_0}\right)\Delta f 2\pi f_{NFP_{mod}} sin\left(2\pi f_{NFP_{mod}} t\right) \tag{46}$$

This has a phase which is only 90° behind the cosine waveform of (40), i.e. 90° advanced compared to the 180° phase of $|R_{NFP}|$ for a droop response (section 8.1.1), and a peak amplitude of $\left(\frac{2H}{f_0}\right)\Delta f 2\pi f_{NFP_{mod}}$.

This leads via (43) to another straight line asymptote on the amplitude/phase NFP plot:

- $|R_{NFP}| = 2H \cdot 2\pi f_{NFP_{mod}}$ on the y axis of the amplitude plot, which crosses the plot diagonally from bottom-left to top-right.
- $\angle R_{NFP} = 270°$ on the y axis of the phase plot, i.e. 90° advanced compared to the 180° phase of the $|R_{NFP}|$ asymptote for a droop response (section 8.1.1).

Another interpretation of (46) is that:

$$\Delta \mathrm{P} = -\left(\frac{2H}{f_0}\right) fs \tag{47}$$

where f is defined by (40) and $s = j\omega$ with $\omega = 2\pi f_{NFP_{mod}}$. The introduction of the differentiation and hence the j term brings in the 90° phase advance relative to the baseline 180° power response phase.

The inertia asymptote line defines an idealistic response expected from a generator during a sustained constant-ROCOF frequency ramp. It ignores the effects of droop response, rotor resonance, and damping. Every device that is claiming to implement an inertial response should provide a response which approaches this line, both in amplitude and phase, over a range of modulation frequencies $f_{NFP_{mod}}$ at which the rotor response is dominant over drooped and damping responses. The approach of the phase, i.e. a noticeable shift from the "default" 180° drooped phase response to a more advanced phase towards 270°, is a particularly important criteria for demonstrating dominance of an inertial response over the relevant range of $f_{NFP_{mod}}$ frequencies. It is possible, over the relevant range of $f_{NFP_{mod}}$ frequencies, to provide a boosted magnitude of response $|R_{NFP}|$, but without a clear phase advance relative to a drooped response at 180 °. This should be interpreted as an enhanced droop/damping response, not as an inertial response.

Likewise, it is possible for a device to offer both inertia and a fast-responding droop response such that the droop response is still significant at higher $f_{NFP_{mod}}$ where (conventionally) inertia and rotor resonance is dominant. In such a case, the phase may rise above 180° but not reach all the way to 270°. This can indicate a mix of significant inertia PLUS fast-acting drooped response.

8.1.2.1 Rotor resonance and damping

A real SM, or a VSM rotor, will not follow the inertia asymptote line to the top-right of the plot. This is fundamentally because (2) and (45) are not accurate during dynamic events, as described in section 4.2. The actual power response is a damped resonance as determined in section 4.9. Therefore:

- A classsic SM with low damping often provides more response than the asymptote predicts, as $f_{NFP_{mod}}$ approaches and moves through the (damped) rotor resonant frequency.
- As $f_{NFP_{mod}}$ increases beyond the (damped) rotor resonant frequency, the actual power response drops away below the asymptote.

8.1.3 NFP plot reponse at higher frequencies.

At modulation frequencies $f_{NFP_{mod}}$ above $f_0/2$ and as $f_{NFP_{mod}} \longrightarrow f_0$, interpretation of the plot becomes conceptually difficult since it describes a modulation of grid frequency at a frequency approaching the grid frequency itself. Therefore, at frequencies above $f_{NFP_{mod}} = f_0/2$, the NFP plot becomes difficult to interpret practically, but can still be of some use, especially when analysing devices which may have relatively high-bandwidth control loops.

Generally, damping (external or internal) tends to provide a power response with a phase of 180° since it is "equivalent" to droop response (see section 4.4). This results in a further "hidden" asymptote which is similar to the droop response asymptote (see section 8.1.1) but instead is valid only at the higher values of $f_{NFP_{mod}}$. This has a contribution to the (V)SM response at higher frequencies.

The other effect at high frequency, is the impact of the various low-pass filter effects in the systems, which:

- make $|R_{NFP}|$ tend towards zero as $f_{NFP_{mod}} \longrightarrow f_0$
- for a grid-forming converter, make $\angle R_{NFP}$ increasingly lag as $f_{NFP_{mod}} \longrightarrow f_0$, but settling at some final value as $f_{NFP_{mod}} \longrightarrow f_0$

One effect that has been noted when acquiring data for NFP plots of non-grid-forming devices, is that:

- for a non-grid-forming converter, $\angle R_{NFP}$ becomes increasingly lagged as $f_{NFP_{mod}} \longrightarrow f_0$, and does not settling at some final value as $f_{NFP_{mod}} \longrightarrow f_0$, but continues to phase-wrap several times as $f_{NFP_{mod}} \longrightarrow f_0$.

8.2 Typical NFP plot examples for GF devices, and their interpretation

The stylised NFP plot shown in Figure 8-1, replotted from the data from [11] illustrates the 2 key asymptotes in red-dotted (D_f=4% droop asymptote) and green-dashed (Inertia asymptote for H=5), plus:

- a grey dashed line "SG trend, true inertia + damping, no control" which shows the response of a stylised synchronous condenser with H=5 which has a real rotor resonance and damping, but no prime mover to provide droop response.
- a solid black line "SG, H = 5s, with IEEEG1 Governor" indicating the response of a SM (of the same design as the synchronous condenser) attached to a steam turbine and IEEEG1 Governor, of total inertia H=5.
- a dashed blue line "DQCI converter, Df = 4% with LPF tau = 0.2s" indicating the response of a grid-following converter using DQ-axis Current Injection control (DQCI).

Because there is no prime mover, the synchronous condenser in Figure 8-1 makes no attempt to provide a response at low frequencies of disturbance. However, it closely follows the inertia asymptote line. Crucially the phase of $\angle R_{NFP}$ makes the 90° advance from 180° to 270° as rotor resonance (and inertial contribution) becomes significant, over the disturbance frequency range of ~0.1 to ~2 Hz in this case. Rotor resonance is at ~2 Hz, and above that frequency, the actual device response magnitude drops rapidly relative to the idealised inertia asymptote, and the phase also drops away.

The SM attached to a prime mover and IEEEG1 governor, shown as the solid black line, has roughly the same response above ~0.5 Hz as the synchronous condenser. However, where $f_{NFP_{mod}} < 0.5$ Hz, the inertial contribution is less dominant, while the drooped prime-mover response becomes more and more dominant as $f_{NFP_{mod}} \longrightarrow 0$. Where $f_{NFP_{mod}} \longrightarrow 0$, $|R_{NFP}| \longrightarrow 1/D_f$ and $\angle R_{NFP} \longrightarrow 180°$. Typically, the amplitude $|R_{NFP}|$ shows a dip between ~0.01 to ~0.5 Hz, as the response curve $|R_{NFP}|$ transitions from the droop asymptote to the inertia asymptote. Essentially at a frequency of ~0.1 Hz, the modulations are too fast for the prime mover to follow, being filtered out by the governor and prime mover responses, and the inertial contribution is also small. Therefore, there is a dip in response in this "middle" frequency region between drooped and inertial response. Also, the phase trajectory typically shows the transition between the 180° phase of the droop asymptote to the 270° phase of the inertia asymptote, as the drooped response tails off and the inertial contribution increases.

Where a faster-responding droop response is possible, the dip between the droop response (lower frequencies) and inertial response zones is reduced. However, if the inertial response is still present, then the clear indicator is the zone of $f_{NFP_{mod}}$ around the (damped) rotor resonant frequency in which the phase $\angle R_{NFP}$ rises from the default 180° phase of the droop asymptote towards the 270° phase of the inertia asymptote. Without this distinctive phase trajectory, the response would be classed as a drooped frequency response, not an inertial response, even if the amplitude trajectory $|R_{NFP}|$ closely followed the inertia asymptote.

The blue dashed line shows the response of a grid-following current-control device. This demonstrates a drooped response which can respond quickly (with a time constant of τ_P =0.2 s, and so $|R_{NFP}|$ does not tail off until ~1 Hz), but zero inertial contribution. This device also shows a grid-following characteristic phase-wrapping of $\angle R_{NFP}$ where $f_{NFP_{mod}}$ approaches and moves above $f_0/2$.

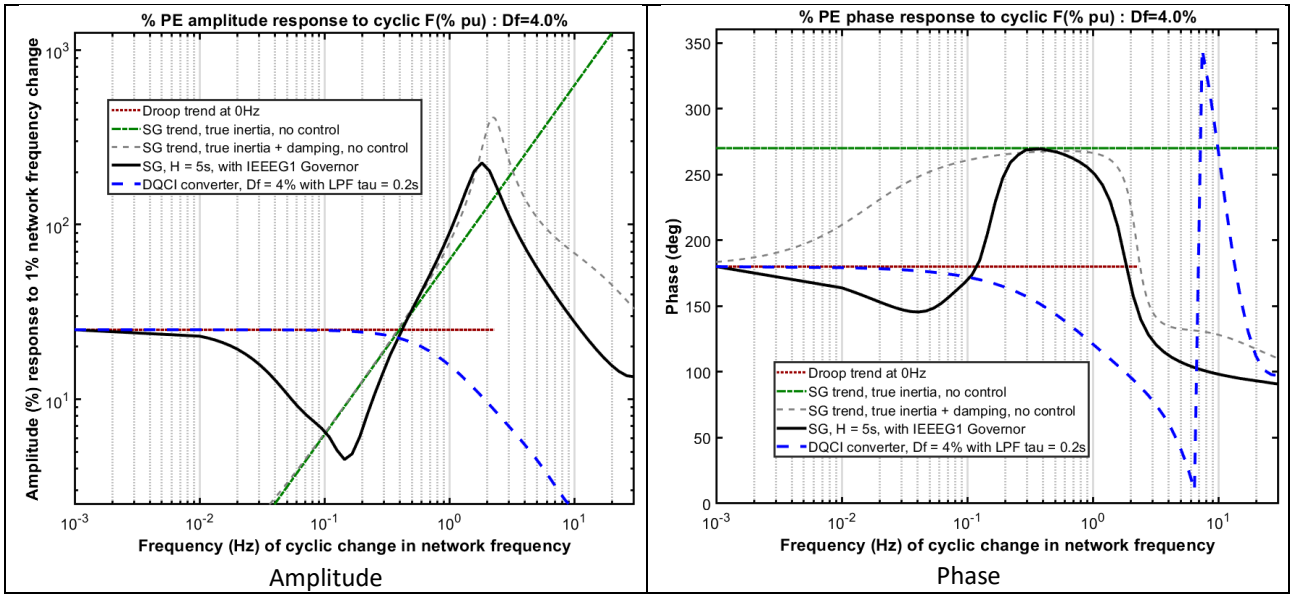

Figure 8-1 : Illustration of the key asymptotes of R_{NFP} on the NFP plot, plus typical SM and SM+PrimeMover responses, plus typical non-grid-forming device (DQCI) response

The shape of the SM/SG response in Figure 8-1, shown as the solid black line, shows all the distinctive properties of a grid-forming device possessing inertia.

- The droop response at the left hand side represents the droop slope. So in this example, the y intercept is 25, representing a 1/25=0.04, hence 4% droop slope, and the phase will be 180°
- The governor and prime mover response begins to tail off at a modulation frequency of ~0.025 Hz (response drops to $1/\sqrt{2}$ of 25 i.e. -3dB), showing that this device has a slow prime-mover response with a time constant of the order of 5 s or more, appropriate for a large turbine.
- The inertial response intersects the inertia asymptote at ~0.2-0.4 Hz, both in amplitude and phase. The fact that the phase response rises a full 90° at ~0.2 Hz to the 270° level shows that the device is providing a truly inertial response. Over the region $0.2 < f_{NFP_{mod}} < 1$ Hz, the inertia contribution is dominant over droop response (which already dropped off by $f_{NFP_{mod}}$ = 0.1 Hz) and damping (which does not become dominant until $f_{NFP_{mod}}$.rises above 1 Hz.
- The rotor resonance at $f_{NFP_{mod}}$ = 2 Hz is lightly damped. This allows the inertial response to exceed the asymptote when the modulation frequency is close to the resonant rotor frequency. It also allows the response phase to achieve the full 270° between ~0.3 and ~0.5 Hz.
- The damping stops the power response rising too far above the predicted inertia asymptote, and stops a sharper rotor resonance. More damping reduces the peak value of the response in this zone of $f_{NFP_{mod}}$, and also tends to reduce the phase from 270° towards 180° as damping power gradually increases and becomes dominant over inertia power as $f_{NFP_{mod}}$.rises above 1 Hz. The damping is still significant up to a frequency of ~15 Hz for a (V)SM with conventional levels of damping.
- As modulation frequency rises past the rotor resonant frequency, rotor damping and the filtering effect of the rotor inertia itself mean that the response amplitude tails off. The response phase also tails off, although for a grid-forming converter it tends to reach a new steady-state value, while a grid-following converter tends to exhibit phase wrapping as frequency increases.

8.3 Basic rules for interpretation

In essence, the NFP plot can be divided into three key regions, described below, and highlighted on Figure 8-2. There can be gaps between the regions, or the regions can overlap, depending on device type/algorithm and parameterisation. The droop and/or inertia regions may not be present at all for some device types/algorithms/parameterisations.

1) Region 1. The active droop region. This appears at the left of the plot. Any device providing a droop response will intercept the asymptote described in section 8.1.1. The magnitude is larger if the droop response is more aggressive, and the phase should be ~180°
2) Region 2. The inertia region. This appears in the middle of the plot. Any device providing a dominantly inertial response will provide a significant magnitude of response, and its phase will be 270°
3) Region 3. The damping region. This appears at the right of the plot. When inertia is present, the damping normally appears as a reduction in the peak resonant magnitude, and then a gradual reduction in response, and return of the phase of the response to 180° and below at the far right of the plot. An exception is that high (e.g. critical) levels of real external damping lead to an elevated resonant peak frequency, and much higher magnitudes to the right of the plot (at higher bandwidths).

- If there is a noticeable dip in magnitude between regions 1 and 2, this signifies that the active droop response (governor, prime mover) tails off before the inertial response becomes significant. Essentially there is a gap between region 1 and region 2, in which the response is small.
- Conversely, if the device provides a drooped response with a small time constant, i.e. a fast frequency response, then regions 1 and 2 may merge into each other. Typically the dip in magnitude between regions 1 and 2 becomes less pronounced, or disappears. The other effect is that the phase of the response where regions 1 and 2 overlap will be influenced both by the 180° phase (or more lagged) of the droop response, and by the 270° of the inertial response, leading to a phase which sits somewhere between 135° and 270° in the regions where regions 1 and 2 overlap. Figure 8-7 and Figure 8-9, shown later, show this for VSM devices with fast-responding droop response.
- All types of damping lead to a response which has a phase of 180° (and lower at the extreme right of the plot), and a magnitude which eventually decreases at the extreme right of the plot
- Lower, conventional amounts of damping simply reduce the magnitude of the rotor resonance, and leave a distinct boundary between regions 2 and 3 at this modulation frequency.
- If damping is more than conventional, i.e. moving towards critical damping, then the impact of region 3 increases and overlaps with region 2.
    - Virtual, internal damping at a high level will severely reduce the magnitude of the resonant peak, and also slightly increase its frequency. It will also tend to move the phase down from 270° back towards 180° in the area where region 3 “moves left” to overlap region 2.
    - Real, external damping for a SM or VSM_{Ext} at a high level will tend to increase the response magnitude as region 2 transitions into region 3, making a new damped resonant peak at a high magnitude with an unconventional frequency, for example ~8 Hz as shown in Figure 8-3and Figure 8-7. However, a real SM with this level of damping does not exist, and implementation of such a VSM_{Ext} device presents challenges, so such a situation may be hypothetical.

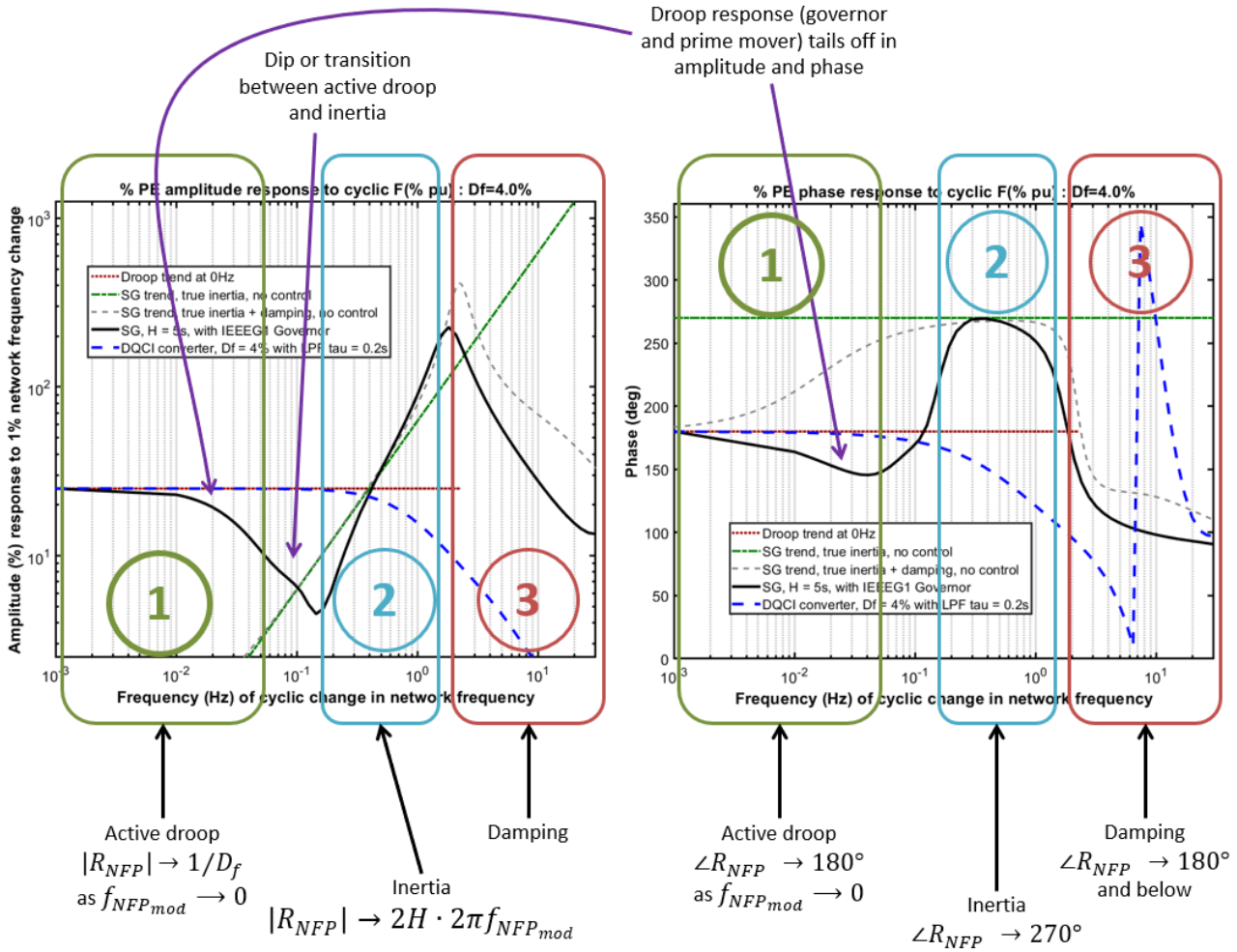

Figure 8-2 : Annotated version of Figure 8-1 NFP plots showing the key regions of response

8.4 NFP plots for example devices

Evaluation of (27) or (28), the power output fluctuations for given frequency fluctuations at different frequencies, reveals the approximate Network Frequency Perturbation plot (NFP plot) for a (V)SM, (in the context of Figure 4-2, ignoring the effects of other interlinked control loops and assuming voltage remains at 1 pu).

Likewise evaluation of (39) reveals the approximate NFP plot for a VSM0H device (Figure 6-2), which provides fast drooped power response but zero inertia.

It is therefore possible to plot generate the NFP plots for the Group A and Group B devices from section 5, and listed explicitly in Table 5-1, together with the VSM0H device described in section 6. To reduce the number of traces per plot, 4 sets of plots are shown:

Group A devices with $H = 4$ plus VSM0H with 4% droop	A1, A3, A5, A7	Figure 8-3
Group A devices with $H = 8$ plus VSM0H with 4% droop	A2, A4, A6	Figure 8-5
Group B devices with $H = 4$ plus VSM0H with 4% droop	B1, B3, B5, B7	Figure 8-7
Group B devices with $H = 8$ plus VSM0H with 4% droop	B2, B4, B6	Figure 8-9

Table 8-1 : NFP plots

Beneath each NFP plot is also shown, for indication, the rotor response functions ϕ_R/ϕ_G from (17) for (V)SM and (31) for VSM0H.

8.4.1 Group A (VSMs without droop response, SM with τ_P=4 s) & VSM0H devices

Following from the general explanation of the plot features in section 8.2, points of note in the NFP plots are:

- Figure 8-3. The SG with conventional controls shows a conventional NFP plot. The droop response trend-line is met at the left of the plot. There is a dip in response at $f_{NFP_{mod}}$ ≈ 0.1 Hz, as droop response is "cut off" and inertial response is not yet dominant. Inertial response is dominant between 0.2 < $f_{NFP_{mod}}$ < 2 Hz, with phase approaching 270° and rotor resonance at ~2 Hz. Damping becomes dominant over inertia with $f_{NFP_{mod}}$ > 2 Hz.
- Figure 8-3. The VSM devices, with no droop response configured, show very low response with low $f_{NFP_{mod}}$, and the response is entirely inertial up to $f_{NFP_{mod}}$ ≈ 2 Hz.
- Figure 8-3. VSM devices with conventional levels of damping show similar performances, whether the damping is internal (device A3) or external (device A8).
- Figure 8-3. Devices with conventional levels of damping show significant damping responses up until $f_{NFP_{mod}}$ ≈ 10-15 Hz.
- Figure 8-3. The viable VSM_{Int} device with critical internal damping A5 shows a smaller inertial contribution at the rotor resonant frequency than devices with lower damping (A3 and A8). Also the damping for device A5 becomes dominant over inertia at a lower $f_{NFP_{mod}}$, drawing the phase down from 270° towards 180° as $f_{NFP_{mod}}$ > 0.5 Hz
- Figure 8-3. The VSM_{Ext} device with critical damping (device A7) shows a response which tracks the inertia asymptote extremely well, in magnitude and phase, up to $f_{NFP_{mod}}$ ≈ 0.5 Hz. At higher $f_{NFP_{mod}} > 0.5$ Hz, the resonant peak is avoided, due to the high level of damping. Also, the device moves into a region between $0.5 < f_{NFP_{mod}} < 40$ Hz in which the response magnitude is very large compared to all the other devices. The response phase reduces from 270° back to 180° (the expected phase of damped/droop response) and then further, in-line with other devices. This emphasises that there is a direct conflict between any requirement for high levels of real, external damping power, and a 5 Hz upper bandwidth. A bandwidth (of power response) up to ~40 Hz could be required if high (critical) levels of external damping were strictly required.
- Figure 8-3. The VSM0H converter shows a flat response over the whole range 0 < $f_{NFP_{mod}}$ < 3 Hz, above which there is a small peak followed by a rapid rolloff. The device provides a drooped/damped response across the whole range of $f_{NFP_{mod}}$, with damping significant up to ~ 15 Hz.
- Figure 8-5. Similar conclusions as for the group A devices with H=4 in Figure 8-3, except that the inertia is doubled in A2, A4 & A6. This affects the slope of the inertia asymptote, the gradient of the VSM inertial responses, and the rotor resonant frequencies which drop by $\sqrt{2}$.

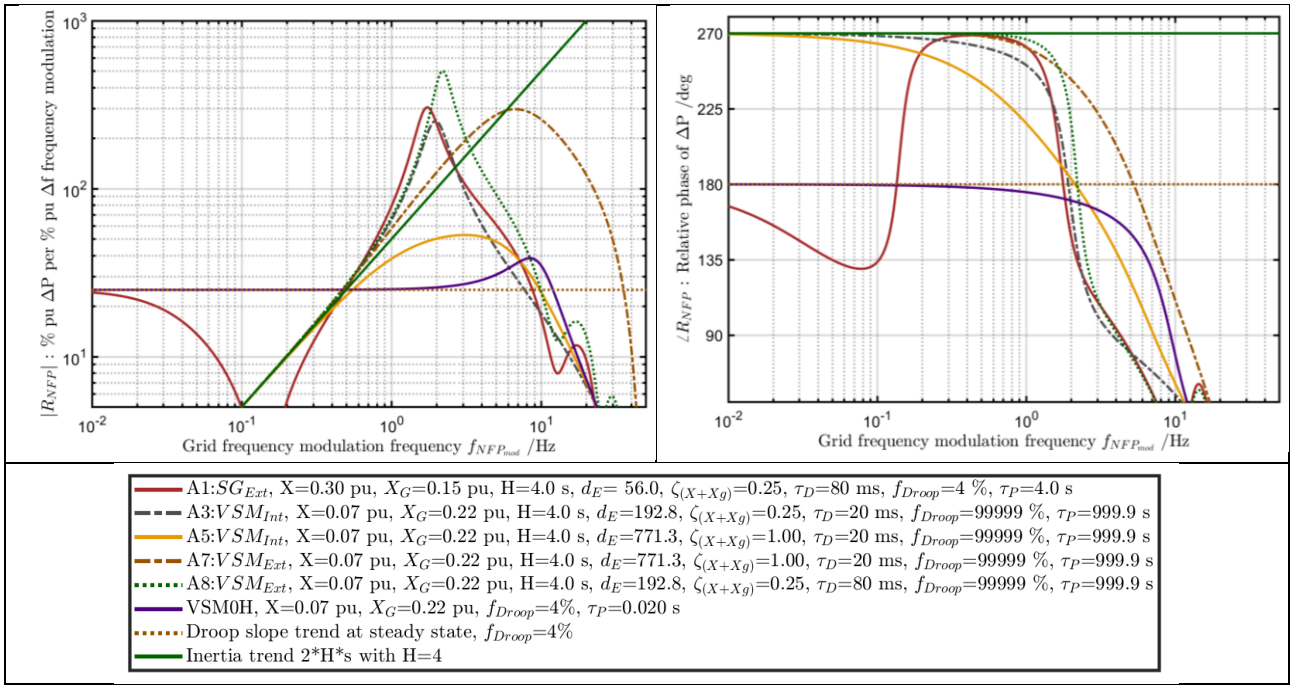

Figure 8-3 : NFP plot for Group A devices with H=4 (A1, A3, A5, A7, A8) plus VSM0H, and asymptotes for droop and inertia

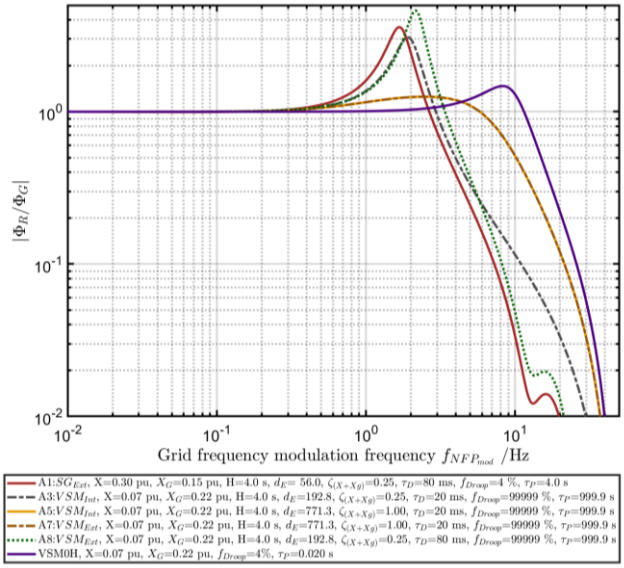

Figure 8-4 : ϕ_R/ϕ_G for Group A devices with H=4 (A1, A3, A5, A7, A8) plus VSM0H

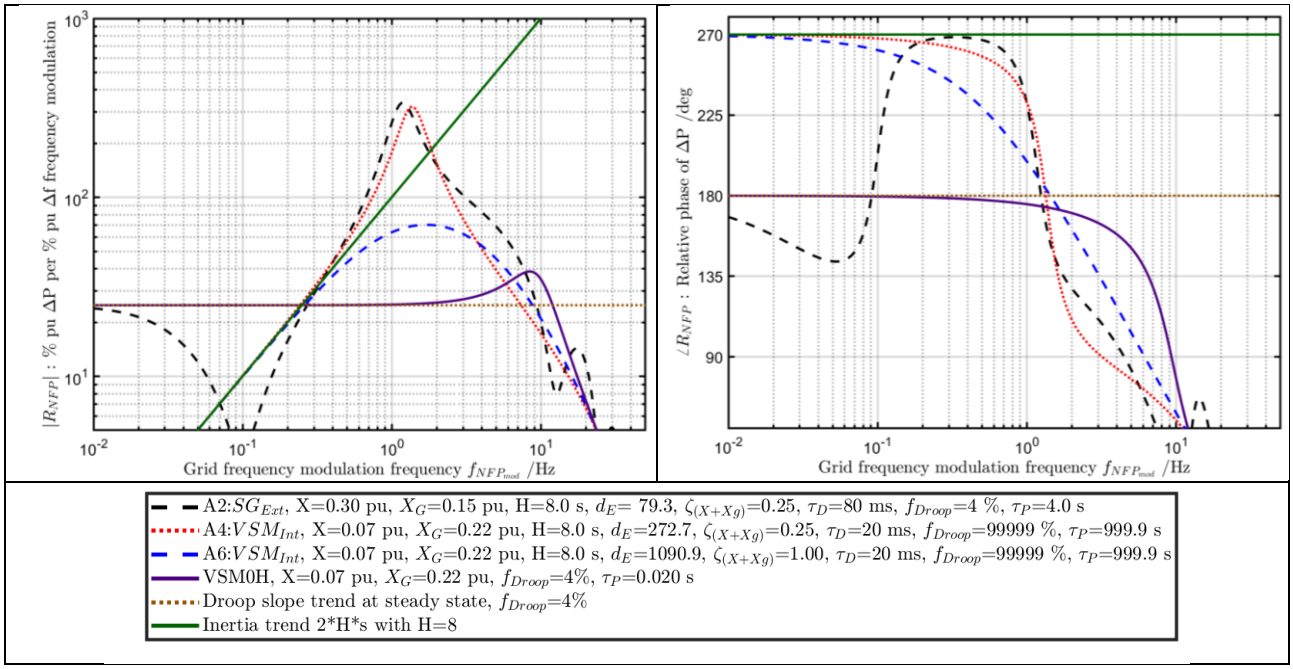

Figure 8-5 : NFP plot for Group A devices with H=8 (A2, A4, A6) plus VSM0H, and asymptotes for droop and inertia

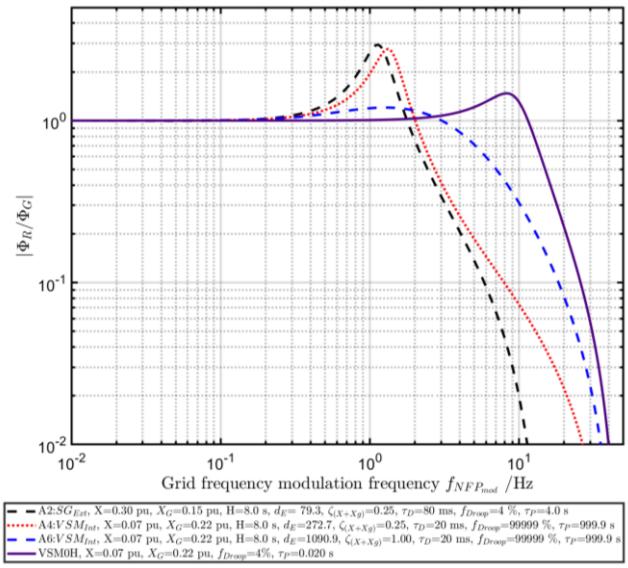

Figure 8-6 : ϕ_R/ϕ_G for Group A devices with H=8 (A2, A4, A6) plus VSM0H

8.4.2 Group B (VSMs with droop response τ_P=1 s, SM with τ_P=10 s) & VSM0H devices

- Figure 8-7. The Group B VSM devices with H=4 contain droop response. This means that, compared to Figure 8-3, the VSM responses for $f_{NFP_{mod}}$ < ~0.3 Hz now also contain droop response and do converge with the droop asymptote.
- Figure 8-7. Because the response time constant of the Group B VSM devices are only τ_P=1 s, compared to the SM which is much slower with τ_P=10 s, the droop response for the VSM devices B3-B8 is dominant until a much higher $f_{NFP_{mod}}$, and the dip in response between the drooped response and the inertial response is less pronounced. In fact, the droop responses and inertial responses for B3-B8 begin to overlap in region of $f_{NFP_{mod}}$ near 0.3 Hz, which leads to the phase of the NFP plot taking longer to transition from 180° towards 270°. As a logical extension to this argument, if drooped response is combined with inertial response, and the time constant on droop response is small, then this can prevent the NFP plot phase from reaching 270°, even if inertial response is genuinely present. Likewise a high damping value can also have the same effect.
- Figure 8-7. The VSM_{Int} device with critical damping (device B5) shows this effect, where the high damping means that the phase of the NFP plot never reaches 270°. In Figure 8-3, the phase of the NFP response for device A5 dropped away from 270° at higher $f_{NFP_{mod}}$ as damping became dominant over inertia. In Figure 8-7, device B5, which is the same as device A5 except that droop response is added, shows the same behaviour at high $f_{NFP_{mod}}$, but additionally the phase at lower $f_{NFP_{mod}}$ does not now reach 270°, because the drooped response is still significant at the lower $f_{NFP_{mod}}$ end of the inertial "zone".
- Figure 8-9. Most conclusions have already been drawn in the points above, but the plot for the group B devices with H=8 and droop responses active for the VSM devices is shown here for completeness and consistency.

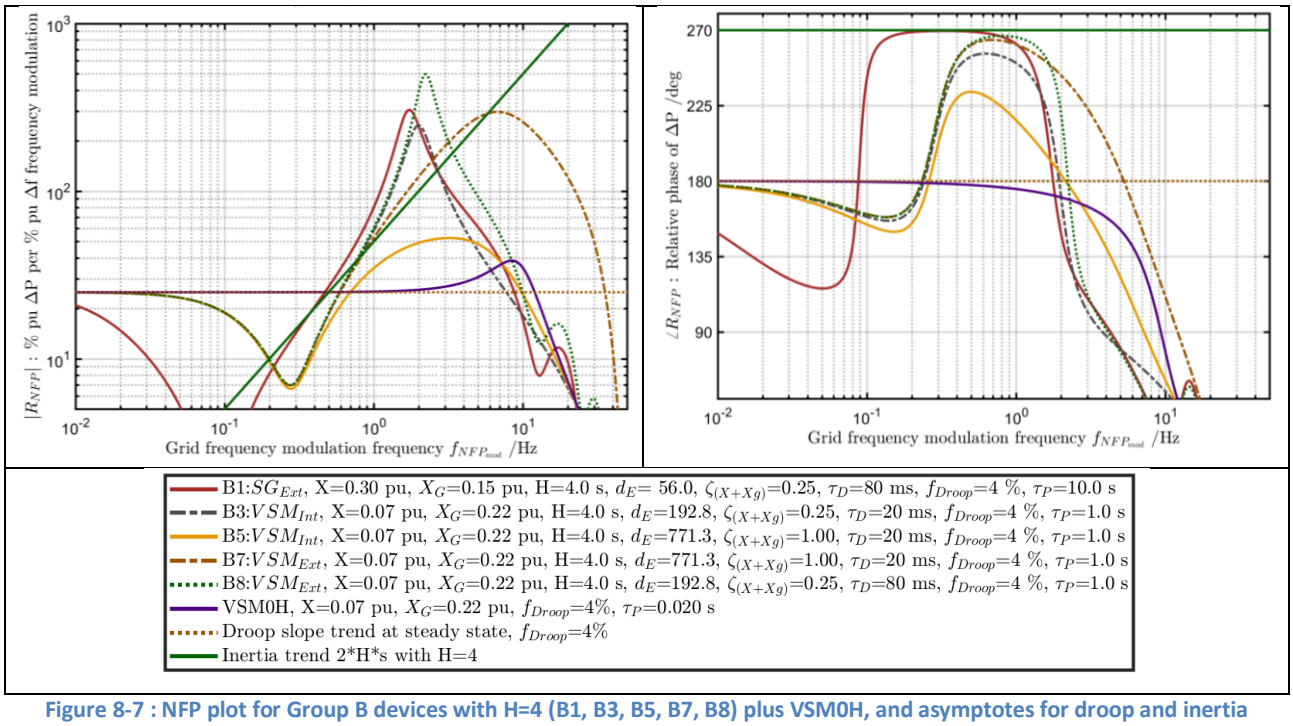

Figure 8-7 : NFP plot for Group B devices with H=4 (B1, B3, B5, B7, B8) plus VSM0H, and asymptotes for droop and inertia

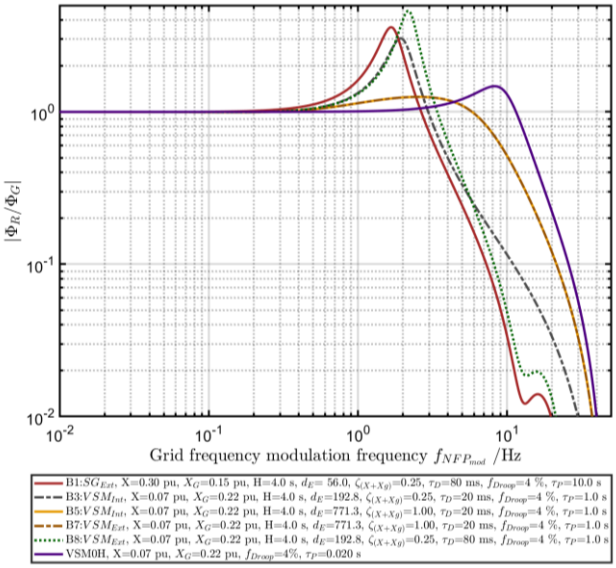

Figure 8-8 : ϕ_R/ϕ_G for Group B devices with H=4 (B1, B3, B5, B7, B8) plus VSM0H

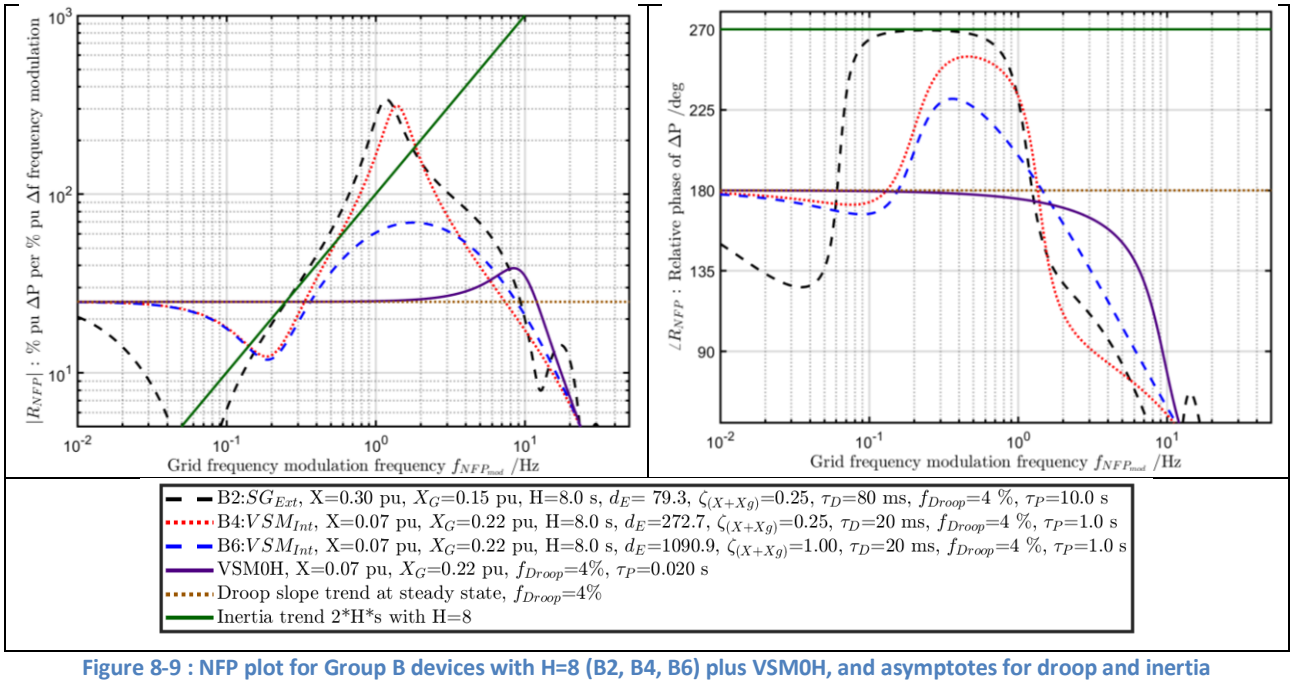

Figure 8-9 : NFP plot for Group B devices with H=8 (B2, B4, B6) plus VSM0H, and asymptotes for droop and inertia

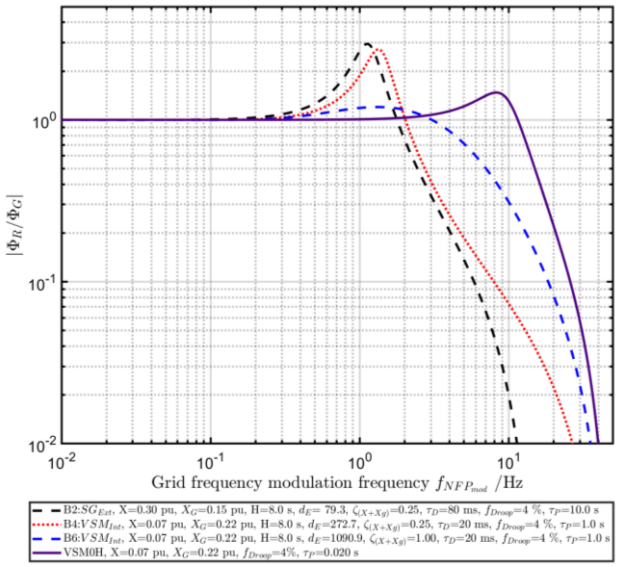

Figure 8-10 : ϕ_R/ϕ_G for Group B devices with H=8 (B2, B4, B6) plus VSM0H

8.5 Extracting NFP plots from background data

The methods described within 8 for defining and generating the NFP plot rely on placing the device (simulated or real) in a test system that is subjected to specific frequency modulations. This can be achieved in simulation, or in a very closely controlled PHIL test environment, or by injecting modulations into the PWM waveforms at the converter bridge. For multi-MVA generators, and any generator installed at a real network location, direct generation of the NFP plot using real device hardware is therefore either unviable, or comes with a (perhaps manageable) risk of inducing local flicker and (inter)harmonics.

It might be possible to extract the NFP plot shapes (amplitude and phase) from background data, gathered over timeframes that encompass a variety of grid phase/frequency trajectories, with current and voltage data gathered at a device point-of-common coupling with the network. A procedure to do this has not yet been created. It might be possible to do effectively, or it might be too difficult to extract the data from “noise” without gathering excessive quantities of data. Further research is required.

9 Use of the NFP plot to produce a specification mask

The NFP plot, introduced in section 8, offers one possible way of characterising a device, and determining its claims of droop response, inertia and damping. The plot does not reveal everything about a device. For example it does not explicitly show "stability", nor the grid stiffness and the device's response to discrete phase steps. However, it would be possible to validate a device's claims of droop (and "fast frequency") response, inertial characteristics and damping, from the NFP plot. The NFP plots can be generated in a variety of ways, as described in section 8.

One part of a specification for grid forming converters could therefore be an assessment of the NFP plot of the device, against a mask defined by the claimed device properties. Examples shown in the figures below give examples of these masks, and how they might be defined.

The first example is for a synchronous machine connected to a steam turbine, with H=8. This is example B2 (Group B, device 2) from section 5 Table 5-1. The idealised NFP plot for such a device is shown as the central lines of the NFP plot shown in Figure 9-1. This is determined using (27). Also shown on Figure 9-1 are upper and lower mask lines. These are determined by evaluating (27) many times, to fully explore the 6-dimensional "cube" of parameter space that encompasses a ±10 % variation of the following 6 parameters from their nominal values:

- Impedances X, X_G
- Inertia H, and damping ζ
- Droop slope D_f, and droop response time constant τ_P

The results of (27) evaluated many times for the different combinations of parameter variations allow the minimum and maximum (lower and upper) masks lines to be determined.

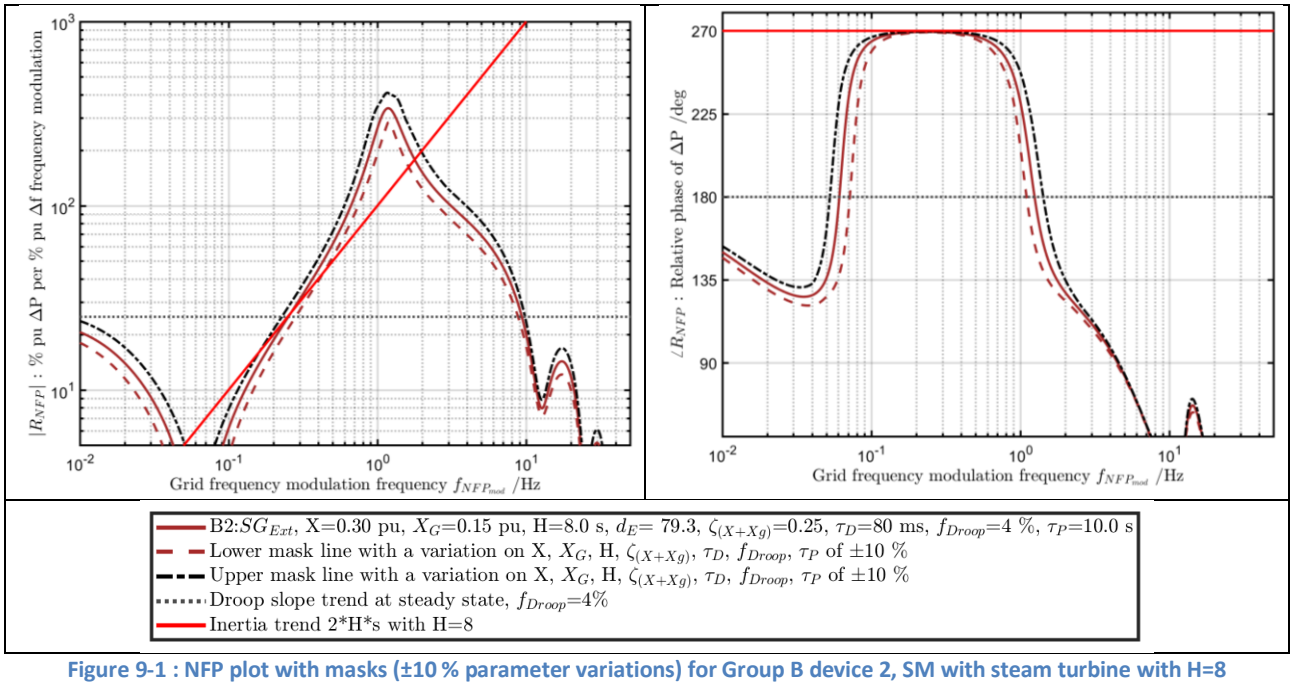

Figure 9-1 : NFP plot with masks (±10 % parameter variations) for Group B device 2, SM with steam turbine with H=8

Figure 9-1 shows that, even considering ±10 % variations on all six parameter values, the lower and upper mask lines are relatively tightly spaced to the idealised nominal performance. Partly this is due to the log-log nature of the plot scales. However, it does show that if a device claims to have a certain performance, with defined inertial and droop responses, it ought to closely resemble the idealised NFP plot, unless the parameters are quite significantly different to those claimed.

The second example, shown in Figure 9-2, is for VSM_{Int} device B5 (Group B, device 5) from section 5 Table 5-1. In this case, the idealised NFP plot central line and masks are determined using (28), with the same ±10 % variation allowed from the nominally declared values.

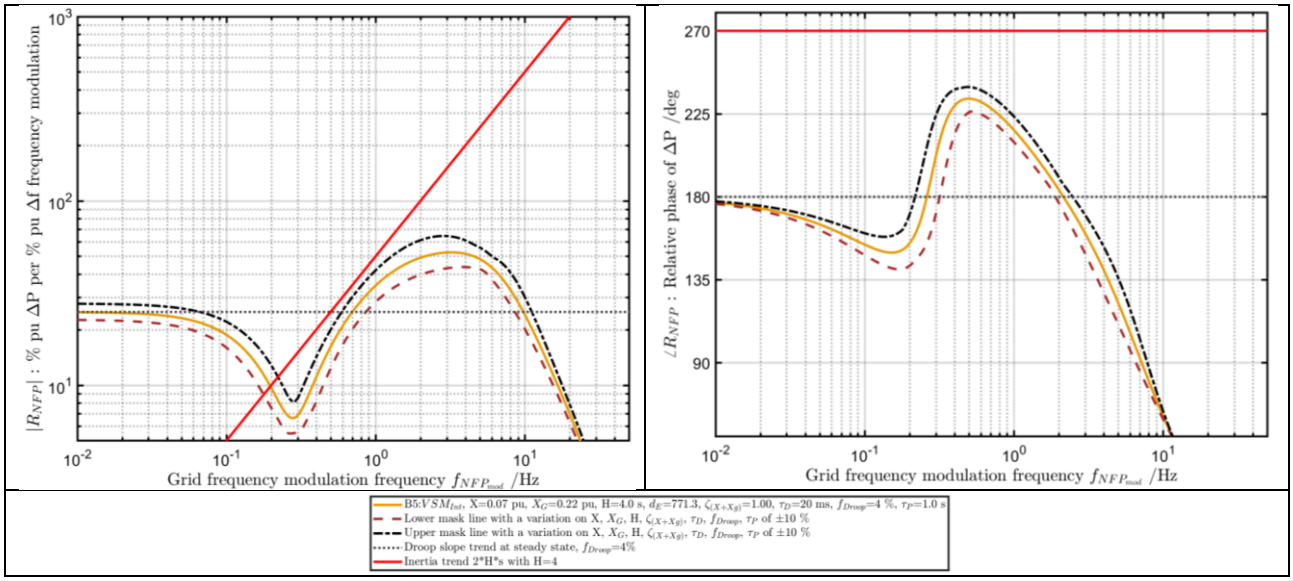

Figure 9-2 : NFP plot with masks (±10 % parameter variations) for Group B device 5, VSM with H=4

Again, the mask lines are relatively tightly constrained to the nominal performance, partly due to the log-log plot style.

Considering the tightness of the mask lines in both Figure 9-1 and Figure 9-2, and the clear differences in shape between the two figures, it appears that the NPF plot might be very useful as a tool for discriminating between device behaviours.

While the droop slope D_f and asymptote is the same for both devices in Figure 9-1 and Figure 9-2:

- The response time τ_P of the VSM_{Int} in Figure 9-2 is much less than that of the SM in Figure 9-1. On Figure 9-2 this is represented as a flat droop response extending to ~0.1 Hz, while in Figure 9-1 the response of the SM is already tailing off at 0.01 Hz. If a device claims to have a fast response, but does not, then this will be clear from the left-hand side of the NFP plot.
- The inertia is H =8 in Figure 9-1 but only H =4 in Figure 9-2. In Figure 9-1 it is clear that the device (and the mask lines) clearly move towards the inertia asymtote, because the damping is small. In Figure 9-2 it is not so clear that the mask moves towards the inertia asymptote. In particular, the phase plot in Figure 9-2 shows only a 45 ° advance in the region of inertial contribution (~0.5 to ~2 Hz), and the phase comes significantly short of meeting the inertia phase asymptote at 270°. This is for two reasons. Firstly, the drooped response is

fast, and so the droop response is still fighting for dominance with inertia at $f_{NFP_{mod}}$ ≈ 0.3 Hz, and this drags the phase of the response towards 180°. Secondly, the damping is high (critical), which means that damping is becoming dominant towards $f_{NFP_{mod}}$ ≈ 5 Hz. This also drags the phase of the response towards 180°. Nevertheless, the mask lines show the boundary that the device ought to fall within, if the device has the claimed parameters, ±10 %.

10 Appendix A : Derivation of time-domain response of (V)SM rotor

Equation (18) is repeated here as (48), the simplified rotor response, ignoring the additional filters.

$$\frac{\phi_R}{\phi_G} \approx \frac{\frac{k_s X}{2H(X+X_G)}s + \frac{\omega_0}{2H(X+X_G)}}{s^2 + \frac{k_s X}{2H(X+X_G)}s + \frac{\omega_0}{2H(X+X_G)}} \tag{48}$$

This can be rewritten using (19) as:

$$\frac{\phi_R}{\phi_G} \approx \frac{2\zeta\omega_n s + \omega_n^2}{s^2 + 2\zeta\omega_n s + \omega_n^2} \tag{49}$$

in which (20)-(25) can all be applied where useful.

If a phase step function of size Δ radians, i.e. Δ/s is applied at ϕ_G, then the response at ϕ_R will be:

$$\phi_R \approx \frac{\Delta}{s}\left[\frac{2\zeta\omega_n s + \omega_n^2}{s^2 + 2\zeta\omega_n s + \omega_n^2}\right] \tag{50}$$

This can be split into two parts:

$$\phi_R \approx \Delta\left[\frac{2\zeta\omega_n}{s^2 + 2\zeta\omega_n s + \omega_n^2} + \frac{\omega_n^2}{s(s^2 + 2\zeta\omega_n s + \omega_n^2)}\right] \tag{51}$$

A final short set of manipulations allows the two parts to be put into forms that can be applied directly to a table of inverse Laplace transforms:

$$\phi_R \approx \Delta\left[\frac{2\zeta\omega_n}{(s+\zeta\omega_n)^2 - (\zeta\omega_n)^2 + \omega_n^2} + \frac{\omega_n^2}{s(s^2 + 2\zeta\omega_n s + \omega_n^2)}\right] \tag{52}$$

where we can define:

$$\omega_d^2 = \omega_n^2(1-\zeta^2) \implies \omega_d = \omega_n\sqrt{(1-\zeta^2)} \tag{53}$$

which is essentially where the equation for the damped natural resonance stems from.

therefore:

$$\phi_R \approx \Delta\left[\frac{2\zeta\omega_n}{(s+\zeta\omega_n)^2 - \omega_d^2} + \frac{\omega_n^2}{s(s^2 + 2\zeta\omega_n s + \omega_n^2)}\right] \tag{54}$$

This expression can now be applied to a standard table of inverse Laplace transforms, assuming $\zeta < 1$:

$$\phi_{R(t)} \approx \Delta\left[\left(\frac{2\zeta\omega_n}{\omega_d}\right)e^{(-\zeta\omega_n t)}sin(\omega_d t) + \left(1 - \frac{e^{(-\zeta\omega_n t)}}{\sqrt{(1-\zeta^2)}}sin(\omega_d t + \text{acos}(\zeta))\right)\right] \tag{55}$$

11 Appendix B : (V)SM rotor analogy to a "mass on a spring in zero gravity"

In this section, screenshots of powerpoint slides show how a (V)SM rotor motion is analgous to a "mass on a spring in zero gravity". By comparing the diagrams, and the form of the motion equations it is possible to see the analogy in the behaviour.

11.1 (V)SM rotor

The VSM rotor motion here is shown, neglecting any extra complications due to grid impedance X_G, and the analysis is confined to the machine stator and rotor interactions.

The VSM rotor analysis is done using pu quantities for torque, impedance (stiffness) and damping. The conversion from SI units to pu quantities is derived on the 2nd figure (Figure 11-2).

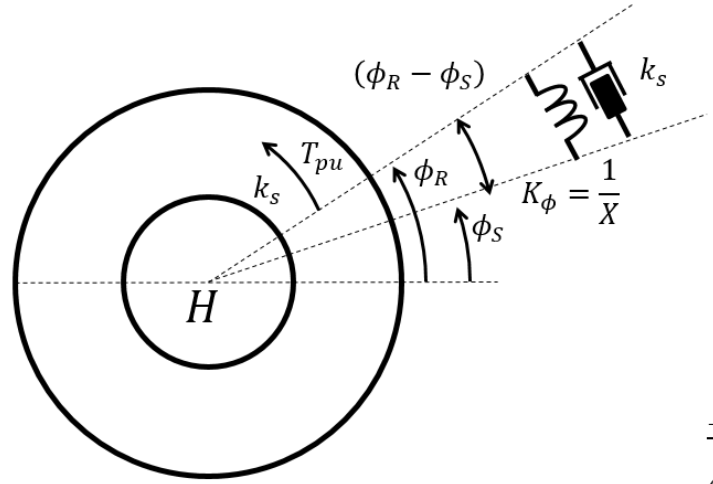

T_{pu}	Torque	pu
ϕ_R	Rotor angle	rad
ϕ_S	Stator electrical angle	rad
H	pu inertia	s
X	Transient impedance	pu
$K_\phi = 1/X$	"Spring stiffness"	1/pu
k_s	damping	pu per pu slip
ω_0	Nominal speed	rad/s

(V)SM Rotor

$$T_{pu} = -\left[(\phi_R - \phi_S)K_\phi + \frac{d(\phi_R - \phi_S)}{dt}\left(\frac{k_s}{\omega_0}\right)\right]$$

$$T_{pu} = \frac{-(\phi_R - \phi_S)}{X} - s(\phi_R - \phi_S)\left(\frac{k_s}{\omega_0}\right)$$

$$T_{pu} = \left(\frac{2H}{\omega_0}\right)\frac{d^2\phi_R}{dt^2}$$ *(Derived on following page)*

$$\frac{-(\phi_R-\phi_S)}{X} - s(\phi_R - \phi_S)\left(\frac{k_s}{\omega_0}\right) = \left(\frac{2H}{\omega_0}\right)s^2\phi_R$$

$$\phi_R\left(\left(\frac{2H}{\omega_0}\right)s^2 + s\left(\frac{k_s}{\omega_0}\right) + \frac{1}{X}\right) = \phi_S\left(s\left(\frac{k_s}{\omega_0}\right) + \frac{1}{X}\right)$$

$$\phi_R = \frac{\phi_S\left(s\left(\frac{k_s}{\omega_0}\right)+\frac{1}{X}\right)}{\left(\left(\frac{2H}{\omega_0}\right)s^2+s\left(\frac{k_s}{\omega_0}\right)+\frac{1}{X}\right)}$$

$$\frac{\phi_R}{\phi_S} = \frac{\left(s\left(\frac{k_s}{2H}\right)+\frac{\omega_0}{2HX}\right)}{\left(s^2+s\left(\frac{k_s}{2H}\right)+\frac{\omega_0}{2HX}\right)}$$

$$s^2 + \frac{k_s}{2H}s + \frac{\omega_0}{2HX} \Leftrightarrow s^2 + 2\zeta\omega_n s + \omega_n^2$$

$$\omega_n = \sqrt{\frac{\omega_0}{2HX}} \qquad \zeta = \frac{k_s}{4H\omega_n} = \frac{k_s\sqrt{X}}{2\sqrt{2H\omega_0}}$$

Figure 11-1 : (V)SM rotor motion analogy to a "mass on a spring"

T_{pu}	Torque	pu
ϕ_R	Rotor angle	rad
ϕ_S	Stator electrical angle	rad
H	pu inertia	s
X	Transient impedance	pu
$K_\phi = 1/X$	"Spring stiffness"	1/pu
k_s	damping	pu per pu slip
ω_0	Nominal speed	rad/s

J	Inertia	kgm/s²
T_N	Torque	N
S	Machine rating	VA

$$E = \frac{1}{2}J\omega^2$$

$$H = \frac{\left(\frac{1}{2}J{\omega_0}^2\right)}{S}$$

$$T_N = J\frac{d^2\phi_R}{dt^2}$$

$$T_N = \left(\frac{2HS}{{\omega_0}^2}\right)\frac{d^2\phi_R}{dt^2}$$

$$T_{pu} = \frac{T_N}{\left(\frac{S}{\omega_0}\right)} = \left(\frac{2H}{\omega_0}\right)\frac{d^2\phi_R}{dt^2}$$

$$T_{pu} = \left(\frac{2H}{\omega_0}\right)\frac{d^2\phi_R}{dt^2}$$

Figure 11-2 : (V)SM rotor motion SI to pu conversion derived

11.2 Mass on a spring in zero gravity

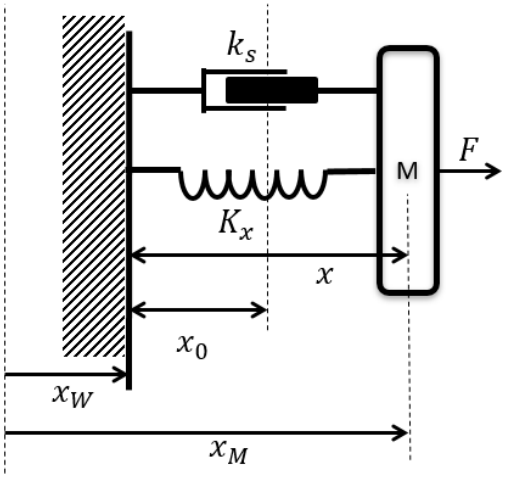

$$x = (x_M - x_W)$$

F	Force	N
x_M	Mass position	m
x_W	Wall position	m
M	Mass	kg
K_x	Spring stiffness	N/m
k_s	damping	Ns/m

Mass on spring

$$F = -\left[(x - x_0)K_x + \frac{dx}{dt}k_s\right]$$

$$F = x_0K_x - (x_M - x_W)K_x - s(x_M - x_W)k_s$$

$$F = Ma$$

$$x_0K_x - (x_M - x_W)K_x - s(x_M - x_W)k_s = Ms^2x_M$$

$$x_M(Ms^2 + sk_s + K_x) = x_W(sk_s + K_x) + x_0K_x$$

$$x_M = \frac{x_W(sk_s+K_x)}{(Ms^2+sk_s+K_x)} + \frac{x_0K_x}{(Ms^2+sk_s+K_x)}$$ (Ignore steady-state offset)

$$\frac{x_M}{x_W} = \frac{(sk_s+K_x)}{M\left(s^2+s\frac{k_s}{M}+\frac{K_x}{M}\right)}$$

$$s^2 + \frac{k_s}{M}s + \frac{K_x}{M} \Leftrightarrow s^2 + 2\zeta\omega_n s + \omega_n^2$$

$$\omega_n = \sqrt{\frac{K_x}{M}} \qquad \zeta = \frac{k_s}{2M\omega_n} = \frac{k_s}{2\sqrt{MK_x}}$$

Figure 11-3 : Mass on a spring in zero gravity